UCLouvain

Institute of Condensed Matter and Nanoscience
Division of Bio and Soft Matter

Synthesis and characterisation of redox-responsive hydrogels based on stable nitroxide radicals

Miriam Khodeir

Jury members:

Prof. Jean-François Gohy (UCLouvain), Supervisor
Prof. Sayed Antoun (ULibanaise), Co-supervisor
Prof. Yann Garcia (UCLouvain), Chairman
Prof. Charles-André Fustin (UCLouvain)
Prof. Christine Jerome (ULiège)
Prof. Evelyne van Ruymbeke (UCLouvain)
Prof. Patrice Woisel (ULille)

Thesis submitted in fulfillment
of the degree of doctor in Sciences

Louvain-la-Neuve 2020

Acknowledgements

This thesis was not only a first professional project, but also a great personal adventure. Now after four years, the time has come to honor all people who assisted and accompanied me throughout this expedition. They let me take advantage of their skills or just listen to my enthusiasm and frustrations. Know that without you, this work would not have become what it is!

This thesis was done at Catholic University of Louvain in Belgium. I thank Pr. Jean-François Gohy, my supervisor, for offering me the opportunity to be a member of his group, for his ideas, confidence and for framed this work with great enthusiasm and optimism. I owe a lot to Prof. Sayed Antoun, my co-supervisor; our discussions crossed all the borders between Lebanon and Belgium during the drafting.

I sincerely thank the members of the jury: Professor Prof. Jean-François Gohy, Professor Sayed Antoun, Professor Yann Garcia, Professor Charles-André Fustin, Professor Christine Jerome, Professor Evelyne van Ruymbeke and Professor Patrice Woisel for reading my manuscript and their constructive remarks that allowed me to improve this one.

Thank you, Jean-François, Alex and Charles-André for always find a time to discuss and answering my questions. And also, for sharing with us best moments with your funny spirit during lunch breaks and the lab day out.

I would like to thanks the people who shared with me their expertise in certain areas. Specially Pr. Evelyne, Jérémy for the rheology analysis, Pr. Alexandru and Bruno for the electrochemical tests, He for the catalyst application part and Olivier for guiding me in the synthesis part during the first months of my thesis. Thanks to Christian for the ESR measurements and Zdravko for the Cryo-TEM measurements and Hélène, Raoul and Etienne for the MS-HPLC and GC-MS analysis.

I also thank all my colleague in the laboratory with whom I have unforgettable moments: Guillaume, Benoît (my personal informatician) and Fadoi with whom I shared the office, my neighbors in work Atul, Jagadeesh (Bob) and Hui, also Lu, Clément, Rowanne, Flanco, Elio, Roland, Sina and the two master students Simon and Louis. All Alex's group, Louis S., Alae Eddine, JD, Xulian, Qi, Xiaozhe, Rico, Luhua. The new arrival: Carla, Zehan, Satyaa, Ashish, Gergeley and Raphael. And our friendly technician support Fabio. Do not forget my master and bachelor students who helped me in this work: Jacinthe, Yannick, Romain, Bejamin and Maria. I wish you all a fully successful future.

Last but not least, I would like to thanks my parents, my sister, my brothers, my cousins specially Raymond and Denise, my friends (Nicole, Mia, Mouna, Massoud, Stephanie, Jessica) and my other half Tannous for their complete support during the whole process of my thesis. Even they are far from me, but their confidence and encouragement are always with me. Without you, I would not have been able to accomplish this thesis.

Just follow your dreams and be patient.

Angelique Kerber

Table of contents

List of symbols

P(M)AA	Poly(meth)acrylic acid
3D	Three-dimensional
A	Shear area
AFM	Atomic force microscopy
C	Spring constant
Cryo-TEM	Cryo-transmission electron microscopy
CSD	Controlled shear deformation
CSR	Controlled shear rate
CSS	Controlled shear stress
CV	Cyclic voltammetry
DLS	Dynamic light scattering
EDTA	Ethylenediaminetetraacetic acid
ESR	Electron spin resonance
F	Shear force
FTIR	Fourier transform infrared
G	Shear modulus
G*	Complex shear modulus
G’	Storage modulus
G’’	Loss modulus
h	Gap width
HA	Hyaluronic acid

IPA	Isopropanol
LCST	Lower critical solution temperature
Li	Lithium
LiPF6	Lithium hexafluorophosphate
LVE	Linear viscoelastic region
Micro-CT	Computed tomography
Mn	Molar mass
n	Shear viscocity
NaCl	Sodium chloride
OEGMA	Oligoethylene glycol methacrylate
$OEGMA_2$	Di (ethylene glycol) methacrylate
OM	Optical microscopy
P(HEA-co-2-NBA)	Poly(hydroxyethylacrylate-co-2-nitrobenzyl acrylate
PANI	Polyaniline
PEG	Poly(ethylene glycol)
PEG-b-PLA	Poly(ethylene glycol)- *bloc*k-Poly(lactic acid)
PEI	Poly(ethylene imine)
PEO	Poly(ethylene oxide)
	Phase shift
PHEMA	Poly(2-hydroxyethyl methacrylate)
PNIPAM	Poly(N-isopropylacrylamide)
Ppy	Polypyrrole
PVA	Poly(vinyl alcohol)

PVP	Poly(vinylpyridine)
SEM	Scanning electron microscopy
SM	Stereo microscopy
SRH	Stimuli-responsive hydrogels
ssDNA	Single-stranded deoxyribonucleic acid
STM	Scannin tunneling microscopy
TEM	Transmission electron microscopy
TEMPO	2,2,6,6-Tetramethyl-1-piperidinyloxy radical
$TEMPO^+$	2,2,6,6-Tetramethyl-1-piperidinyloxoammonium cation
TMPM	2,2,6,6-Tetramethylpiperidin-4-yl methacrylate
v	Velocity
γ	Shear rate
Δgelastic	Elastic free Energy
Δgmix	Energy of mixing
τ	Shear stress

General Introduction

The past decade has witnessed a decided move from static and passive materials to biodegradable, dynamic, and stimuli responsive materials in the laboratory and the industry.

Hydrogels, a unique class of soft materials, are made out of a 3D network of crosslinked hydrophilic macromolecules, which possess the ability to immobilize high amounts of water. These materials form the networks of polymer chain by either physical interactions or chemical bonds, and are often classified as physical or chemical gels, respectively. Physical interactions commonly include hydrophobic, hydrogen bonding and metal ion-ligand interactions, among others, while chemically cross-linked hydrogels result from a broad spectrum of chemical reactions.

The researchers made significant progress in developing hydrogels with greater sophistication and complexity in contrast to the early days of hydrogel synthesis that used rather straightforward chemistry to crosslink hydrophilic polymers in the design of, for example, contact lenses. It was the boom in research the so-called “smart” hydrogels that exhibit responsiveness to a variety of external stimuli such as changes in pH, temperature or redox potential, and that enable a precise control over fundamental material properties, such as swelling, porosity, physical structure, and modulus.[1] This level of external control, has meet the demand for a wide range of applications of hydrogels within medical and industrial fields: well-controlled drug delivery; inexpensive and accurate biosensors; artificial muscles; or effective scaffolds for tissue engineering.[2]

This evolution of hydrogels as a new class of the crosslinked polymers can be appreciated by analysing the number of articles on the topic: doing a quick query for the word "hydrogel" on PubMed it is easy to see the clear exponential tendency in the number of articles (**Figure 1**)

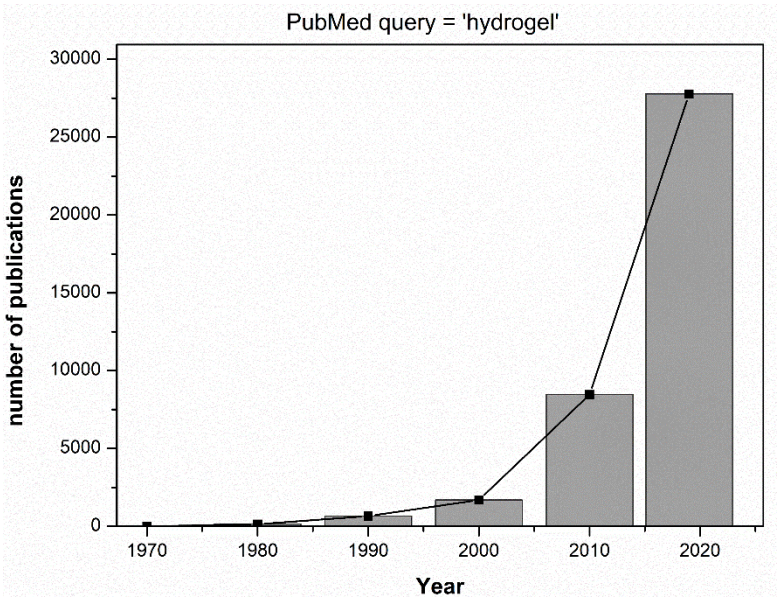

Figure 1. *Histogram showing the increase in publications related to the keyword 'hydrogels' during the past 50 years.*

A historical overview of the major developments in hydrogel research over the last 50 years is presented in **Figure 2**, starting with the relatively simple, chemically crosslinked networks of the 1960s and concluding with today's 'smart' hydrogels.[3]

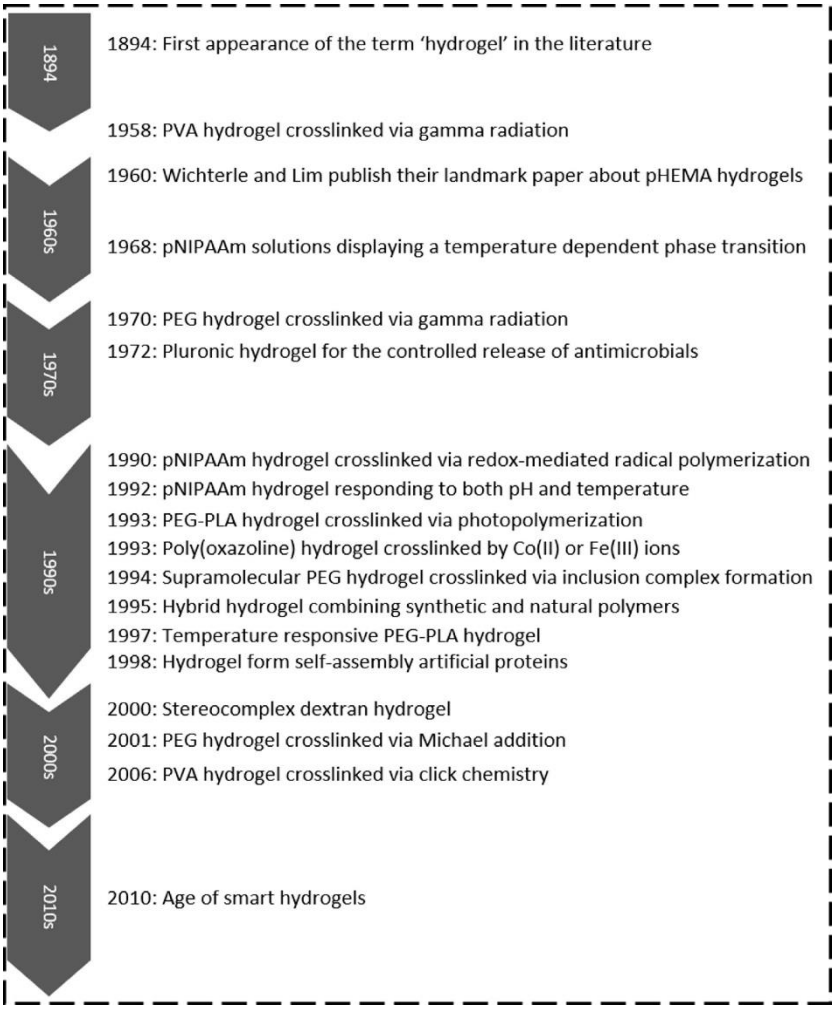

Figure 2. *Timeline presenting a selection of the most important events in the history of hydrogel research.*[3]

Increasing demands on the properties and functionalities of such materials led to the development and design of new synthetic strategies. It provided the production of advanced materials like the ones that will be discussed in the first chapter of this manuscript, in which the concepts, basics and characteristics of hydrogels and the so-called 'smart' hydrogel are briefly presented.

And as research continues toward finding novel mechanisms for stimuli-responsiveness and innovative applications of the responsive hydrogels, the main focus of this thesis is the development of new responsive hydrogels that can release guest molecules upon a redox stimulus. To obtain redox-responsive behavior, we have introduced in the hydrogel the 2,2,6,6-tetramethyl-1-piperidinyloxy (TEMPO) stable nitroxide radical that can be reversibly oxidized into an oxoammonium cation ($TEMPO^+$). Water solubility is provided by the presence of the (oligoethylene glycol) methacrylate (OEGMA) for the first type of studied hydrogel or N-isopropylacrylamide (NIPAM) comonomer for the second type of investigated hydrogel.

Chapters 2 and 3 are dedicated to the synthesis, electrochemical and mechanical characterizations of the first type of hydrogel in their two forms: the reduced one coined as P(TEMPO-*r*-OEGMA), and the oxidized one P($TEMPO^+$-*r*-OEGMA). A preliminary demonstration of the concept of encapsulation/release of a model molecule is also provided for those hydrogels.

Chapter 4 describes the second type of hydrogel containing the NIPAM co-monomer, which is well known in the scientific literature for its thermo-responsive properties and bio-applications. Once again the reduced P(TEMPO-*r*-NIPAM) and oxidized P($TEMPO^+$-*r*-NIPAM) states are characterized into detail.

To end with chapter 5, that details some application of our P(TEMPO-*r*-OEGMA) based hydrogels. The first application describes the electrochemically-controlled release of aspirin from our redox-responsive gels deposited on carbon-printed electrodes and the other application is related to the use of the same hydrogels as catalytic scaffolds (due to the presence of TEMPO radicals) for the oxidation of alcohols.

All these chapters will demonstrate the development of a new class of redox responsive hydrogels based on stable nitroxide radicals that exhibit interesting physicochemical properties making them very promising candidates for practical use in a wide range of applications.

1 C. Echeverria, S. Fernandes, M. Godinho, J. Borges and P. Soares, *Gels*, 2018, **4**, 54.

2 M. Mahinroosta, Z. Jomeh Farsangi, A. Allahverdi and Z. Shakoori, *Mater. Today Chem.*, 2018, **8**, 42–55.

3 S. J. Buwalda, K. W. M. Boere, P. J. Dijkstra, J. Feijen, T. Vermonden and W. E. Hennink, *J. Control. Release*, 2014, **190**, 254–273.

Abstract

Stimuli-responsive hydrogels have the unique property of undergoing a phase transition. This property has attracted much interest for their application in the field of medicine and biotechnology. Aqueous solutions of linear polymers of the poly(N-substituted acrylamides), poly(ethylene glycol methacrylates) families and their three-dimensional macroscopic (hydrogels) or microscopic (nano- and microgels) networks demonstrate such a phase transition behavior. In particular, polymers of this family have the ability to respond to temperature and are characterized by a lower critical solution temperature (LCST). Moreover, redox-responsive polymers such as those based on 2,2,6,6-tetramethyl-1-piperidinyloxy-methacrylate (TEMPO), also gained a lot of attention in recent years. The aim of the present thesis is the synthesis and characterisation of stimuli-responsive hydrogels prepared from the above-mentioned polymers. The effect of both redox and temperature stimuli on the mechanical and electrochemical characteristics of these hydrogels is studied and their possible application for the precise encapsulation/release of guest molecules and as catalytic scaffolds for alcohol oxidation is demonstrated.

Résumé

Les hydrogels stimuli-répondants présentent la propriété unique de subir une transition de phase. Cette propriété a suscité beaucoup d'intérêt pour leur application dans le domaine de la médecine et de la biotechnologie. Les solutions aqueueses de polymères linéaires des familles des poly(acrylamides N-substitués) et des poly(méthacrylates d'éthylène glycol) ainsi que leurs réseaux macroscopiques tridimensionnels (hydrogels) ou microscopiques (nano- et microgels) montrent un tel comportement de transition de phase. En particulier, les polymères de cette famille ont la capacité d'être sensibles la température, et sont caractérisés par une température de solution critique inférieure (LCST). De plus, les polymères sensibles à l'oxydoréduction comme ceux basés sur le méthacrylate de2,2,6,6-tétraméthyl-1-pipéridinyloxy (TEMPO) ont également attiré beaucoup d'attention ces dernières années. Le but de la présente thèse est la synthèse et la caractérisation d'hydrogels stimuli-répondants préparés à partir des polymères susmentionnés. L'effet des stimuli redox et de la température sur les caractéristiques mécaniques et électrochimiques de ces hydrogels est étudié et leur application dans l'encapsulation / libération contrôlée de molécules hôtes et comme catalyseurs pour l'oxydation des alcools est démontrée.

Chapter 1

State of the art

Table of contents

1.1 Hydrogels

The aim of this introduction is to provide the reader with the basic concepts that will be used further in this thesis. This introduction will not provide an exhaustive list and description of all the stimuli-responsive hydrogels that have been reported so far since this list would be extremely long. This introduction will rather show some typical examples of stimuli-responsive hydrogels and will focus on their swelling and rheological properties since those ones will be thoroughly investigated in this thesis. Finally, some applications of stimuli-responsive hydrogels will be described.

1.1.1 Brief history of hydrogels

The term 'hydrogel' dates back to an article published in 1894 by Lee, Kwon and Park.[1] This material was not a hydrogel as we describe it today; it was indeed a colloidal gel made with inorganic salts. The first ever hydrogel reported in 1949 for biomedical implant was poly(vinyl alcohol) (PVOH) cross-linked with formaldehyde and marketed with the trade name Ivalon.[2] Later in 1958, Danno prepared PVOH hydrogels cross-linked by passing gamma radiation through an aqueous solution.[3] Du Pont de Nemours scientists reported in 1936 the synthesis of poly(2-hydroxyethyl methacrylate) (pHEMA) describing it as a hard, brittle and glassy polymer.

Then, (pHEMA) hydrogels were developed much later, by Wichterle and Lim[4] in 1960 for contact lenses application and it was the start of the revolution featuring present day hydrogels. This crosslinked network material has been described with a high water affinity without dissolution and a structural integrity which belong to the typical modern hydrogel properties.[5] Hydrogels are in fact the first materials developed for human body uses[6,7] and show later a great interest from biomaterial scientists for many years.[8,9] Those biomedical applications gained particular attention from the decade of 70's[10] especially in the field of stimuli sensitive hydrogels, the so-called smart hydrogels of modern times. As a typical example, inorganic groups were introduced on the pHEMA backbone to manipulate the pH

sensitivity in the pHEMA membranes and to study sodium chloride (NaCl) permeability control of these membranes as a function of pH.[11]

The aims, goals and the number of materials changed and enlarged constantly over the years. As suggested by Buwalda et al.,[12] the history of hydrogels belongs to different eras:
- First generation hydrogels (sixties onwards) comprise a wide range of cross-linked hydrogels with relatively high swelling and good mechanical strength
- Second generation hydrogels (start of seventies) capable of a response to specific stimuli, such as variations of temperature, pH or concentration of specific molecules in solution
- Third generation hydrogels comprising stereo complexed materials such as those based on poly(ethylene glycol)-*block*-poly(D/L-lactide)[13] and supramolecular interactions such as those based on host-guest interactions with e.g. cyclodextrin.[14]

This progress in hydrogel science leads to an increasing interest in the development of the so called "smart hydrogels" that are able to modify their properties in response to stimuli (**Figure 1.1**). The important and influential work of Lim and Sun[15] in 1980 proved the successful application of calcium alginate microcapsules for cell encapsulation. Later on, Yannas and co-workers[16] explored hydrogels made of natural polymers such as collagen and shark fish cartilage for artificial burn dressings.

Hydrogels based on both natural and synthetic polymers have continued to be of interest for encapsulation of molecules and recently, hydrogels gained much attention for organ and tissue reparative and regenerative matrices in the field of tissue engineering.[1]

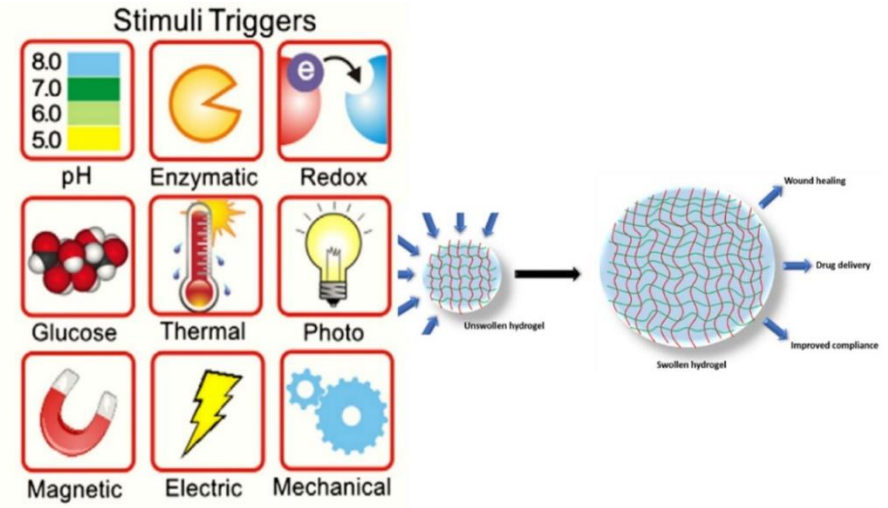

Figure 1.1 *Swelling of a hydrogel in response to various chemical and physical stimuli.*[17,18]

1.1.2 Definition of hydrogels

A three-dimensional network of polymer chains made of natural or synthetic or hybrid materials possessing high degree of flexibility due to large water content is called a hydrogel (**Figure 1.2**).

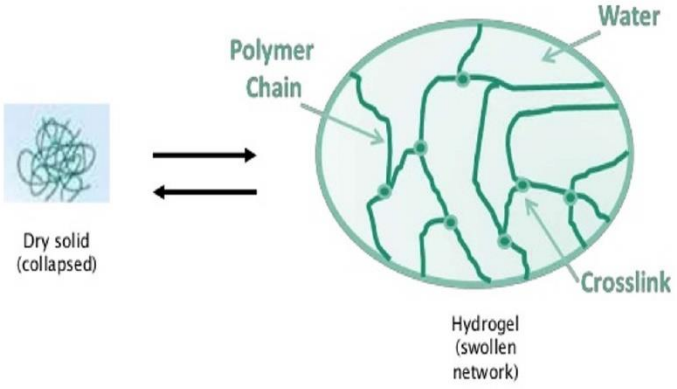

Figure 1.2 *Crosslinked polymer network in dry and water-swollen (hydrogel) state.*[19]

The absorption of water in hydrogels is due to the presence of hydrophilic groups on the polymer chains such as $–NH_2$, –OH, –COOH etc. Swelling phenomena come along with capillary action and osmotic pressure while hydrogels resist dissolution thanks to the cross-linking between polymer chains. Hydrogels can be chemically crosslinked by covalent bonds between different functional groups on the polymer chains via special cross-linking agents, or physically crosslinked through supramolecular interactions such as hydrogen bonds established between different polymer chains. The difference between physical and chemical cross-linked gels is shown in **Figure 1.3**.

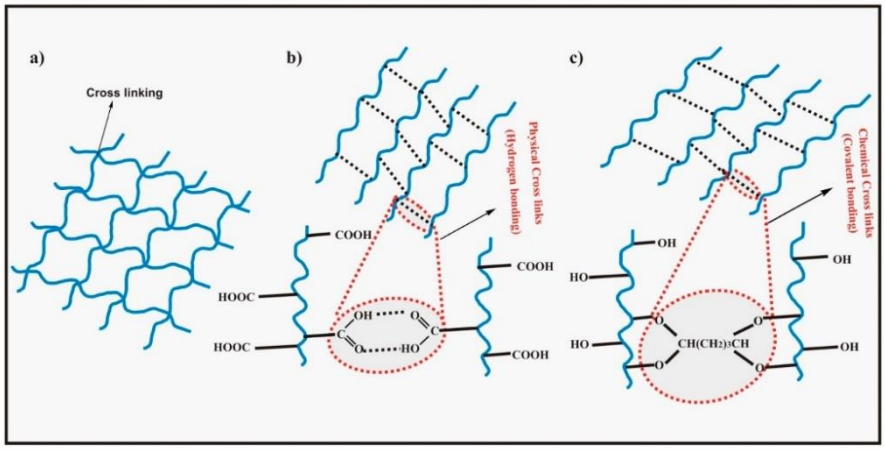

Figure 1.3 *(a) Hydrogel matrix; (b) physically cross-linked hydrogel matrix (hydrogen bonds between carboxylic acid groups); (c) chemically cross-linked hydrogel matrix (acetal groups).*[20]

The equilibrium swelling capacity of a hydrogel is a balance between swelling and elastic forces. The modulation of the contribution of each force leads to hydrogels with different swelling capacities and determines some important properties of the hydrogel, including diffusion characteristics, internal transport and mechanical strength. Many of these properties are controlled not only by the degree of swelling, but also by the chemical nature of the polymer network and the network morphology.

Due to their high-water content, softness, rubbery nature, hydrophilicity, superabsorber character, viscoelasticity, biodegradability and their similarity with extra cellular matrix, some hydrogels resemble strongly biological tissues, resulting in a high interest for biomedical applications such as drug delivery and tissue engineering, with minor toxicity or tissue damage. Another feature of the so-called 'smart hydrogels' is their reversible response to different stimuli like pH, temperature, electric field, magnetic field, ionic strength of solution, and biological molecules[21,22] that make them particularly important for a wide range of applications.

1.1.3 Classification of hydrogels

Hydrogels are classified based on numerous factors like biodegradability, type of cross-linking, source, ionic charge, preparation method, physical properties, and the response nature of the hydrogels to external stimuli.[23] The complete classification of hydrogels is shown in **Figure 1.4**.

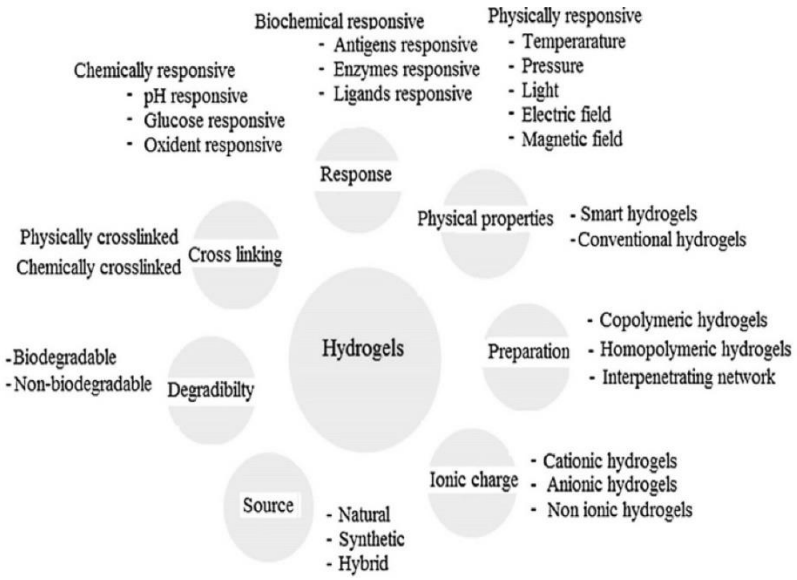

Figure 1.4 *Classification of hydrogels based on different properties.*[23]

1.1.4 Stimuli responsive hydrogels

During the last few decades, a significant amount of research has been performed to develop hydrogels with stimuli-responsive properties where external triggers like temperature, pH, light, shear forces, chemicals, magnetic and electrical fields cause some changes in the properties of the hydrogel materials such as swelling, porosity, physical structure, and modulus. Examples of different stimuli sensitive hydrogels and their mechanisms of response are presented in **Table 1.1**.[20]

Nature of stimulus	Stimulus	Mechanism	Polymers	References
Physical stimuli	Temperature	Shift in temperature changes polymer-polymer and polymer-water interaction responsible for swelling and drug release.	Chitosan-Poly(acrylamide)	24
	Pressure	Swelling under increased pressure and vice versa. This is due to an increase in lower critical solution temperature (LCST) value of hydrogels with pressure. The LCST is the temperature below which thermoresponsive hydrogels swell.	Poly(N-isopropylacrylamide), poly(N,N-diethylacrylamide)	25,26
	Light	Exposure to light (UV and visible light) reversibly changes the hydrogel from its flowable form to non-flowable form and vice versa	Poly(trimethyleniu m iminium trifluorosulfonimide) and 2,6-bis(benzoxal-2-yl)pyridine blend	2,27

Electric field	Changes in electrical charge distribution within the hydrogel's matrix on the application of electric field cause swelling–deswelling and is consequently responsible for the on-demand drug release.	Polythiophene and polypyrrole	25,28
Magnetic field	When a magnetic field is applied, it causes pores in the gel leading to drug release.	Magnetite nanoparticles and poly(acrylamide) composite hydrogels	29
Ultrasound irradiation	Exposure to ultrasound temporarily breaks the ionic cross-links in the hydrogels and the drug is released. Cross-links are reformed on discontinuation of the ultrasound waves. This facilitates on-demand drug release.	Calcium alginate Poly(lactic acid) Poly(acrylic…?	30,31

	pH	Shift in pH causes change in the charge on the polymer chains leading to swelling and drug release.	Poly(acrylic acid), Guar gum succinate, Kappa-carrageenan/poly(vinyl alcohol)	32–34
	Ionic strength	Change in ion concentration also causes swelling and drug release.	Kappa carrageenan-g-poly(acrylic acid) hydrogels	35
Chemical stimuli	CO_2	In CO_2 sensors, a pH sensitive hydrogel disc comes in contact with a bicarbonate solution. On exposure to CO_2, the pH of solution changes resulting in swelling or deswelling of the hydrogel which causes a change in pressure which is a measure of the partial pressure of CO_2.	Poly(2-hydroxyethylmethacrylate)-co-(2-dimethylaminoethylmethacrylate)	36,37
	Glucose	Hydrogels show swelling in response to increased glucose concentration. The complex formed between glucose and phenylboronic acid drives the swelling of the hydrogels and consequently insulin release.	Poly(acrylamide)-co-(3-acrylamidophenyl-boronic acid)	38

	Redox	Disulfide linkages incorporated in hydrogels cleave in the reductive environment (high level of glutathione concentration = 0.5–10 mM) in intracellular matrix and release bioactive molecules/drugs .	[poly(ethylene glycol) monomethyl ether]-graft-[disulfide linked poly(amido-amine)] and α-cyclodextrin glycidylmethacrylate	39
Biological stimuli	Enzyme	Enzymes cause hydrogel degradation and consequently the drug release. This is called a chemically controlled drug release mechanism.	Glycidylmethacrylate dextran-g-poly(acrylic acid)	40
	Antigen	Hydrogels sense the free antigen and undergo swelling followed by drug release.	N-succinimidylacrylate based antigen-antibody entrapment hydrogel	23,21
	DNA	Single stranded (ss) DNA grafted hydrogels show swelling in the presence of ssDNA.	Single stranded DNA probe-g-poly(acrylamide) hydrogels	41

Table 1.1 *Different stimuli sensitive hydrogels and their mechanisms of response.*[20]

Some hydrogels are elaborated to exhibit dual responsiveness with external stimuli such as temperature and pH. Those stimuli-responsive properties of hydrogels lead to extremely diversified applications in the biomedical domain especially for drug delivery applications.[42–44] As a typical example, pH- and thermo-responsive hydrogels in **Figure 1.5** show changes in mechanical and drug release properties with the change in the temperature and pH of the external environment.

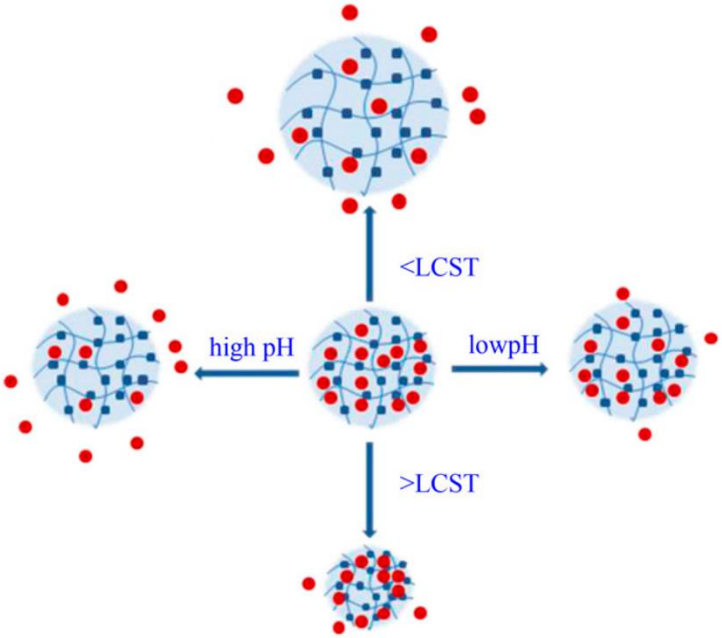

Figure 1.5 *pH and temperature responsive hydrogels.*[45]

1.1.4.1 Redox-responsive hydrogels

Among all the different stimuli described above, change in the redox state is particularly attractive to polymer scientists because it is one of the most relevant triggers targeted in biomedical research.[46] In humans, a healthy redox state is extremely important in various daily cellular functions such as cell cycle regulation, which includes cell proliferation, cell differentiation, and cell death. The representative cellular redox couple, as example, is glutathione/glutathione disulfide

(GSH/GSSG), which is works constantly to buffer the level of reactive oxygen species to keep the redox environment regulated.[47]

The design of redox active network usually involves incorporation of redox responsive centers in the polymer main chain, in the side groups or as cross-linking moieties. Especially valuable are those gels that are capable of responding reversibly, in a controllable manner to redox stimuli. Redox stimuli may be applied chemically or electrochemically.

A wide range of redox gels based on ferrocene, viologen, conjugated polymers, tetrathiafulvalene, transition metal ions and disulfide bonds has been developed with various dimensions, including macroscopic gels, microgels and nanogels. Ferrocene is one of the most widely used redox center due to its low bio-toxicity, commercial availability and plays a key role in the fabrication of redox-responsive hydrogels (RRHs).[48] Harada, Nakahata, and coworkers have contributed significantly in this area using host–guest polymers[49], and one of their works involved redox-responsive self-healing hydrogels that used cyclodextrins and ferrocene as host–guest to achieve redox sensitivity.[50,51] The transition in oxidation state of ferrocene (**Figure 1.6**) in gel system can induce various responsive behavior of their properties like hydrophilicity, color, morphology, expansion-contraction, sol-gel transitions and so on.[52] These redox responsive gels have been explored for the application in actuators, biosensors, molecular delivery systems and so on. [52]

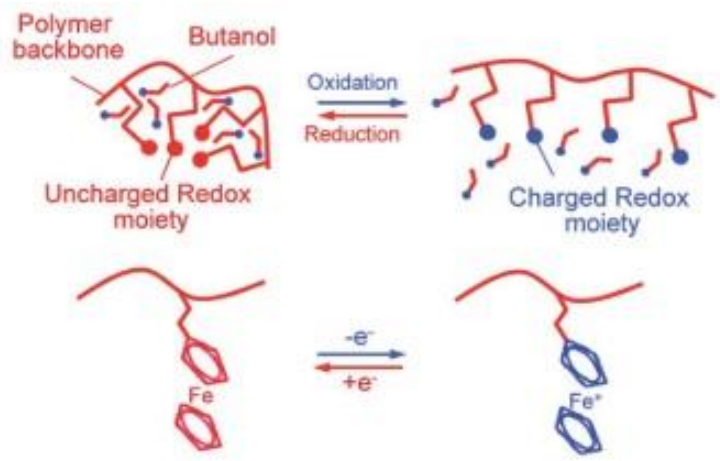

Figure 1.6 *Schematic diagram showing the absorption of organic molecules (e.g. butanol as shown here) by the polymer in the uncharged state and the subsequent release of the organic molecules on oxidation of the ferrocene groups in the polymer.*[53]

On another hand, the viologen as redox center, can be cited in the context of the development of redox-responsive hydrogels. As example, the work of Kao et al.,[54] they synthesized a Vinyl benzyl viologen (VBV) and utilized to obtain all-in-one thermally cured electrochromic devices (ECDs). (**Figure 1.7**) The vinyl moiety of VBV monomer could react with methyl methacrylate (MMA) to yield bulky VBV/poly(methyl methacrylate) (PMMA) chains and even cross-linked network without the assistance of additional crosslinker. Both the bulky VBV/PMMA chains and the resulting polymer network can hinder the aggregation of the viologens and reduce the possibility of dimerization, rendering enhanced cycling stability.

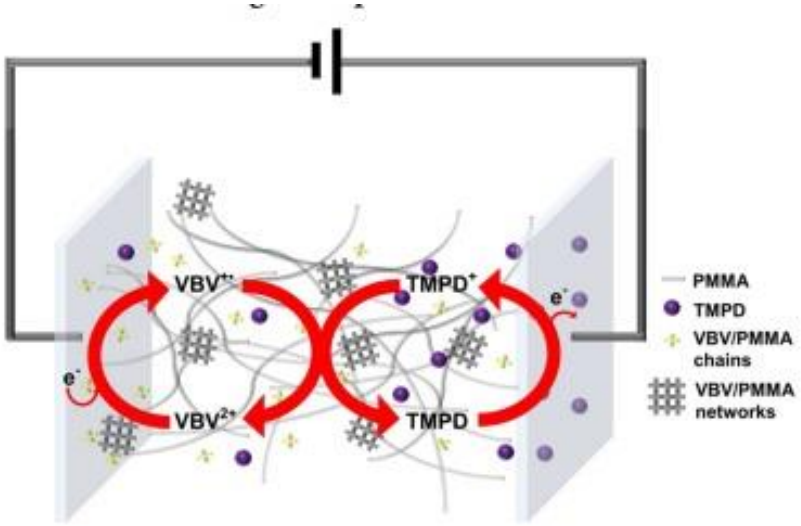

Figure 1.7 *Working Principle of the VBV-Based ECD.*[54]

Hydrogel materials with a high mechanical strength, such as nanocomposite gels,[55] slide-ring gels[56] and tetra-PEG gels,[57] have been also reported. Among them are the double network (DN) gels reported by Gong et al.,[58] which show a high mechanical strength because of two isolated polymer networks, formed from soft and hard networks, which delocalize the stress on the gel network effectively. They used in their work an inclusion complex of βcyclodextrin (CD) and methylviologen (MV) as a stimuli responsive supramolecular bond cross-linking the gel networks. (**Figure 1.8**) CD is a cyclic oligosaccharide which is well-known for its use as a host molecule, entrapping various functional guest molecules.[59] MV is a redox responsive molecule and reduced MV (MV^0) is strongly entrapped into the cavity of CD.[60] They also demonstrated the reversing of the effects of the supramolecular bonds to the stimuli responsiveness of hydrogel materials. Some researchers reported stimuli responsive DN gels due to host–guest interactions.[61]

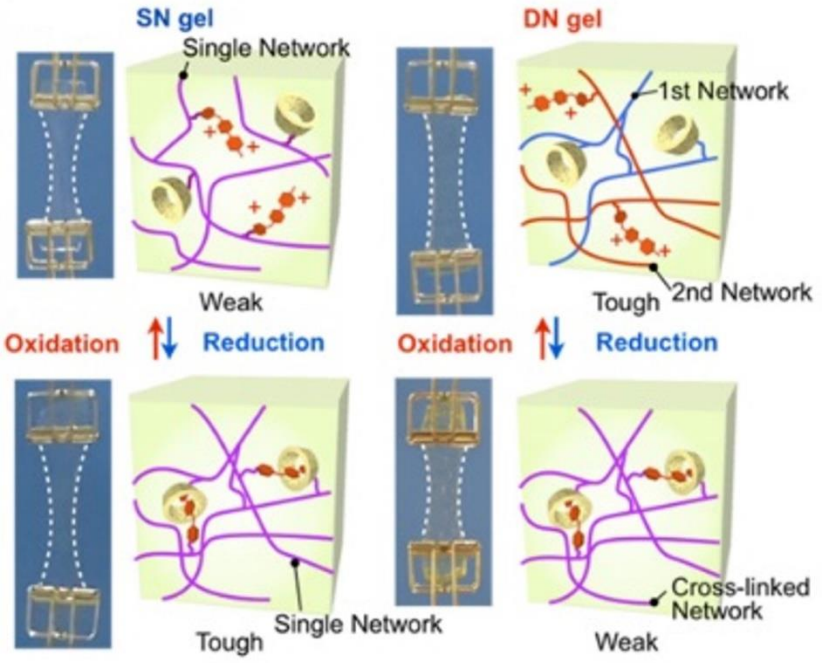

Figure 1.8 *Photographs of the SN and DN gels just before breaking by tensile elongation and schematic representations of polymer network structures of the SN and DN gels before and after redox reactions.*[62]

Recently, design and synthesis of multi- responsive hydrogels with satisfying responsiveness get the research interest due to their great importance in practical applications and being closer to the complex responsive behavior found in nature. Among the rare dual redox/temperature responsive hydrogel, the work of Vancso et al. can be cited here, they chose to introduce an poly(ferrocenylsilane) based poly(ionic liquid) which is composed of alternating ferrocene and silane units in the vinylimidazolium group into PNIPAM hydrogel and synthesized dual-responsive hydrogels which can be reversibly oxidized and reduced by chemical and electrochemical means.[63] Yan et al. prepared a dual-responsive poly(ionic liquid) electrolyte by copolymerization of NIPAM, diallyl- viologen and ionic liquid. The LCST values of the electrolytes can be adjusted by changing the molar ratio of NIPAM/ionic liquid.[64]

The area of redox responsive networks is expected to continue its expansion, due to their versatile applications.

1.1.5 Important Properties of hydrogels

A hydrogel is a composite made of a solid (polymer) and a liquid (water). The final properties of a hydrogel are affected by the polymer-to-water ratio. In the following, some of the important hydrogel properties are discussed.

Mechanical tests are important to gather information about the hydrogel network and the possible range of application. The mechanical behavior of hydrogels relies on the theories of rubber elasticity and viscoelasticity. Those theories are based on time-independent recovery of the chain orientation and time-dependent recovery of the structure. Those theories are used to describe the mechanical behavior, to analyze the polymer structure and to determine the effective molecular weight between cross-links as well as getting information about the number of elastically active chains.

Different variables and causes affect the mechanical properties of hydrogels: the used monomers, the polymerization conditions, the cross-link density, the degree of swelling, and the medium in which the material is swollen. For example, by increasing the crosslinking degree a high stiffness gel is obtained, in contrast with a low crosslinking degree material. Hence, different analysis should be performed according to the material, the conditions and the aim of the study.

1.1.5.1 Swelling properties

The most important property of hydrogels is their ability to swell, when put in contact with water without allowing dissolution to occur. A low- or a high-swelling hydrogel is characterized by a high- or low-polymer/water ratio, respectively. Hydrogels, with superior stability in their swollen state (e.g. hydrogels for contact lenses), require a high solid content; while a low-solid-content hydrogel (e.g. superabsorbent in baby diapers) is desirable when superior swelling capacity is a major

requirement. The solid/liquid content of hydrogels is essentially determined by the cross-linker/monomer ratio used during the hydrogel's synthesis or post-synthesis.

Because water acts as a plasticizer in a hydrophilic polymer network system, the swelling process of hydrogels can be considered under rubbery state and the most widely used theory to explain the swelling for neutral hydrogels is the equilibrium swelling theory of Flory and Rehner[65,66] that takes into account the free energy of mixing ΔGmix from the polymer and solvent interaction and the elastic free energy ΔGelastic from the crosslinked network:[67]

$$\Delta G_{system} = \Delta G_{mix} + \Delta G_{elastic}$$

The first step of the swelling process is the contact of water with the hydrogel surface, then it will penetrate into the polymeric network. In this case, $\Delta G_{mix} \ll 0$, $\Delta G_{elastic} > 0$ and $\Delta G_{mix} + \Delta G_{elastic} < 0$. The meshes of the network in the rubbery phase will start expanding, so the swelling is favored and water diffuses into the network. Achilleos et al.[68] have developed a technique for the real-time visualization of dynamic deformation profiles during gel swelling processes. The system, which is based on caged photo-activated fluorophores covalently attached to the gel network, can provide quantitative information on transport fields such as polymer deformation and concentration. Based on this technique and other simulations,[69] it is obvious that swelling is not a continuous process. The influence of an osmotic driving force opposed by the cross-links owing to an elastic retractive force, balances the stretching of the network and prevents its deformation. During the swelling process, ΔGmix and ΔGelastic both increased until $|\Delta G_{mix}| = |\Delta G_{elastic}|$ and $\Delta G_{system} = \Delta G_{mix} + \Delta G_{elastic} = 0$. In this situation, no more driving force is acting for swelling and the equilibrium swelling is reached where the elasticity and osmotic forces are balanced.

When the total chemical potential is equal to zero, the change in chemical potential due to mixing is balanced by elastic retractive forces. The change in chemical potential due to elastic forces can be expressed by using the theory of rubber elasticity, while the contribution of mixing to chemical potential change is determined using the heat and the entropy of mixing.[70] With equaling these two contributions, the molecular weight between two cross-links (M_c) in the absence of a solvent can be expressed as:[71]

$$\frac{1}{\overline{M_C}} = \frac{2}{\overline{M_N}} - \frac{(\bar{v}/V_1)\left[\ln(1-v_{2,s})+v_{2,s}+x_1 v_{2,s}^2\right]}{v_{2,s}^{1/3}-(v_{2,s}/2)} \qquad (1)$$

Where M_N is the average molecular weight of the polymer chains prepared in the absence of cross-linker, υ and V_1 are the specific and the molar volume of water, respectively. $\upsilon_{2,s}$ is the polymer volume fraction in the fully swollen state, and χ_1 is the polymer–solvent interaction parameter.

The presence of water changes the chemical potential, so that a new term is required for the volume fraction density of the polymer chains. Thus, the above original Flory–Rehner model can be rewritten by incorporating $\upsilon_{2,r}$, a term describing the polymer fraction in the relaxed state according to the theory of Peppas and Merrill:[72,71]

$$\frac{1}{\overline{M_c}} = \frac{2}{\overline{M_N}} - \frac{\left(\frac{\bar{v}}{V_1}\right)\left[\ln(1-v_{2,s})+v_{2,s}+x_1\, v_{2,s}^2\right]}{v_{2,r}\left[\left(\frac{v_{2,s}}{v_{2,r}}\right)^{\frac{1}{3}}-\left(\frac{v_{2,s}}{2v_{2,r}}\right)\right]} \qquad (2)$$

When ionic groups are present in the network, the swelling equilibrium of the matrix becomes more complicated. New terms concerning the ionic strength, I and the dissociation constants, K_a, and K_b have to be added to Eq. (2). Equivalent expressions for anionic and cationic gels are formulated as shown in Eqs. (3) and (4), respectively.[73]

$$\frac{V_1}{4I}\left(\frac{V_{2,s}^2}{\bar{v}}\right)\left(\frac{K_a}{10^{-pH}-K_a}\right)^2 = \left[\ln\left(1-v_{2,s}\right)+v_{2,s}+x_1 v_{2,s}^2\right]+\left(\frac{V_1}{\bar{v}\overline{M_c}}\right)\left(1-\frac{2\overline{M_c}}{\overline{M_N}}\right)v_{2,r}\left[\left(\frac{v_{2,s}}{v_{2,r}}\right)^{1/3}-\left(\frac{v_{2,s}}{2v_{2,r}}\right)\right] \quad (3)$$

$$\frac{V_1}{4I}\left(\frac{V_{2,s}^2}{\bar{v}}\right)\left(\frac{K_b}{10^{pH-14}-K_a}\right)^2 = \left[\ln\left(1-v_{2,s}\right)+v_{2,s}+x_1\, v_{2,s}^2\right]+\left(\frac{V_1}{\bar{v}\overline{M_C}}\right)\left(1-\frac{2\overline{M_C}}{\overline{M_N}}\right)v_{2,r}\left[\left(\frac{v_{2,s}}{v_{2,r}}\right)^{1/3}-\left(\frac{v_{2,s}}{2v_{2,r}}\right)\right] \quad (4)$$

The mesh size is described by the correlation length (ξ) which is defined as the linear distance between two adjacent crosslinks. ξ can be described by the equation:[72]

$$\xi = v_{2,s}^{-1/3}\left(\bar{r}_o^2\right)^{1/2} = \alpha\left(\bar{r}_o^2\right)^{1/2} \quad (5)$$

where α is the elongation of the polymer chains in any direction, and $(r^2{}_0)^{1/2}$, the unperturbed end-to-end distance of the polymer chains between the cross-linking points.

Assuming an isotropic swelling, the end-to-end distance and the pore size of a swollen polymeric network (**Figure 1.9**) can be calculated using the equation:[72]

$$\xi = v_{2,s}^{-1/3}\left(\frac{2C_N\overline{M_C}}{\overline{M_r}}\right)^{1/2} l \quad (6)$$

where l is the length of the bonds along the backbone chain, and C_N, is the Flory characteristic ratio that represent the average correlation over all bonds and it is interesting to note that for all polymers $C_N > 1$ and as $N \rightarrow \infty$ C_N approaches a finite value $C\infty$ and M_r the molecular weight of the repeating units..

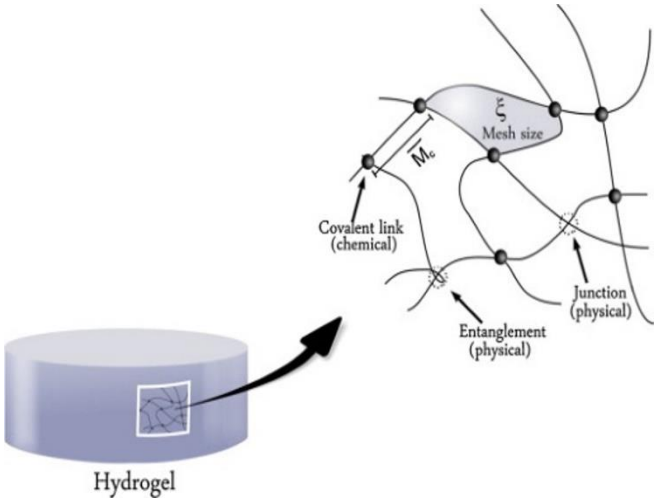

Figure 1.9 *A cross-linked hydrogel structure with the mesh size and the average molecular weight between the cross-linking points* M_C.[23]

Swelling is affected by numerous physicochemical conditions or structural factors.[74,75] The nature of the polymer and the cross-linking degree, are the important ones that determine the swelling ratio. For highly cross-linked hydrogels, smaller mesh size and less swelling are observed in comparison to slightly cross-linked ones.

The swelling kinetics depends on two phenomena of solvent penetration into the matrix.[76,77] The first one is the diffusion-controlled also known as Fickian type behavior. The diffusion of water molecules through the hydrogel matrix occurs much faster than the relaxation of the polymer chains, and the swelling is controlled by a concentration gradient. The second one is the relaxation-controlled situation where the swelling is controlled by the rate of polymer relaxation.

It becomes clear that the composition of the surrounding medium can influence some characteristics of the gel network such as the cross-linking density or chemical nature of the polymer backbone that will in turn macroscopically alter the swelling behavior. Such changes can

result from physiochemical stimuli such as changes in temperature, pH, etc. or from biochemical stimuli as described in 1.1.4.

Finally, the so-called “degree of swelling” or “water uptake” is often used to characterize hydrogels and can be defined as the weight ratio between the difference in hydrogel weight in both dry and swollen state over the weight of the dry gel:[1]

$$Water\ uptake = \frac{swollen\ weight - dry\ weight}{dry\ weight} \times 100$$

1.1.5.2 Rheological properties and concepts

Rheology is a branch of physics that studies the deformation and flow behavior of liquid and liquid-like material (oil, blood, ketchup, polymer solution and melts) and describes the interrelation between force, deformation and time. The term originates from the Greek word “rhei” meaning “to flow”. But it also includes the study of elastic materials that do not flow, such as solid-like materials. Rheometry is the measuring technology used to determine flow properties and viscoelastic properties of a material: fluids flow at different speeds and solids can be deformed to a certain extent. Depending on the physical behavior of materials such as oil, honey, hand cream, sweet jelly, plastic materials, wood, and metals; they can be defined as liquids, solids, and, in between, highly viscous, semi-solid substances. The fundamental principles and the basics of rheology are briefly presented in the following.

Rheometers can be used for shear tests and torsional tests to determine many rheological parameters, in contrast to viscometers that can measure only the viscosity of a sample. They operate with continuous rotation (one direction of motion) and rotational oscillation (**Figure 1.10**).

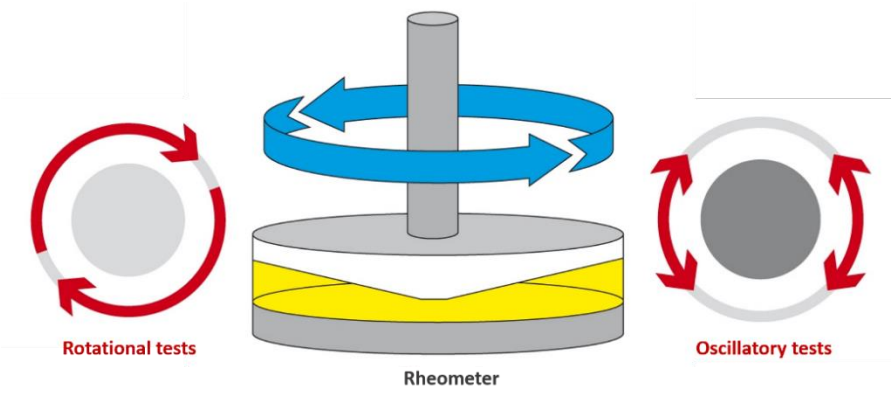

Figure 1.10 *Measuring principle of a typical rheometer for rotational tests with continuous rotation (left) or rotational oscillation (right)*[78]

For example, when the test of viscosity is made in a beaker with a spindle, the measurement will be relative to the beaker size, spindle size and filled volume. (**Figure 1.11, a**) Hence, the sample shape cannot be defined so the measurements are empirical.

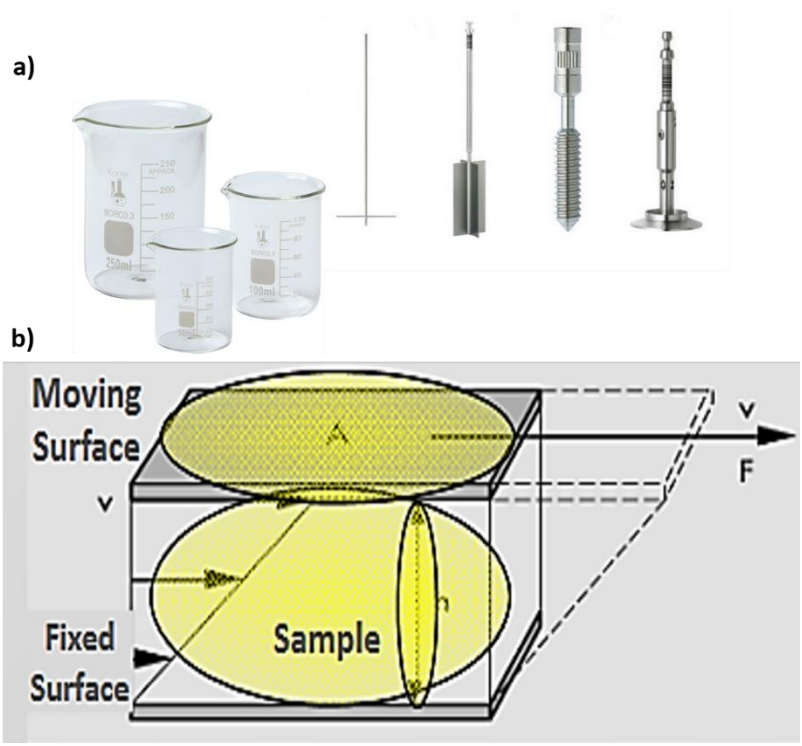

Figure 1.11 *a) Spindle for viscosity test b) Calculation of shear stress and shear rate using the two-plates model with shear area A, gap width h, shear force F, and velocity v* [78]

For absolute measurements, the system requires a defined flow field or sample shape by using the two-plate model (sample is sheared between a fixed and moving surface), a relatively narrow shear gap (h) and a known sample area (shear field, A) (**Figure 1.11, b**) that will be defined by specific standards for measuring systems. These standards describe the following measuring geometries (**Figure 1.12**): cone-plate, concentric cylinders and plate-plate.

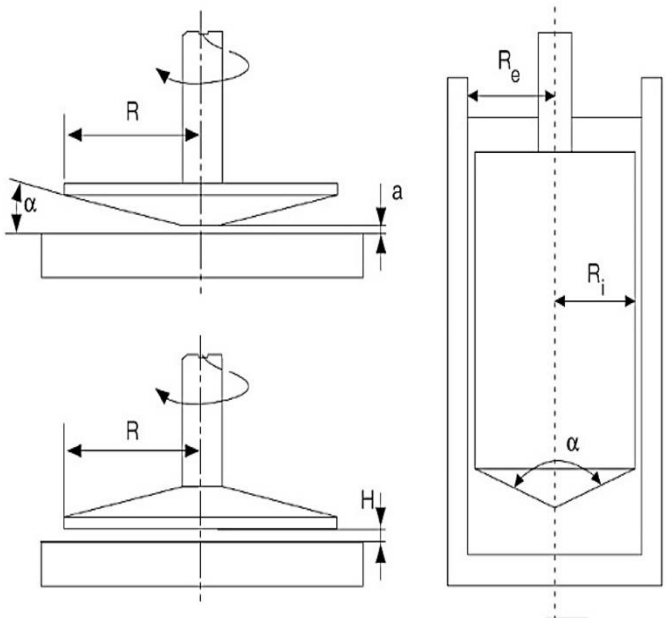

Figure 1.12 *Measuring systems: cone-plate (with radius R, cone angle α, truncation a); plate-plate (with radius R, distance between plates H); and concentric cylinders (with bob radius R_i and cup radius R_e and internal angle α at the tip of the bob)* [78]

The elasticity or viscosity of a system can be determined by quantification of the forces and deformations. An applied force will induce different magnitudes of deformation depending on the size of the material. In order to determine material properties independently to the size and shape of the system, two key rheological concepts are used: stress and strain.

Stress is defined as the amount of force applied to a given area of the sample and has the SI unit of Pa (N/m2). Strain is defined as the amount of deformation in a given material and is often given in terms of percent. In a simple shear deformation, the symbols σ or τ are often used for stress and γ for the strain. The shear stress is defined as $\sigma = F/A$ where F is the shear force (in N) and A is the shear area A (in m^2).

The shear strain is defined as $\gamma = s / h$ where s is the deflection path s (in m) and h is the shear gap (in m).

i. Viscosity

The viscosity modulus is the quantity that tells you how fast the material will flow under a specific constraint and time. The law of viscosity is defined as: $\eta = \tau / \dot{\gamma}$ where τ is the shear stress (in Pa) and $\dot{\gamma}$ is the shear rate (in s^{-1}). These three parameters, namely shear stress, shear rate, and viscosity, can only be precisely measured in uniform flow conditions. To measure the viscosity behavior a yield point is defined that represents the lowest shear-stress value above which a material will behave like a fluid, and below which the material will act like a – sometimes very soft – solid. In another word, this yield is the minimum force that must be surpassed in order to break down a sample structure at rest, and thus make it flow.

ii. Elasticity

The elastic modulus is the quantity that allows you to predict how much a material will deform elastically when you apply a certain amount of stress. An ideal elastic system follows Hooke's law, which states that the force is proportional to the deformation, or in terms of stress and strain: $\sigma = G^*\gamma$ where G is the elastic shear modulus (rigidity of the system) and γ as defined earlier. The higher the G value, the stiffer the material. The law of elasticity can be compared with the law of springs: $F / s = C$, where F is the force acting on the spring, s is the deflection path and C is the spring constant, which describes the stiffness of a spring.

iii. Viscoelasticity

Many materials show a viscous (liquid) and elastic (solid) mixed behavior when sheared and are called viscoelastic materials (**Figure 1.13**). Gels like all polymer systems show viscoelastic behavior.

Different rheological techniques can be used to test the viscoelastic behavior of materials, including creep testing, stress relaxation and oscillatory testing. The oscillatory shear rheometry is the most effective way to measure viscoelasticity on a rotational rheometer. This will be discussed in the following.

Figure 1.13 *From left to right: water as an ideally viscous liquid, hair shampoo as an example of a viscoelastic liquid, followed by a viscoelastic solid, such as hand cream, and the Eiffel Tower as an example of an ideally elastic solid made of metal.*[78]

Oscillatory testing involves oscillating the sample between two plates, with the upper plate moving and the lower plate remaining stationary at a given stress or strain amplitude and frequency. The oscillations are applied in a sinusoidal manner (sine curve). The oscillations are so small that the inherent structures in a sample are measured without perturbation or destruction. The force required to keep the lower plate in position is measured and the signal is rheologically evaluated as shear stress τ. The results are shown in a diagram over time as a sinusoidal curve of the shear stress and the shear strain, where four cases can be laid out: [79]

1) Ideal elastic material: no phase shift or loss factor tan (δ) between the preset and the response sine curve i.e. steel or stone (**Figure 1.14, left**).

2) Viscoelastic material: the sine curves of shear strain and shear stress show a phase shift (δ). It is always between 0° and 90° in this case (**Figure 1.14, right**).

3) Fluid sample: the phase shift is between $90° \geq \delta > 45°$. For ideally viscous flow behavior, it is equal to 90°.

4) Solid, gel-like material, δ is between 45° > δ ≥ 0°. i.e. hand creams, sweet jelly, and tire rubber.

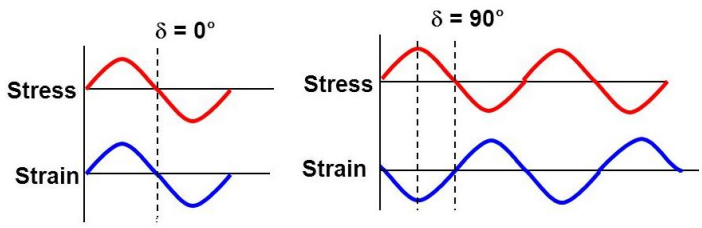

Figure 1.14 *Direct comparison of ideally elastic behavior (left) with no phase shift, and ideally viscous behavior (right) with 90° phase shift between the two curves.*

This phase difference, which describe the viscous and elastic components contribution in the total material stiffness or resistance to deformation, can be expressed as complex shear modulus (G*) and is defined as the ratio of the applied stress (or strain) to the measured strain (or stress): [78]

$$G^* = \sigma_{max}/\gamma_{max}$$

Moreover, the elastic portion of G* is called the storage modulus (G' in Pa) since it represents the storage of energy that acts like a driving force for reforming the structure into its original shape and thus describes the solid-state behavior of the sample. The viscous portion is called the loss modulus (G" in Pa) since it represents the energy loss which is no longer available for the further behavior of the sample material and thus describe the liquid-state behavior of the sample.

Due to the bonds inside the viscoelastic solids and gel-like material, for example chemical bonds or physical-chemical interactions, the elastic modulus is higher than the viscous modulus (G' > G") in this kind of sample (**Figure 1.12**). In contrast, the viscoelastic liquids, mainly composed of unlinked individual molecules, show a higher loss

modulus than storage modulus (**Figure 1.15**). During the analysis of results, the loss factor tan δ is plotted in addition to the curves of G' and G" and allows the easy spotting of a phase transition in the sample. This phase transition may correspond to the sol/gel transition point or simply the gel point where the behavior of the sample has changed during the measurement from the liquid or sol state to the solid or gel state and vice versa.

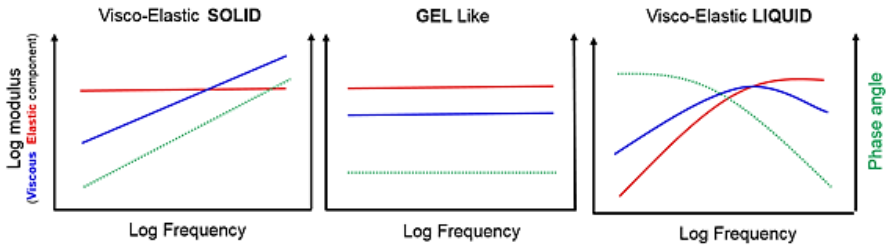

Figure 1.15 *Typical frequency response for a viscoelastic solid, viscoelastic liquid and a gel in oscillatory testing.*[80]

It is important when measuring the previously defined viscoelastic characteristics that measurements are made in the linear viscoelastic region (abbreviated: LVE region) where the test is carried out without destroying the structure of the sample (**Figure 1.16**). More frequently, the curve of G' as a function of applied strain is followed to determine the plateau-value where G’ is constant. And the linearity limit is first calculated in an amplitude sweep test that shows the strain as a percentage.

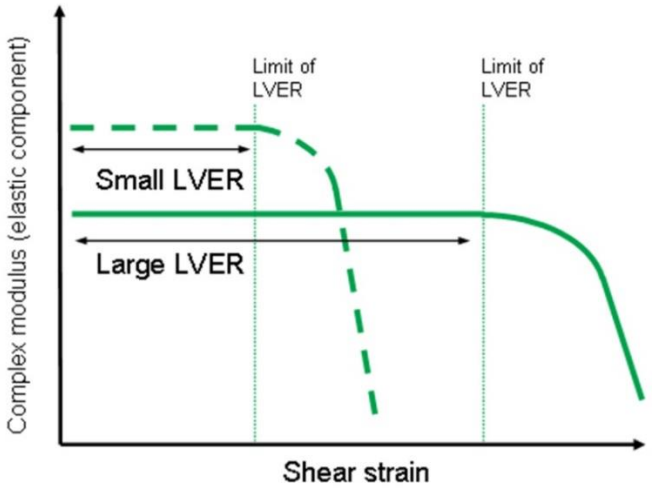

Figure 1.16 *Illustration showing the LVE for different materials as a function of applied strain.*[80]

Rotational rheometers operate in one of two operation modes: 'controlled shear stress, CSS or CS' or 'controlled shear rate, CSR or CR' which differ with the preset parameters. In the case of time-dependent flow behavior, shearing is kept constant and three intervaltimes will be followed: 1) with very low preset shear rate to simulate behavior at rest 2) with strong shear to simulate structural breakdown of the sample during processing 3) with very low shear to simulate structural regeneration at rest after application using the same preset low shear rate as in the first interval. But not all the materials present a structural regeneration aspect, it is more a gel formation or curing in a constant shear condition.

Moreover, temperature-dependent flow behavior can be also recorded with constant shearing and a preset time-dependent temperature profile. As a result, the melting or softening of samples can be followed when temperature is increased, or the crystallization, solidification or cold gelation when temperature is decreased

In terms of measurements, two main tests are performed for a sample:

1) Amplitude sweeps: To study the deformation behavior of samples in the non-destructive deformation range and to define the upper limit of this range. Usually, the deformation amplitude is increased beyond this limit to determine when the inner structure of the material gets softer, starts to flow, or breaks down in a brittle way. The measuring results are usually presented as a diagram with strain (or shear stress) plotted on the x-axis and storage modulus G' and loss modulus G" plotted on the y-axis, both axes being on a logarithmic scale.

2) Frequency sweeps: To study the time-dependent behavior of a sample in the non-destructive deformation range. High frequencies are used to simulate fast motion on short timescales, whereas low frequencies simulate slow motion on long timescales or at rest. In frequency sweeps, the amplitude is constant while the oscillation frequency is increased or decreased step-wise from one measuring point to the next. The results of frequency sweeps are usually presented in a diagram with the (angular) frequency plotted on the x-axis and storage modulus G' and loss modulus G" plotted on the y-axis, with both axes on a logarithmic scale. Frequencies can be stated in one of two ways: As frequency f in Hz or as angular frequency ω in rad/s or in s^{-1}.

Beyond that, there are many more rheological parameters that can affect rheological behavior. Special measuring instruments and equipments are also available but are out of the scope of this thesis.

1.1.5.3 Porosity and permeation

Pores in hydrogels can exist as smaller pores within the network or formed by phase separation during synthesis. The ‘tortuosity’ is a parameter that represent, the pore size distribution, the average pore size and the pore interconnections of the hydrogel matrix and is usually difficult to quantify.

The concentration of the chemical cross-links, the concentration of the physical entanglements and the net charge of polyelectrolytes can affect the pore-size distribution of hydrogels which is quantified using the composition of the hydrogel. The latter is expressed as a function of the concentrations of monomer (T%) and cross-linker (%C).[1]

While keeping in mind that the porous structure of ahydrogel is also affected by the properties of the solution medium, like dissolving ionic solutes (Donnan effects) or by dissolving uncharged solutes (osmotic effects). There are many techniques to investigate the porosity of hydrogels like Archimedes methods, mercury porosimetry (destructive assay) , gas adsorption, liquid extrusion porosity (including the permeability essay) and the X-ray microtomography (non-destructive high- resolution radiography).[1] But the limitation with these techniques is that they require a change in the pore solvent and/or temperature which causes the shrinking or swelling of the gel or requires mathematical manipulation and assumption, which may introduce unwanted artifacts. Moreover, all these techniques are commonly coupled with optical and electronic microscopies which are still expensive techniques both in terms of money and time for a qualitative and/or quantitative assay.

The control hydrogel porosity and microarchitecture remain very important for creating functional engineered tissues one of the most relevant example. Hydrogels have been used as scaffolds for tissue engineering applications because of their biocompatibility and similarities to native extracellular matrix. The porosity of these scaffolds materials plays an important role in directing tissue formation and function.[81] It is also necessary to allow homogeneous cell distribution and interconnection throughout engineered tissues. In addition, increase in the degree of porosity can have a beneficial effect on the mechanical properties, with the stiffness of the scaffold decreasing as porosity increases,[82] and the mechanical characteristics varying greatly with fluid flux caused by deformation.[83] New techniques in the future will certainly improve the ability to control the

porosity and microarchitecture of hydrogels and will drive the research closer to their goals.

1.1.5.4 Crosslinking

The crosslinking degree and type of crosslinks are governing the swelling, mechanical, rheological properties of hydrogels. Hydrogel networks can be obtained via two main ways.[84] The first one is the physical crosslinking using non-covalent and/or supramolecular interactions such as hydrophobic or ionic interactions between chains, hydrogen bonding between chains, etc. The second way is the chemical crosslinking that occurs via the formation of covalent bonds between chains. Many possibilities exist to create such covalent bonds such as Michaelis-Arbuzov reaction, Michael's reaction, nucleophile addition and so on.[85]

By controlling the degree of crosslinking, it is possible to achieve desirable material properties for many different applications. For example, a hydrogel with high degree of crosslinking presents a small mesh size letting the network absorb less solvent than the one with low degree of crosslinking with bigger mesh size. In this way, a wide range of applications starting from the same original polymer can be developped.[86,87]

1.1.6 Applications: From the lab to the market

Hydrogels from many synthetic and natural polymers have been produced with their end use being mainly in industrial fields and in pharmaceutical-biomedical fields (**Figure 1.17**).[88]

Both, natural to purely synthetic polymers, possess their own advantages and limitations. For example, naturally derived hydrogels are difficult to standardize and modify but generally present a goodperformance. Indeed, synthetic hydrogels are highly customizable, but the difficulty with this type is to obtain more complex mechanical properties and a controlled bioactivity. Consequently, the research is focused now onhydrogel systems that come out with more designed and controllable properties. A significant progress is recorded in this

context in the fields of polymer chemistry, synthetic chemistry, supramolecular chemistry, and complex hydrogel networks.

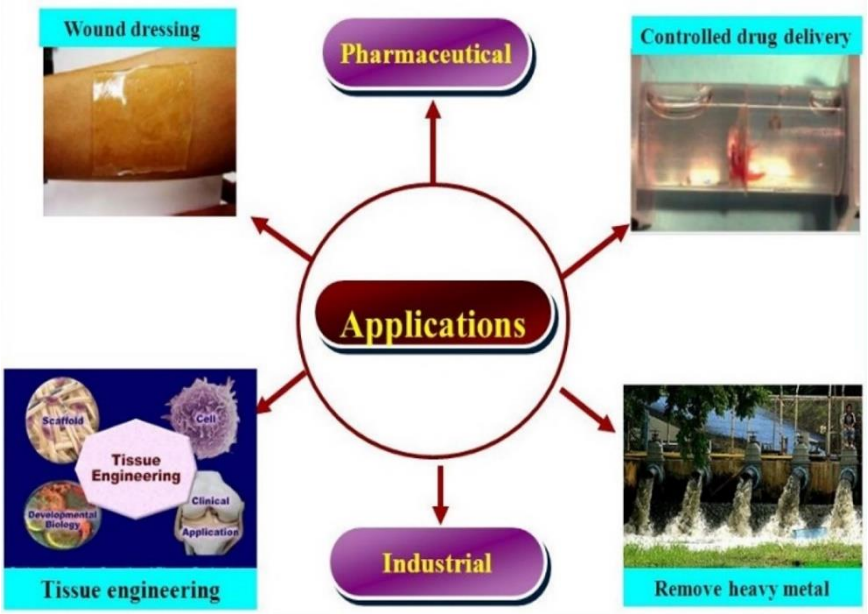

Figure 1.17 *Applications of hydrogels*

Due to their high-water absorption capacity and biocompatibility, hydrogels have been used for a variety of purposes ranging from contacts lenses (crosslinked pHEMA), diapers and wound dressing to transdermal patches, dental materials, implants, injectable polymeric systems, and other controlled drug delivery devices (PEG hydrogels). In **Table 1.2**, we summarize some of the hydrogel applications and the type of polymers used.

Applications	Polymers
Wound care	polyurethane, poly(ethylene glycol), poly(propylene glycol) poly(vinyl pyrrolidone),polyethylene glycol and agar [89]
Drug delivery, pharmaceutical	poly(vinyl pyrrolidone)[90], chitosan, poly(acrylic acid), acrylic acid, carboxymethyl cellulose
Dental Materials	Hydrocolloids [91] Hyaluronan
Tissue engineering, implants	Poly(vinylalcohol), poly(acrylic acid), hyaluronan, collagen [92]
Injectable polymeric system	Polyesters, polyphosphazenes, polypeptides, chitosan, hairpin-peptide [93]
Technical products (cosmetic, pharmaceutical)	Starch, gum Arabic, xanthan, pectin, carrageenan, gellan, guar gum, chitin , chitosan, poly (vinyl methyl ether), poly(N-isopropyl acryl amide) [94]
Others (agriculture, waste treatment, separation, etc.)	poly (vinyl methyl ether), poly(N-isopropyl acryl amide) [Xanthan, starch, poly(vinylalcohol) [95]

Table 1.2 *Applications of hydrogels and types of polymers used.*[88,96]

Stimuli-responsive hydrogels undergo significant physical or chemical changes in response to external variations. Well-designed devices with stimuli-responsive polymers can act like living organisms to "sense and react" and produce desirable responses without human intervention. In this context, this class of hydrogels presents a wide range of application such as:

1) Sensing and biosensing[97] *e.g.*, (poly(N-isopropylacrylamide)-co-methacrylic acid (pNIPAm-co-MAAc) hydrogel on a surface plasmon resonance (SPR) sensor surface with indium tin oxide microheaters embedded to allow for surface plasmon resonance signal tuning.
2) Controlled drug delivery[98] *e.g.*, (poly(N-isopropylacrylamide) temperature-sensitive hydrogels as drug delivery vehicles, the significant change between ambient temperature and physiological temperature has been targeted as a mechanism for the delivery of proteins and small molecules, such as ibuprofen and insulin.
3) Photosensitive hydrogels[72] *e.g.*, poly(hydroxyethylacrylate-co-2-nitrobenzyl acrylate (p(HEA-co-2-NBA)) for tissue culture.
4) Electrically-responsive hydrogels[99] *e.g.*, poly(2-(acrylamide)-2-methylpropanesulfonic acid) (PAMPS) gels for artificial muscles.
5) Shear stress responsive hydrogels[100] *e.g.*, the crosslinked hyaluronic acid (HA) hydrogels, Cyclodextrins-poly(ethylene oxide) (CDs-PEO) for injectable applications for drug delivery and tissue engineering scaffolds, arthritis treatment, biofilm disruption etc.

As detailed in the introduction part, the stimulus-responsive hydrogels are becoming increasingly attractive for a wide range of applications. The present thesis is dedicated to the synthesis and characterization of such “smart” hydrogels, which respond to redox and temperature changes and the study of their mechanical and electrochemical properties described in this introduction (e.g. rheology, swelling, redox activity).

1.2 Objective of the thesis

Recently considerable attention has been put on hydrogels. As a class of material, hydrogels are unique, they consist of a self-supporting, water- swollen three-dimensional (3D) viscoelastic network which permits the diffusion and attachment of molecules and cells. Over the years, the interest in stimuli responsive hydrogels (SRH) has grown exponentially. The properties of SRH may be valuable in different fields as we detailed in the section above. Today, hydrogels still fascinate material scientists and biomedical researchers due to their biocompatibility and the similarity of their physical properties to natural tissues and great strides have been made in terms of their formulations and applications.

The delivery of active molecules by rearrangement of hydrogels can involve the gel swelling/deswelling due to stimuli-induced changes in physico-chemical parameters of the network-forming polymer (a, **Figure 1.18**), the triggered attachment/release of functional compounds onto/from the interior gel network (b, **Figure 1.18**) or the gel dissolution/formation upon triggered degradation/formation of crosslinking points (c, **Figure 1.18**).

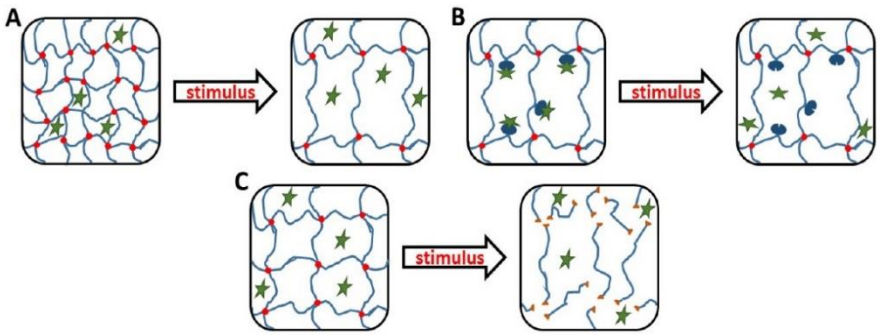

Figure 1.18 *Schematic representation of different mechanisms of stimuli-responsive hydrogels* [101]

Guest molecules delivery from hydrogels was studied by variation of temperature with gels based on poly(N-isopropyl amide) (PNIPAM)[102] or poly[oligo (ethylene glycol) methacrylate] (POEGMA)[103] where the increase of the temperature induces the collapse of the polymeric chains and the deswelling of the hydrogels. A similar approach was applied to pH sensitive gels based on poly(meth)acrylic acid (P(M)AA),[104] poly(ethylene imine) (PEI)[105] or poly(vinyl pyridine) (PVP).[106] Photo responsive gels may release via the three aforementioned mechanism depending on the localisation of the photosensitive moieties.[107] Hydrogels based on disulphide cross-linkers can be cited, where the stiffness of gels decrease leading to the release of their guest molecules when the disulphide bond are broken by a redox stimulus.[108] Another example of redox-responsive hydrogels involves ferrocene functions that can change the hydrophilic-hydrophobic balance of the hydrogel depending on the redox state of the ferrocene moieties.[52] Final examples of redox responsive polymer involve conducting polymers, such as polyaniline (PANI) or polypyrrole (PPy), where clusters of conductive polymers are entrapped into the hydrogels.[109,110] The electrochemical stimuli, induce change in the conductive polymers that become, in this case, hydrophilic and allow the encapsulated drugs to diffuse through the hydrogel. However, still the redox responsive hydrogels need to be more developed compared to other stimuli.

In this project, we aim at developing redox-responsive hydrogels valuable for different applications. We decided to produce SRHs that can release their guest molecules upon the trigger of redox stimuli that can be either redox reagents or electrochemical triggers. The advantages of the electrochemical stimulus versus other typical stimuli is that it can be controlled in time and most of the electrochemical processes do not require particular reagents limiting by products. Moreover, the trigger parameter, such as current intensity and reaction time, can easily bemodulated to adequately comply with the system.

To obtain a redox responsive hydrogel, we have decided to focus our attention on the 2,2,6,6-tetramethyl-1-piperidinyloxy (TEMPO) group. TEMPO is a stable nitroxide radical that can be easily oxidized into its oxoammonium counterpart or reduced into an aminoxyl function (**Figure 1.19**). TEMPO derivatives are largely used in chemistry, for the synthesis of organic molecules or polymers, and in the biomedical field as imaging enhancer (MRI) or radical scavenger of reactive oxygen species (and thus anticipated as new anti-oxidant therapies).[111] Moreover, the redox equilibrium of nitroxides, and especially TEMPO, was used in the recent years for the production of energy storage devices.[112,113] For the energy storage application, scientists developed a polymer bearing TEMPO moieties, poly(TEMPO methacrylate) or PTMA. Here, we propose to introduce this polymer into hydrogels in order to obtain redox responsive hydrogels.

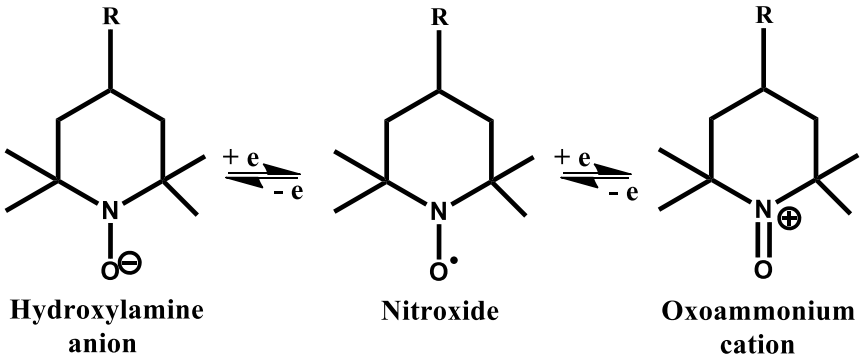

Figure 1.19 *Oxidation and reduction of TEMPO.*

Since TEMPO is hydrophobic, TEMPO methacrylate should be copolymerised with a hydrophilic monomer in order to obtain hydrogels. Therefore, we propose to synthesise chemically crosslinked hydrogels based on TEMPO and on oligo(ethylene glycol) methacrylate (OEGMA, hydrophilic unit) or N-isopropylacrylamide (NIPAM, hydrophilic units). The hydrogel formation will be realised in two steps: the first step consists in the synthesis of a precursor hydrogel by the conventional radical copolymerisation of 2,2,6,6-tetramethylpiperidin-4-yl methacrylate (TMPM), POEGMA or PNIPAM and the crosslinker agent. In the second step, PTMPM will be oxidised into TEMPO to obtain the desired redox responsive P(TEMPO-*r*-OEGMA) or P(TEMPO-*r*-NIPAM) hydrogels. Several hydrogels will be synthesised and the lattice parameters of the hydrogels will be varied by tuning the molar ratio of the crosslinker agent and of the TEMPO units (molar ratio between TEMPO/OEGMA or TEMPO/NIPAM) to obtain hydrogels with different characteristics.

Once the desired hydrogels will be obtained, we will study their swelling behaviour in aqueous media. Their redox properties will be studied in solution via a chemical and electrochemical oxidation of the TEMPO repeating units into $TEMPO^+$ units. Also, we will perform the mechanical characteristics (rheology) for all the investigated hydrogels. All these tests will allow us to determine the optimal conditions for the design of redox responsive hydrogels.

Those materials would allow a precise control of the delivery of guest molecules from the matrix with an electrical stimulus. To achieve this, we propose the encapsulation of guest molecules driven by electrostatic interactions, where the anionic guest molecules will be complexed to the oxidised $TEMPO^+$ function of the hydrogels. The reduction of the $TEMPO^+$ will induce the disappearance of the electrostatic interaction between the guest molecules and the hydrogel matrix and thus the diffusion of the guest molecules out of the hydrogel.

Finally, in order to broaden the scope of application of our system, we will also test our TEMPO-containing hydrogels as scaffolds for the oxidation of alcohol.

Bibliography

1 N. Chirani, L. H. Yahia, L. Gritsch, F. L. Motta and C. G. Natta, *J. Biomed. Sci.*, 2015, **4**, 1–23.

2 C. M. Kirschner and K. S. Anseth, *Acta Mater.*, 2013, **61**, 931–944.

3 Akibumi Danno, *J. Phys. Soc. Japan*, 1958, **13**, 722–727.

4 Q. Vinh, D. Phu, J. Hyung and D. Sung, *Eur. Polym. J.*, 2015, **72**, 602–619.

5 O. Whicterle and D. Lim, *Nature*, 1960, **185**, 117–118.

6 S. C. Lee, I. K. Kwon and K. Park, *Adv. Drug Deliv. Rev.*, 2013, **65**, 17–20.

7 J. Kopecek, *Biomacromolecules*, 2007, **28**, 5185–5192.

8 H. Kono and T. Teshirogi, *Int. J. Biol. Macromol.*, 2015, **72**, 299–308.

9 P. N.A., *CRC Press Inc.*, 1987, **21**, 184.

10 W. Y. Seow and C. A. E. Hauser, *Mater. Today*, 2014, **17**, 381–388.

11 K. Jindrich, *J. POLYM. SCI. PART A POLYM. CHEM*, 2009, **47**, 5929–5946.

12 S. J. Buwalda, K. W. M. Boere, P. J. Dijkstra, J. Feijen, T. Vermonden and W. E. Hennink, *J. Control. Release*, 2014, **190**, 254–273.

13 H. Mao, C. Wang, X. Chang, H. Cao, G. Shan, Y. Bao and P. Pan, *Mater. Chem. Front.*, 2018, **2**, 313–322.

14 F. Van De Manakker, M. Van Der Pot, T. Vermonden, C. F. Van Nostrum and W. E. Hennink, *Macromolecules*, 2008, **41**, 1766–1773.

15 Lim F. and Sun A.M., *Science (80-.).*, 1980, **210**, 908–910.

16 I. V Yannas, E. Lee, D. P. Orgill, E. M. Skrabut and G. F. Murphyt, *Proc. Natl. Acad. Sci. USA*, 1989, **86**, 933–937.

17 I. P. Harrison and F. Spada, *Pharmaceutics*, 2018, **10**, 2–13.

18 Y. Lu, W. Sun and Z. Gu, *J. Control. Release*, 2014, **194**, 1–19.

19 A. Kumar, K. A. Amarnath, K. Jawahar, N. Kumar and R. Farshi, *Asian J. Appl. Sci. Technol.*, 2018, **2**, 995–998.

20 M. Rizwan, R. Yahya, A. Hassan, M. Yar, A. D. Azzahari, V. Selvanathan and F. Sonsudin, *Polymers (Basel).*, 2017, **9**, 2–37.

21 T. Miyata, T. Uragami and K. Nakamae, *Adv. Drug Deliv. Rev.*, 2002, **54**, 79–98.

22 R. V Ulijn, N. Bibi, V. Jayawarna, P. D. Thornton, S. J. Todd, R. J. Mart, A. M. Smith and J. E. Gough, *Mater. Today*, 2007, **10**, 40–48.

23 F. Ullah, M. B. H. Othman, F. Javed, Z. Ahmad and H. M. Akil, *Mater. Sci. Eng. C*, 2015, **57**, 414–433.

24 A. Khan, M. Bisyrul and H. Othman, *J. Polym. Res.*, 2013, **20**, 1–8.

25 Y. Qiu and K. Park, *Adv. Drug Deliv. Rev.*, 2001, **53**, 321–339.

26 L. Pan, A. Chortos, G. Yu, Y. Wang, S. Isaacson, R. Allen, Y. Shi, R. Dauskardt and Z. Bao, *Nat. Commun.*, 2014, **5**, 1–8.

27 C. Alvarez-lorenzo, L. Bromberg and A. Concheiro, *Photochem. Photobiol.*, 2009, **85**, 848–860.

28 B. Jeong and A. Gutowska, *Trends Biotechnol.*, 2002, **20**, 305–311.

29 M. Namdeo, S. K. Bajpai and S. Kakkar, *J. Biomater. Sci.*, 2009, **20**, 1747–1761.

30 N. Huebsch, C. J. Kearney, X. Zhao, J. Kim, C. A. Cezar and Z. Suo, *Proc. Natl. Acad. Sci. USA*, 2014, **111**, 9762–9767.

31 A. Zardad, Y. E. Choonara, L. Claire, P. Kumar, M. Mabrouk, P. Pavan, D. Kondiah and V. Pillay, *Polymers (Basel).*, 2016, **8**, 359.

32 D. Schmaljohann, *Adv. Drug Deliv. Rev.*, 2006, **58**, 1655–1670.

33 D. S. Seeli and M. Prabaharan, *Int. J. Biol. Macromol.*, 2016, **84**, 10–15.

34 H. Hezaveh and I. I. Muhamad, *Chem. Eng. Res. Des.*, 2012, **91**, 508–519.

35 N. Rasool, T. Yasin, J. Y. Y. Heng and Z. Akhter, *Polymer (Guildf).*, 2010, **51**, 1687–1693.

36 X. Li, R. Xie, F. Luo, Z. Jia, K. Shi, X. Ju and W. Wang, *J. Taiwan Inst. Chem. Eng.*, 2019, **94**, 135–142.

37 C. Xiong, K. Peng, X. Tang, Z. Ye, Y. Shi and H. Yang, *RSC Adv.*, 2017, **7**, 34669–34675.

38 Y. Dong, W. Wang, O. Veiseh, E. A. Appel, K. Xue, M. J. Webber, B. C. Tang, X. Yang, G. C. Weir, R. Langer and D. G. Anderson, *Langmuir*, 2016, **32**, 8743–8747.

39 J. Yu, H. Fan and J. Chen, *Soft Matter*, 2011, **7**, 7386–7394.

40 I. Kim and I. Oh, *Arch. Pharm. Res.*, 2005, **28**, 983–987.

41 Y. Murakami and M. Maeda, *Biomacromolecules*, 2005, **6**, 2927–2929.

42 A. S. Hoffman, *Adv. Drug Deliv. Rev.*, 2013, **65**, 10–16.

43 J. Brassinne, F. Zhuge, C. Fustin and J. Gohy, *Gels*, 2015, **1**, 235–255.

44 L. Zha and F. Alexis, *Soft Matter*, 2011, **7**, 5908–5916.

45 K. Madhusudana Rao, B. Mallikarjuna, K. S. V. Krishna Rao, S. Siraj, K. Chowdoji Rao and M. C. S. Subha, *Colloids Surfaces B Biointerfaces*, 2013, **102**, 891–897.

46 W. Cheng and Y. Liu, *Redox-responsive hydrogels*, Elsevier Ltd, 2017.

47 E. H. Sarsour, M. G. Kumar, L. Chaudhuri, A. L. Kalen and P. C. Goswami, *Antioxidants Redox Signal.*, 2009, **11**, 2985–3011.

48 I. Tomatsu, A. Hashidzume and A. Harada, *Macromol. Rapid Commun.*, 2006, **27**, 238–241.

49 A. Harada, Y. Takashima and M. Nakahata, *Acc. Chem. Res.*, 2014, **47**, 2128–2140.

50 K. Miyamae, M. Nakahata, Y. Takashima and A. Harada, *Angew. Chemie - Int. Ed.*, 2015, **54**, 8984–8987.

51 M. Nakahata, Y. Takashima, H. Yamaguchi and A. Harada, *Nat. Commun.*, 2011, **2**, 511–516.

52 J. Wu, L. Wang, H. Yu, Zain-ul-Abdin, R. U. Khan and M. Haroon, *J. Organomet. Chem.*, 2017, **828**, 38–51.

53 X. Sui, X. Feng, M. A. Hempenius and G. J. Vancso, *J. Mater. Chem. B*, 2013, **1**, 1658–1672.

54 S. Y. Kao, H. C. Lu, C. W. Kung, H. W. Chen, T. H. Chang and K. C. Ho, *ACS Appl. Mater. Interfaces*, 2016, **8**, 4175–4184.

55 H. J. Li and K. Haraguchi, *Polym. Prepr. Japan*, 2006, **55**, 1077.

56 K. Mayumi, M. Tezuka, A. Bando and K. Ito, *Soft Matter*, 2012, **8**, 8179–8183.

57 M. Kurakazu, T. Katashima, M. Chijiishi, K. Nishi, Y. Akagi, T. Matsunaga, M. Shibayama, U. Il Chung and T. Sakai, *Macromolecules*, 2010, **43**, 3935–3940.

58 W. Yang, H. Furukawa and J. P. Gong, *Adv. Mater.*, 2008, **20**, 4499–4503.

59 Q. Hu, G. Tang and P. K. Chu, .

60 A. Mirzoian and A. E. Kaifer, *Chem. - A Eur. J.*, 1997, **3**, 1052–1058.

61 W. Sun, B. Xue, Y. Li, M. Qin, J. Wu, K. Lu, J. Wu, Y. Cao, Q. Jiang and W. Wang, *Adv. Funct. Mater.*, 2016, **26**, 9044–9052.

62 S. Tamesue, S. Noguchi, Y. Kimura and T. Endo, *ACS Appl. Mater. Interfaces*, 2018, **10**, 27381–27390.

63 X. Feng, K. Zhang, P. Chen, X. Sui, M. A. Hempenius, B. Liedberg and G. J. Vancso, *Macromol. Rapid Commun.*, 2016, **37**, 1939–1944.

64 F. Chen, Y. Ren, J. Guo and F. Yan, *Chem. Commun.*, 2017, **53**, 1595–1598.

65 P. J. Flory and J. Rehner, *J. Chem. Phys.*, 1943, **11**, 521.

66 P. J. Flory, *J. Chem. Phys.*, 1950, **18**, 6–10.

67 Q. Chai, Y. Jiao and X. Yu, *Gels*, 2017, **3**, 6.

68 E. C. Achilleos, R. K. Prud, K. N. Christodoulou, K. R. Gee and I. G. Kevrekidis, *Chem. Eng. Sci.*, 2000, **55**, 3335–3340.

69 H. N. Masazumi KOJIMA, Shuichi ANDO, Katsuo KATAOKA, Toyohiko HIROTA, Kazuharu AOYAGI, *Chem. Pharm. Bull.*

70 F. Edwards, *Br. Polym. J.*, 1977, **9**, 140–3.

71 N. A. Peppas and E. W. Merrill, *J. Appl. Polym. Sci.*, 1977, **21**, 1763–1770.

72 M. C. Koetting, J. T. Peters, S. D. Steichen, A. Nicholas, U. States, U. States, U. States and U. States, *Mater. Sci. Eng. R Reports*, 2015, **93**, 1–49.

73 E. M. White, J. Yatvin, J. B. Grubbs, J. A. Bilbrey and J. Locklin, *J. Polym. Sci. Part B Polym. Phys.*, 2013, **51**, 1084–1099.

74 J. M. G. Swann, W. Bras, P. D. Topham, J. R. Howse and A. J. Ryan, *Langmuir*, 2010, **26**, 10191–10197.

75 M. Gao, K. Gawel and B. T. Stokke, *Soft Matter*, 2011, **7**, 1741–6.

76 O. T. Kim SW, Bae YH, *Pharm. Res.*, 1992, **9**, 283–290.

77 N. A. Peppas and A. R. Khare, *Adv. Drug Deliv. Rev.*, 1993, **11**, 1–35.

78 Https://wiki.anton-paar.com/be-en/basics-of-rheology/, Basics of rheology.

79 P. A. Janmey, P. C. Georges and S. Hvidt, in *Methods in Cell Biology*, 2007, vol. 83.

80 M. Worldwide, https://cdn.technologynetworks.com/TN/Resources/PDF/WP160620BasicIntroRheology.pdf, https://cdn.technologynetworks.com/TN/Resources/PDF/WP160620BasicIntroRheology.pdf.

81 J. W. Nichol and A. Khademhosseini, *Soft Matter*, 2009, **5**, 1312–1319.

82 S. Gerecht, S. A. Townsend, H. Pressler, H. Zhu, C. L. E. Nijst, J. P. Bruggeman, J. W. Nichol and R. Langer, *Biomaterials*, 2007, **28**, 4826–4835.

83 N. Annabi, J. W. Nichol, X. Zhong, C. Ji, S. Koshy, A. Khademhosseini and F. Dehghani, *Tissue Eng. - Part B Rev.*, 2010, **16**, 371–383.

84 J. Maitra and V. K. Shukla, *Am. J. Polym. Sci.*, 2014, **4**, 25–31.

85 G. yed K. H., A.-A. Saphwan and Op. Glyn, in *Intech*, Progress in Molecular and Environmental Bioengineering. In: Carpi A. Analysis and Modeling to Technology Applications., 2011.

86 H. Sung, D. Huang, W. Chang, R. Huang and J. Hsu, *J. biomed Mater Res*, 1999, **46**, 520–530.

87 L. M. Weber, C. G. Lopez and K. S. Anseth, *J. biomed Mater Res*, 2009, **90**, 720–729.

88 S. K. Singh, A. Dhyani and D. Juyal, *pharma Innov. J.*, 2017, **6**, 25–32.

89 J. M. Rosiak and F. Yoshii, *Nucl. Instruments Methods Phys. Res. Sect. B Beam Interact. with Mater. Atoms*, 1999, **151**, 56–64.

90 M. Kumar, G. Bhatt and C. J. Duffy, *Int. J. Geogr. Inf. Sci.*, 2009, **23**, 1569–1596.

91 A. Devi, U. Nautiyal, S. Kaur and K. Komal, *Asian Pacific J. Heal. Sci.*, 2014, **1**, 92–105.

92 M. D. Fahmy, B. Shah, M. Razavi, H. Jazayeri, F. Fahimipour, J. White, R. Masri and L. Tayebi, *RSC Smart Mater.*, 208AD, **2017-Janua**, 77–87.

93 C. Yan, A. Altunbas, T. Yucel, R. P. Nagarkar, J. P. Schneider and D. J. Pochan, *Soft Matter*, 2010, **6**, 5143–5156.

94 S. Benamer, M. Mahlous, A. Boukrif, B. Mansouri and S. L. Youcef, *Nucl. Instruments Methods Phys. Res. Sect. B Beam Interact. with Mater. Atoms*, 2006, **248**, 284–290.

95 V. Van Tran, D. Park and Y. C. Lee, *Environ. Sci. Pollut. Res.*, 2018, **25**, 24569–24599.

96 Syed K. H. Gulrez, S. Al-Assaf and G. O. Phillips, in *Progress in Molecular and Environmental Bioengineering*, 2011, vol. 51, pp. 2–35.

97 I. Willner, *Acc. Chem. Res.*, 2017, **50**, 657–658.

98 R. Francis, D. K. Baby and D. S. Kumar, *J. Appl. Polym. Sci.*, 2012, **124**, 5079–5088.

99 M. Bassil, J. Davenas and M. EL Tahchi, *Sensors Actuators, B Chem.*, 2008, **134**, 496–501.

100 M. Guvendiren, H. D. Lu and J. A. Burdick, *Soft Matter*, 2012, **8**, 260–272.

101 K. L. Daniel Klinger, *Polymer (Guildf).*, 2012, **53**, 5209–5231.

102 A. A. Naddaf, I. Tsibranska and H. J. Bart, *Chem. Eng. Process. Process Intensif.*, 2010, **49**, 581–588.

103 M. M. Shoaib, V. Huynh, Y. Shad, R. Ahmed, A. H. Jesmer, G. Melacini and R. G. Wylie, *RSC Adv.*, 2019, **9**, 18978–18988.

104 S. S. Halacheva, T. J. Freemont and B. R. Saunders, *J. Mater. Chem. B*, 2013, **1**, 4065–4078.

105 C. Englert, L. Tauhardt, M. Hartlieb, K. Kempe, M. Gottschaldt and U. S. Schubert, *Biomacromolecules*, 2014, **15**, 1124–1131.

106 A. Arizaga, G. Ibarz and R. Piñol, *J. Colloid Interface Sci.*, 2010, **348**, 668–672.

107 C. Wang, G. Zhang, G. Liu, J. Hu and S. Liu, *J. Control. Release*, 2017, **259**, 149–159.

108 M. Ejaz, H. Yu, Y. Yan, D. A. Blake, R. S. Ayyala and S. M. Grayson, *Polymer (Guildf).*, 2011, **52**, 5262–5270.

109 G. H. Wang and L. M. Zhang, *Carbohydr. Polym.*, 2018, **202**, 523–529.

110 J. Hur, K. Im, S. W. Kim, J. Kim, D. Y. Chung, T. H. Kim, K. H. Jo, J. H. Hahn, Z. Bao, S. Hwang and N. Park, *ACS Nano*, 2014, **8**, 10066–10076.

111 Y. Zhu, Y. Matsumura, M. Velayutham, L. M. Foley, T. K. Hitchens and W. R. Wagner, *Biomaterials*, 2018, **177**, 98–112.

112 T. Janoschka, S. Morgenstern, H. Hiller, C. Friebe, K. Wolkersdörfer, B. Häupler, M. D. Hager and U. S. Schubert, *Polym. Chem.*, 2015, **6**, 7801–7811.

113 D. C. Bobela, B. K. Hughes, W. A. Braunecker, T. W. Kemper, R. E. Larsen and T. Gennett, *J. Phys. Chem. Lett.*, 2015, **6**, 1414–1419.

Chapter 2

Synthesis and characterisation of redox hydrogels based on stable nitroxide radicals

Table of contents

2.1 Introduction

Hydrogels have received considerable attention over the past 50 years due to their exceptional promise in a wide range of applications.[1] Hydrogels can be defined as polymer networks consisting of inter- and intra-molecularly connected polymer chains that possess the ability to absorb large amounts of water while maintaining their three-dimensional structure.[2] The stimuli-responsive hydrogels (SRHs), also called 'smart' hydrogels, represent a broad class of hydrogels being actively investigated, and some of them have been considered for practical use.[3-5] SRHs can be defined as hydrogels that are able to modify their equilibrium swelling in response to external stimuli such as pH,[6,7] temperature, [7,8] redox, [9,10] light, [11,12] and electrical field.[13]

A lot of work has been carried out on temperature-sensitive SRHs using poly(N-isopropylacrylamide) (PNIPAM) as thermo-responsive unit. Indeed, PNIPAM exhibits a lower critical solubility temperature (LCST) around 32 °C in aqueous medium and is therefore very useful for preparing smart materials for biological applications.[14-17] However, in recent years, scientists reported very interesting alternatives to PNIPAM. New families of polymers exhibiting either LCST or upper critical solubility (UCST) behaviors in water have been described in the literature. [18-21] Among them, thermo-responsive polymers containing short oligo(ethylene glycol) side-chains have gained rapid success in fundamental polymer science but also in applied materials research.[21] Early reports by Aoshima and co-workers [22] and Ishizone and co-workers [23] demonstrated that some of those polymers exhibit a LCST behavior in aqueous medium. It was afterwards shown that these stimuli-responsive properties can be finely adjusted via macromolecular design, and in particular using co-polymerization approaches.[24-26]

As far as redox responsive SRHs are concerned much less work has been performed. Hydrogels based on disulphide cross-linkers can be cited, where the gels dissolve and release their guest molecules when the disulphide bonds are broken.[27] Other systems involve ferrocene functions that can change the hydrophilic-hydrophobic balance of the gel depending on the redox state of the ferrocene moieties.[27,28] Other examples of redox responsive polymers involve conducting polymers, such as polyaniline (PANI) or polypyrrole (PPy), where clusters of conductive polymer are entrapped into the hydrogels. When submitted to an electrical current the conducting polymer becomes hydrophilic and allows the encapsulated drug to diffuse out of the hydrogel.[29,30]

Our strategy described in this chapter, is to design a redox responsive hydrogel that can encapsulate negatively charged hydrophilic molecules upon oxidation and release them upon reduction. To obtain this redox responsive hydrogel, we decided to focus our attention on the 2,2,6,6-tetramethyl-1-piperidinyloxy (TEMPO) group as redox-active component. TEMPO is a stable nitroxide radical that can be easily oxidised into its oxoammonium counterpart or reduced into an aminoxyl functions.[31] Nitroxide radicals, and especially TEMPO derivatives, are largely used in chemistry for the synthesis of organic molecules or polymers,[32] and in the biomedical field as imaging enhancer in electron spin resonance (ESR) techniques or as radical scavenger of reactive oxygen species (and thus anticipated as valuable candidates for anti-oxidant therapies).[33] Moreover, the redox equilibrium associated to nitroxide radicals, and especially TEMPO, has been used in the recent years for the production of energy storage devices.[34,35] For the energy storage application, scientists developed a polymer bearing TEMPO moieties, poly(TEMPO methacrylate) abbreviated as PTMA.[34] In the present work, we have introduced this polymer into a hydrogel in order to produce redox responsive SRHs.

A precursor of the hydrogel will be firstly synthetized by conventional radical polymerisation. This polymeric network will be obtained from a mixture of 2,2,6,6-tetramethylpiperidin-4-yl methacrylate (TMPM), oligo(ethylene glycol) methyl ether methacrylate with an average molar mass of 300 g/mol ($OEGMA_{300}$) and di(ethylene glycol) dimethacrylate ($OEGMA_2$) as cross-linker. In the second step, the secondary amine of TMPM units will be oxidised into TEMPO-methacrylate **(**TEMPO) to obtain the desired redox responsive hydrogel. The final step will be the oxidation of the nitroxide radical units of TEMPO into oxoammonium ones ($TEMPO^+$). In this case the encapsulation of the molecules would be driven by electrostatic interactions between the anionic molecules and the positively charged $TEMPO^+$ units of the hydrogels. The reduction of the $TEMPO^+$ into TEMPO will finally allow the disappearance of those electrostatic interactions and thus the diffusion of the guest molecules out of the hydrogel (**Figure 2.1**).

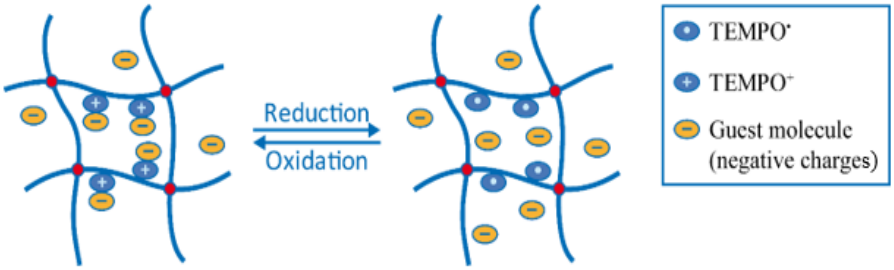

Figure 2.1 *Schematic representation of redox hydrogels for the encapsulation/release of negatively charged molecules.*

2.2 Synthesis

The investigated hydrogels were synthesized via a three-step methodology as detailed in the experimental section of this chapter, using conventional radical polymerization. (**Scheme 2.1**)

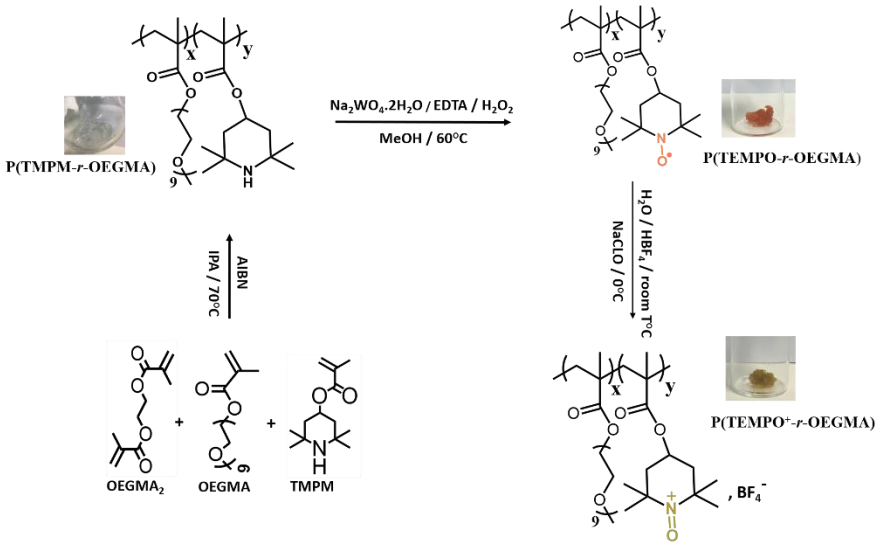

Scheme 2.1 *Synthesis of P(TEMPO$^+$-r-OEGMA) hydrogels*

A precursor poly(2,2,6,6 tetramethylpiperidin-4-yl methacrylate-random-oligoethylene glycol methacrylate) (P(TMPM-*r*-OEGMA)) hydrogel was firstly synthetized.

Regarding this step of the process, ^{1}H NMR spectra of the supernatant of the polymerization medium were systematically recorded in order to monitor the polymerization reaction leading to the P(TMPM-*r*-OEGMA) precursor hydrogel. As a typical example, the ^{1}H NMR spectrum of the supernatant of the polymerization medium for the P(TMPM-*r*-OEGMA) hydrogel prepared with X_{TEMPO} = 0.4 and X_{CL} = 0.03 is shown in **Figure 2.2** after overnight polymerization. This spectrum reveals no vinyl peaks (around 4.6 - 6.5 ppm) indicating a full consumption of the monomers according to the precision limit inherent to ^{1}H NMR spectroscopy.

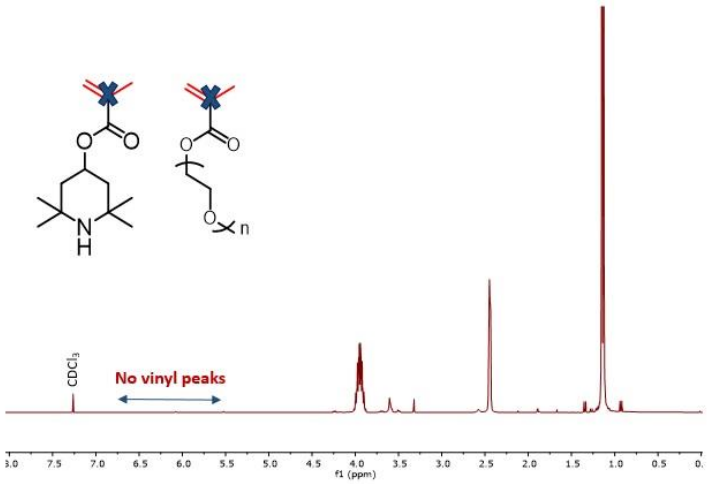

Figure 2.2 *Typical, ^{1}H-NMR spectrum of the supernatant of the polymerisation medium in deuterated chloroform for the investigated P(TMPM-r-OEGMA) hydrogels after overnight polymerization. (X_{TEMPO}=0.2; X_{CL}=0.03)*

In addition, the ^{1}H NMR spectrum of the P(TMPM-*r*-OEGMA) precursor network swollen in deuterated acetonitrile in the NMR tube (**Figure 2.3**) revealed a network composition corresponding to the comonomer feed and hence demonstrating the complete incorporation of the comonomers into the synthesized network. Same results were obtained for all the synthesized networks.

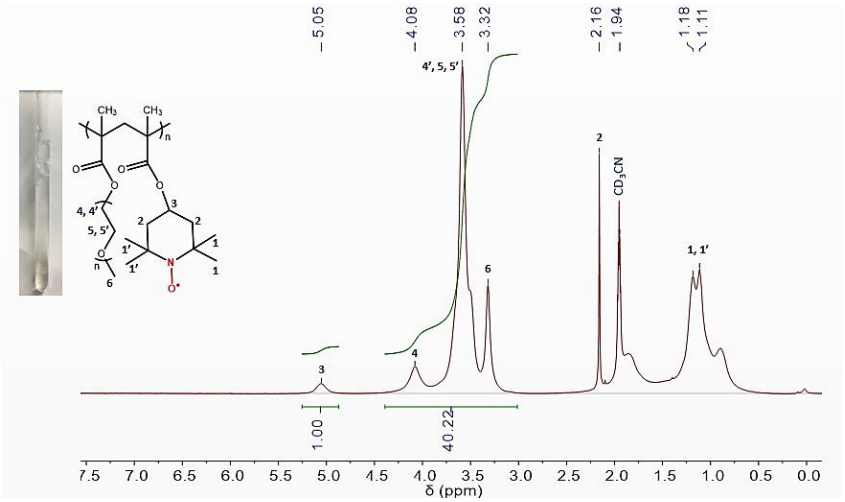

Figure 2.3 *Typical ^{1}H-NMR spectrum for all the non-oxidized P(TMPM-r-OEGMA) after overnight polymerization. (Gels are swelled directly in NMR tube in deuterated acetonitrile to reach equilibrium and homogenous aspect before analysis). (X_{TEMPO}=0.2; X_{CL}=0.03).*

In a second step, the secondary amine of TMPM units has been oxidized into a nitroxide radical to lead to TEMPO groups. An orange sticky poly(2,2,6,6-tetramethylpiperidinyloxy methacrylate-random-oligoethyleneglycol methacrylate) (P(TEMPO-*r*-OEGMA)) hydrogel was finally obtained.

TEMPO groups were finally chemically oxidized into oxoammonium counter anion to obtain the oxidized (P(TEMPO^{+}-*r*-OEGMA)) hydrogel.

As first view, FTIR spectra were recorded after oxidation to confirm the presence of TEMPO^{+} in our hydrogels. Indeed, the characteristic band of the N-O radical at 1540 cm^{-1} in the P(TEMPO-r-OEGMA) hydrogels was observed to shift at 1570 cm^{-1} (characteristic of the N=O bond) in the P(TEMPO^{+}-r-OEGMA) samples (**Figure 2.4**).

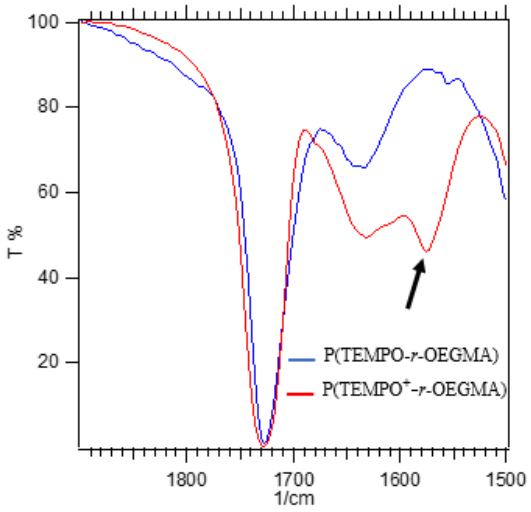

Figure 2.4 *Typical infrared (FTIR) spectra for all the oxidized P(TEMPO$^+$-r-OEGMA) (red curve) and all the radical form P(TEMPO-r-OEGMA) (blue curve) hydrogels. (X_{TEMPO}=0.4; X_{CL}=0.01)*

2.3 Electrochemical performances

2.3.1 Electron spin resonance

The oxidation of the P(TMPM-r-OEGMA) precursor into the P(TEMPO-r-OEGMA) hydrogel was macroscopically observed by the apparition of the orange color characteristic of the nitroxide radicals (**Scheme 2.1**). The oxidation yield of TEMPO radical units to oxoammonium ones was further determined by Electron spin resonance (ESR). This method indicates an oxidation yield of ca. 99% and confirms that a high level of oxidation has been reached for all the investigated hydrogels. As a typical example, **Figure 2.5** (red line) shows for the P(TEMPO-r-OEGMA) hydrogel with X_{TEMPO} = 0.4 and X_{CL} = 0.03 a spin density of around 1.15x10^{-3}mol/g with the typical signal shape for polymeric organic radicals that confirms the presence of TEMPO radicals in this hydrogel.

Finally, the P(TEMPO-r-OEGMA) hydrogels were converted into P(TEMPO$^+$-r-OEGMA) ones by the chemical oxidation of the nitroxide radicals into oxoammonium cations using NaClO. This reaction can be visually monitored by the change of color of the hydrogel from orange to yellow (**Scheme 2.1**). ESR was also used to monitor this reaction. As a typical example, a spin ratio of ca. 10^{-6} mol/g was measured for the P(TEMPO$^+$-r-OEGMA) hydrogel with X_{TEMPO} = 0.4 and XCL = 0.03 and no characteristic signal belonging to radical species was clearly visualized (**Figure 2.5**, green line). From the spin density measurement, we deduce that only ca. 0.1% of the TEMPO units are not oxidized into TEMPO$^+$, which practically means that the conversion of TEMPO units into TEMPO$^+$ ones is quantitative. Similar results have been obtained for all the investigated hydrogels.

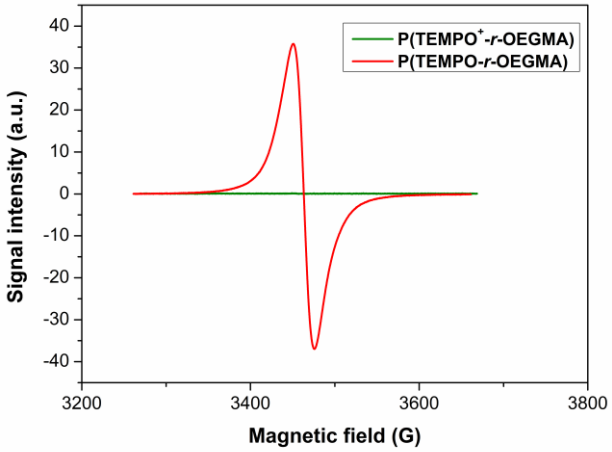

Figure 2.5 *Electron spin resonance spectra of the P(TEMPO-r-OEGMA) (red line) and P(TEMPO$^+$-r-OEGMA) (green line) hydrogels. (X_{TEMPO} = 0.4 and X_{CL} = 0.03)*

2.3.2 Cyclic Voltammetry

Beside chemical oxidation of the P(TEMPO-*r*-OEGMA) hydrogels into P(TEMPO$^+$-*r*-OEGMA) ones, the redox reactions occurring in those materials can also be electrochemically triggered. To this aim,

cyclic voltammetry measurements (CV) were performed to firstly confirm the presence of redox responsive TEMPO groups in our materials and secondly to study the reversibility of the redox reactions. Since performing the CV experiments directly with the hydrogels was not possible with our experimental set-up, we have used a methodology previously optimized for the investigation of TEMPO-containing polymer in Li-ion battery applications.[38]

Practically, this means that the CV experiments have been performed in the solid state with an electrode prepared by blending P(TEMPO-*r*-OEGMA) or P($TEMPO^+$-*r*-OEGMA) dried sample with conducting carbon black, in half-cell configuration against a metallic lithium counter electrode used as reference. **Figure 2.6** shows the reversible oxidation (blue line) of the nitroxide radicals into the oxoammonium cations for P(TEMPO-*r*-OEGMA) and the reversible reduction (red line) of the oxoammonium cations into nitroxide radicals for P($TEMPO^+$-*r*-OEGMA) both around 3.6V vs Li/Li^+ with well-defined peaks for the samples prepared with X_{TEMPO} = 0.3 and X_{CL} = 0.03. This confirms the presence of TEMPO groups in our hydrogels and the reversibility of the redox processes associated to these groups. Moreover, the CV was performed for 5 cycles for each electrode and same results was obtained confirming the stability of the nitroxide radical in our system. Similar results have been obtained for all the investigated samples evidencing their reversible redox responsive behavior.

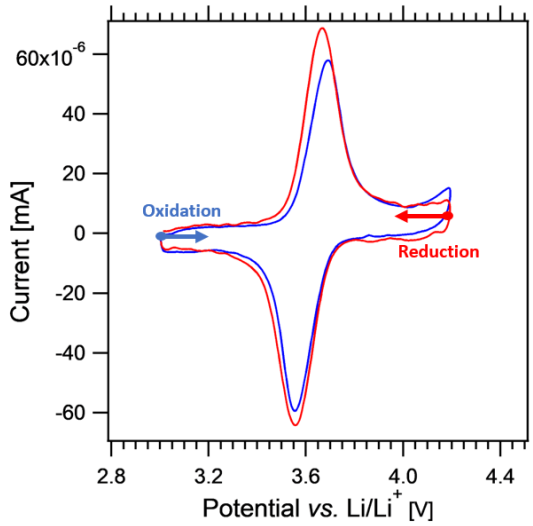

Figure 2.6 *Cyclic voltammetry of P(TEMPO-r-OEGMA) (in blue) and P(TEMPO$^+$-r-OEGMA) (in red) electrodes in half-cell configuration with lithium as counter electrode at 0.5 mV/s (1 cycle is depicted for each electrode).(X_{TEMPO} = 0.3 and X_{CL} = 0.03)*

2.4 Morphological analysis: Cryo-TEM microscopy

Cryogenic-transmission electron microscopy (Cryo-TEM) was further used to obtain details about the microstructure of these hydrogels. As shown in **Figure 2.7** for a X_{TEMPO} = 0.2 and X_{CL} = 0.03 system, the sample has been diluted 100X and the fibrils may correspond to deformed hydrogel pieces. However, the observation of a structure shows that there are insoluble parts (hydrophobic domains) in our hydrogels . that aggregate in some insoluble units into insoluble domains. Indeed, a similar microstructure was found by Zhai et al.[39] for hydrogels formed from β-cyclodextrin and an anionic surfactant containing a biphenyl group and in which the formation of hydrophobic nanodomains was also hypothesized. In our case, we believe that TEMPO units are at the origin of those hydrophobic domains. Indeed, TEMPO groups are basically hydrophobic and not water-soluble. The TEMPO groups randomly located in the P(TEMPO-*r*-OEGMA) network could then aggregate into hydrophobic domains making our

system a combination of a chemically crosslinked hydrogel (through the $OEGMA_2$ units) and a physically crosslinked hydrogel (through the TEMPO hydrophobic domains).

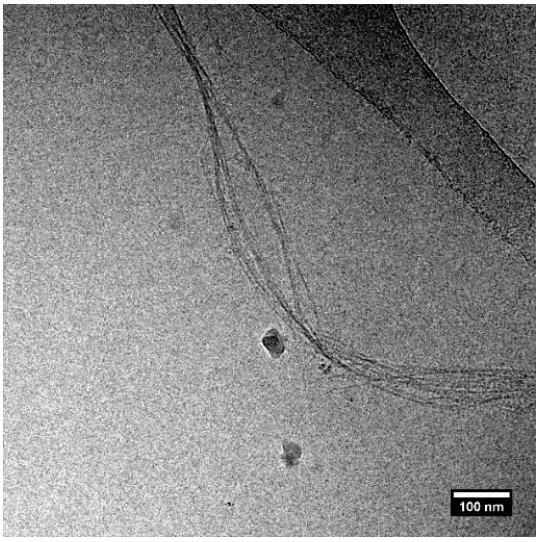

Figure 2.7 *Cryo-TEM image for a P(TEMPO-r-OEGMA) hydrogel (X_{TEMPO}= 0.2 and X_{CL}=0.03).*

2.5 Mechanical properties

2.5.1 Swelling Test

Swelling tests were then performed on all the P(TEMPO-*r*-OEGMA) hydrogels (**Table 2.1**). In Table 2.1, all the synthesized hydrogel are listed in accordance to the two parameters described: X_{TEMPO} and X_{CL}. A threshold in cross-linker seems to be needed to obtain a hydrogel. This threshold is equal to 0.03 for all the tested X_{TEMPO}.

The swelling factor SF, defined as

$$SF = (Ws - Wd)/Wd \qquad (1)$$

Where Ws is the weight of hydrogel in the swollen state at the equilibrium and Wd is the weight of the hydrogel in the dry state after elimination of extractable fraction, was measured as a function of X_{TEMPO} and X_{CL} (**Figure 2.8 and 2.9**).

X_{CL} \ X_{TEMPO}	0	0,1	0,2	0,3	0,4
0,014	Liquid 	Liquid 	Liquid 	Visco-elastic liquid 	Visco-elastic liquid 
0,02	liquid 	liquid 	liquid 	Visco-elastic liquid 	Visco-elastic liquid 
0,03	Gel 	Gel 	Gel 	Gel 	Gel 
0,04	Gel 	Gel 	Gel 	Gel 	Gel 
0,05	Gel 	Gel 	Gel 	Gel 	Gel 

Table 2.1 Library of different aspects obtained by free radical polymerization according to two parameters: X_{TEMPO} and X_{CL}.

The equilibrium state was determined by regularly weighting the hydrogel during the swelling process until it reached a constant weight. This was typically achieved after 24h (**Figure 2.8**). However, the hydrogels were further equilibrated to reach a total time of 48h before measurement, to be sure to be at the equilibrium.

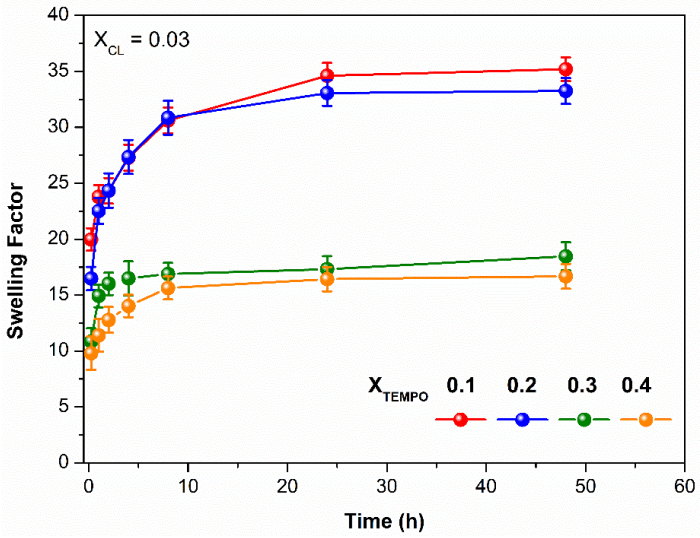

Figure 2.8 *Kinetic swelling study of P(TEMPO-r-OEGMA) hydrogels with varying $X_{TEMPO;}$ error bars represent average swelling ratio ± standard deviation where n = 3.*

The best results in terms of swelling factors and structure of the gels were obtained for X_{CL} = 0.03 (**Figure 2.9**). Lower X_{CL} eventually leads to viscous fluids instead of gels (**Table 2.1**) and lower swelling factors are observed for higher X_{CL} (**Figure 2.9**).

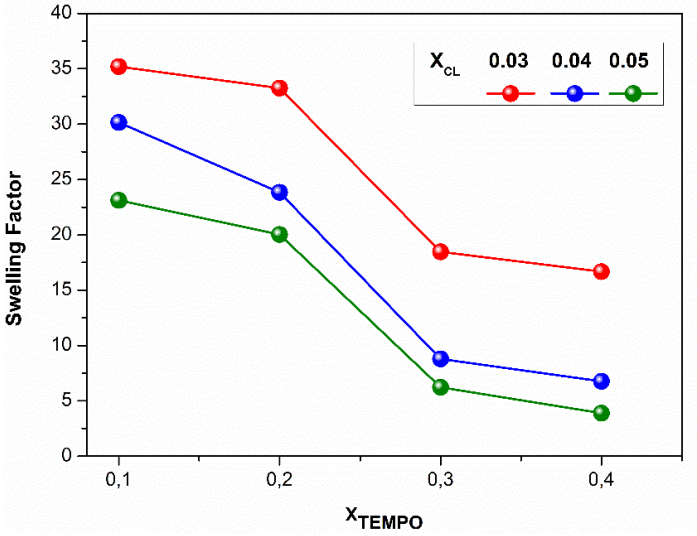

Figure 2.9 *The equilibrium swelling factor of the hydrogels for different cross-linker equivalent*

Those results can be easily understood by taking into account that a too low concentration in crosslinking units impedes the formation of a continuous network of polymer chains in the hydrogel while a high concentration of those groups reduces the mesh size and is detrimental to high swelling ratio. More discussion for the different aspects of hydrogels with the different molar ratio of cross-linker will be presented in chapter 3. In this respect, X_{CL} being equal to 0.03 seems to be the best compromise. Indeed, P(TEMPO-r-OEGMA) hydrogels with varying X_{TEMPO} ratio and X_{CL} fixed to 0.03 display swelling factors around 35 for X_{TEMPO} 0.1 and 0.2 (**Figure 2.8**), meaning that 0,025 g of dry sample absorb around 1 g of water. For X_{TEMPO} 0.3 and 0.4 the swelling factor decreases by nearly a factor two, which can be explained by the increase in hydrophobicity provided by the TEMPO units. In addition, the fraction of chains which are not trapped in the network has been experimentally determined by preparing the P(TEMPO-*r*-OEGMA) gels with X_{TEMPO} of 0.1, 0.2, 0.3 and 0.4 with an excess of D_2O compared to the previously determined swelling ratios at equilibrium (**Figure 2.8**). After equilibration for 48h, gels with a

supernatant sol fraction were obtained. The amount of free chains released by the network has been further determined by measuring the amount of chains extracted in the sol fraction using ^{1}H NMR with an internal standard. This amount is approximately the same in the four analyzed samples and is 10.6 +/- 0.5 wt%. The same experiment was performed for the reference P(OEGMA) gel with X_{TEMPO}=0 and an amount of 20.5 wt% was determined.

2.5.2 Rheology experiments

The viscoelastic properties of the P(TEMPO-*r*-OEGMA) hydrogels were also investigated by rotational rheometry. Again, only hydrogels with X_{CL} fixed to 0.03 were investigated. Their viscoelastic response was measured as a function of the oscillation frequency for the different X_{TEMPO} values. As shown in **Figure 2.10**, the storage modulus (G') is superior to the loss modulus (G") in the whole experimental frequency window, confirming the formation of a gel.

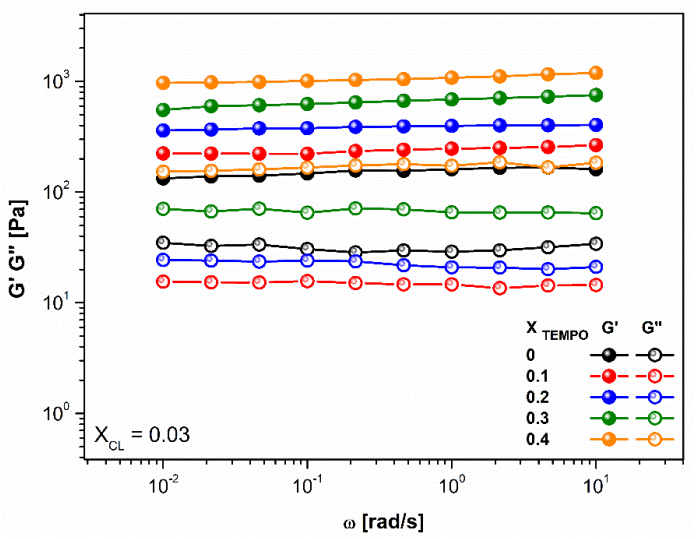

Figure 2.10 *Frequency sweep plots of storage and loss moduli versus frequency for P(TEMPO-r-OEGMA) hydrogels with different* X_{TEMPO}.

Nevertheless, without TEMPO, the level of the storage modulus of the hydrogel is very low (~150Pa), which suggests that the gel contains only few chemical crosslinks which effectively contribute to the polymer network. Based on the modulus, the average molar mass between two active crosslinks, M_{XX}, can be estimated based on the relationship:

$$G_N^0 = \frac{c\,\rho_{melt} RT}{M_{XX}}, \qquad (1)$$

with ρ_{melt} being the density of OEGMA in the melt state and c, the concentration of the network, which is equal to 1.6 wt% for all the gels analysed here. The parameter υtrapped, which represents the weight fraction of segments trapped between two active crosslinks, allows accounting for the fact that dangling ends do not participate to the network elasticity. If we consider that all segments contribute to the network (i.e. υtrapped=1) a value of 320 kg/mol is found for M_{XX}, which is most probably larger than the average molar mass in number of the chains, M_{chain}, if these ones are not crosslinked. Indeed, if we perform the polymerization with only TMPMP and OEGMA and without $OEGMA_2$ crosslinker, one can roughly estimate M_{chain} as equal to 180 kg/mol with a molar mass dispersity of 1.8 as measured by SEC. The fact that M_{XX} is found to be larger than M_{chain} suggests that a large fraction of the polymer is not trapped into the network and therefore, does not contribute to the sample elasticity. This is consistent with the observation that at slightly lower crosslinking density, $X_{CL}=0.02$, the sample shows a liquid behavior, the crosslink density being too low to lead to the formation of a network (**Table 2.1**).

In order to estimate the fraction of dangling ends, a statistical algorithm has been developed,[40] based on the assumptions proposed by Flory: *1)* All monomers have the same probability to be crosslinked, *2)* this probability does not depend on the position of the other crosslinks along the chain, *3)* Intramolecular crosslinks are not taken into account. Starting from the estimated molar mass distribution of the non-crosslinked chains and from the molar mass of an OEGMA unit, equal to 300 g/mol, large ensemble of chains is generated, along which

crosslinkers are included in a statistical way, with a certain probability p_X. The chains composition is then analyzed, which allows us to determine $\upsilon_{trapped}$ and M_{strand} and consequently, the elastic plateau modulus in function of p_X. It must be noted that same results could have been obtained analytically.[41,42] However, due to the sample dispersity and to the low level of crosslinks per chain, a statistical algorithm has been preferred.[40]

Figure 2.11 presents the values of p_X of the different samples, which have been determined such that the corresponding values of $\upsilon_{trapped}$ and M_{strand} lead to the right level of plateau modulus, through Eq. 1 (see insert in **Figure 2.11**). The observed diminution of the elastic modulus at low frequency could be attributed to an experimental error during the measurements as at these frequencies we have low sensitivity detection for the machine.

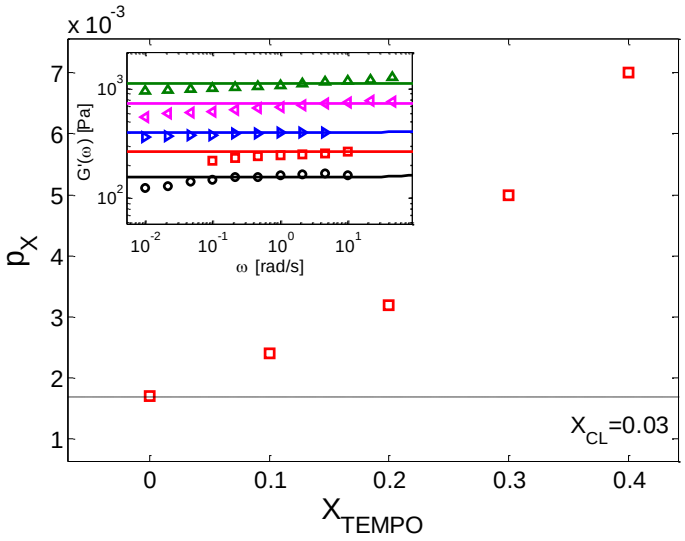

Figure 2.11 *Crosslinking probability p_X in function of X_{TEMPO}, determined such as the corresponding value of $\upsilon_{trapped}$ and M_{strand} lead to the right level of plateau modulus (see Insert: Experimental (symbols) versus theoretical (line) data, for X_{TEMPO} = 0 (o), 0.1 (□), 0.2 (>), 0.3 (<) and 0.4 (Δ)).*

The corresponding molar mass distributions of free chains, dangling ends and trapped segments are shown in **Figure 2.12**, in case of X_{TEMPO}=0, and compared to the distribution of the non-crosslinked sample (X_{CL}=0). It is found that within this sample, 22.7 wt% of the chains are linear (i.e. with no crosslink), 50 wt% of the chain segments are dangling ends and only $\upsilon_{trapped}$ = 27.3 wt% of the chain's segments are trapped between two crosslinks, i.e. only ¼ of the sample contributes to the elastic plateau. This value agrees with the fraction of P(OEGMA) chains experimentally extracted from the hydrogel (20.5 wt%). Furthermore, the average molar mass in number of a molecular segment between two crosslinks or chain extremities, M_{strand}, is 87 kg/mol. This molar mass is also in good agreement with the Mn found by SEC analysis of the fraction of non-entrapped chains in the gels (86 kg/mol and Đ of 1.8).

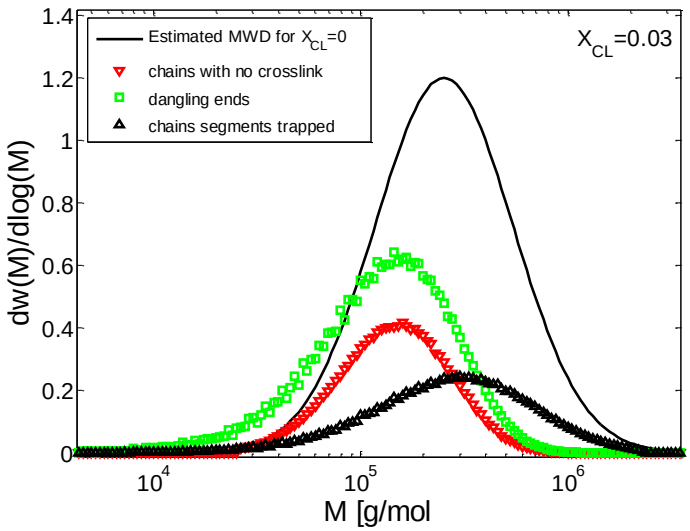

Figure 2.12 *The sample X_{CL}=0.03 and X_{TEMPO}=0 is divided into several contributions: The MWD distribution of the chains containing zero crosslink, of the dangling ends (excluding the chains with no crosslinks), and of the chain segments trapped between the first and the last crosslinks. For comparison, the MWD of the chains with no crosslink (X_{CL}=0, M_n = 180kg/mol, PDI=1.8) is also presented.*

By adding TEMPO units, the storage modulus G' increases (**Figure 2.10**). Since these units are insoluble in water, we hypothesize that TEMPO groups aggregate into hydrophobic domains that could be at the origin of the nanostructures observed by cryo-TEM (**Figure 2.7**). As suggested before, those hydrophobic domains could play the role of additional physical crosslinks to the chemical crosslinks provided by $OEGMA_2$ units, which explains the increase in elastic modulus of our hydrogels with increasing X_{TEMPO}.

The constant storage modulus observed in **Figure 2.10** for the samples containing TEMPO units means that the lifetime of the corresponding hydrophobic domains is long since their relaxation is not observed within the experimental frequency window. In order to investigate their reversible behaviour, strain sweeps have been performed from low to high strain amplitude and then, from high to low strain. Results are shown in **Figure 2.13** for X_{TEMPO} = 0.1 and 0.4. For both samples, a hysteresis is observed, which can be seen as a signature of the reversible bonds: while the network structure is partially broken at high strain in order to allow the sample to deform, the network is reformed when coming back to low strain amplitude.

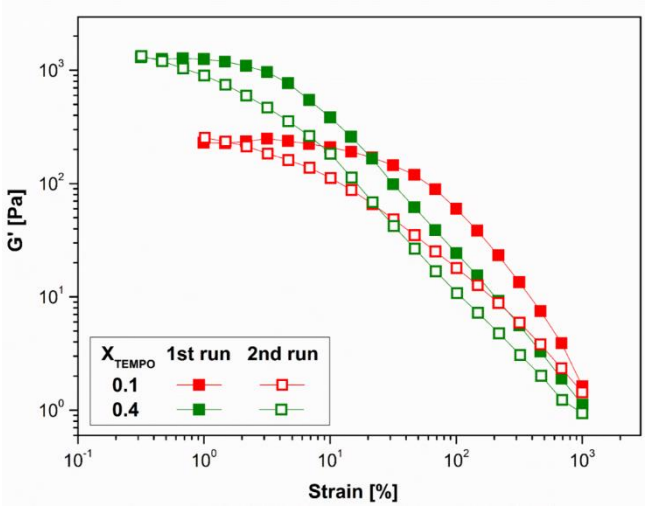

Figure 2.13 *Storage modulus of the P(TEMPO-r-OEGMA) hydrogels with X_{CL}=0.03 and X_{TEMPO}=0.1 (red) or 0.4 (green), from low to high (filled symbols) or high to low (empty symbols) amplitude of deformation.*

It is also observed that the hydrogels show a resistance *versus* strain till approximately 10% and 3% with X_{TEMPO}=0.1 and 0.4, respectively, before losing their elasticity. (**Figure 2.13**) The lower resistance found with X_{TEMPO}=0.4 is consistent with the fact that the network is denser and therefore, the physical crosslinks have to break at lower strain in order to allow the sample flowing.

Regarding the oxidized form $TEMPO^+$ containing hydrogels, a frequency sweep was performed that confirms gel formation. While comparing the rheological properties of the P(TEMPO-r-OEGMA) and P($TEMPO^+$-*r*-OEGMA) hydrogels (**Figure 2.14**), we observe that the charged gel displays higher moduli than the non-charged one. Although the hydrophobic TEMPO domains should disappear upon oxidation of their nitroxide radicals into soluble oxoammonium cations, we hypothesize that the resulting cationic units induce a stretching of the polymer chains due to polyelectrolyte behavior and a stiffening of the gel due to large charge densities leading to electrostatic repulsions. This showed that the elastic modulus of hydrogels varies depending on the presence or not of charged group in their structure. This is unexpected

because both the polymer concentration and the chemical crosslink density of the hydrogels subjected to mechanical measurements were the same. The results could be explained with the effect of the electrostatic interaction of charged groups on the elastic free energy increases the modulus. More detailed description for $TEMPO^+$ containing hydrogels will be presented in chapter 3.

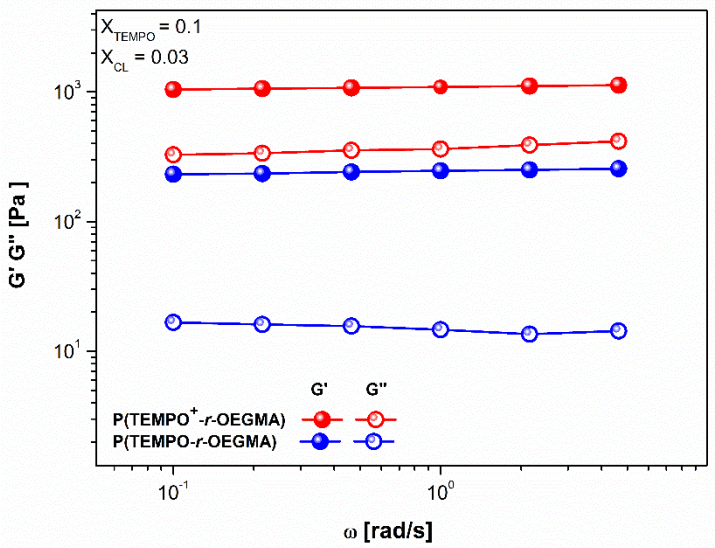

Figure 2.14 *Frequency sweep plots of storage and loss moduli versus frequency for P(TEMPO-r-OEGMA) and P(TEMPO$^+$-r-OEGMA) hydrogels with X_{TEMPO} = 0.1 and X_{CL} = 0.03.*

2.6 Encapsulation properties

In order to demonstrate the encapsulation abilities of our hydrogels, we have designed a proof-of-concept experiment taking opportunity of the presence of positively charged units in the oxidized P(TEMPO-*r*-OEGMA) hydrogels to encapsulate a negatively charged model molecule, namely eosin B. (**Figure 2.15**)

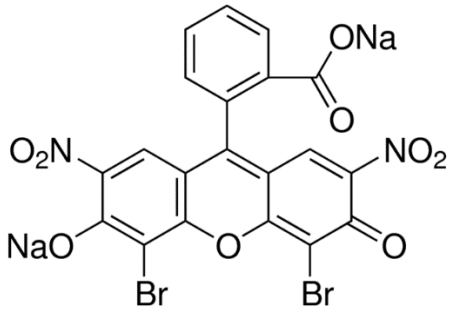

Figure 2.15 Chemical structure of eosin B molecule.

Eosin B was selected since it is a chromophore that can be easily visually followed by its pink-red color. In a first experiment we used water containing eosin B at a concentration of 5g/L to realize the equilibrium swelling of either the P(TEMPO-*r*-OEGMA) or the P($TEMPO^+$-*r*-OEGMA) hydrogels. As macroscopically observed in **Figure 2.16**, both P(TEMPO-*r*-OEGMA) and the P($TEMPO^+$-*r*-OEGMA) (both prepared from the network with X_{TEMPO} = 0.4 and X_{CL} = 0.03) do form hydrogels with encapsulated eosin B. However, the supernatant from the hydrogel prepared from the P($TEMPO^+$-*r*-OEGMA) (**Figure 2.16 (a)**) seems to be colorless while the one from the P(TEMPO-*r*-OEGMA) sample (**Figure 2.16 (b)**) still presents the same characteristic pink color as the one of the starting eosin B solution at t_0. This preliminary observation suggests that some specific interactions are existing between P($TEMPO^+$-*r*-OEGMA) and eosin B that could explain the sequestration of eosin B molecules into the hydrogel. In the case of the P(TEMPO-*r*-OEGMA) hydrogel, eosin B seems to be homogeneously dispersed in the hydrogel and in the supernatant.

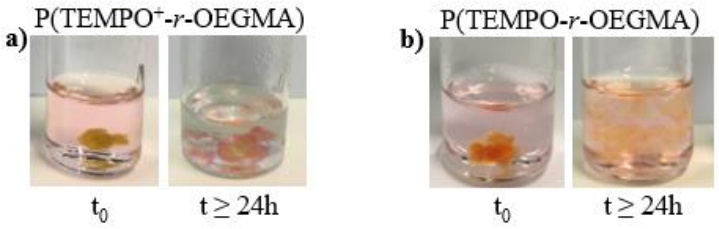

Figure 2.16 *Encapsulation of eosin B via two strategies a) electrostatic interaction (+/-) b) entrapping in the interior gel network by swelling phenomena (hydrogels prepared from the networks with* $X_{TEMPO} = 0.4$ *and* $X_{CL} = 0.03$*)*

This observation was confirmed by UV-Vis measurements realized on the supernatant after equilibration. As observed in **Figure 2.17**, the characteristic absorption peak of eosin B at 514 nm is still observed in the supernatant of the P(TEMPO-*r*-OEGMA) hydrogel while it totally disappeared in the supernatant of the P(TEMPO$^+$-*r*-OEGMA) sample. This observation points towards strong electrostatic interactions between the charged TEMPO$^+$ units and negatively charged eosin B molecules in the case of the P(TEMPO$^+$-*r*-OEGMA) hydrogel. In the experimental conditions used for this experiment with an initial concentration of $8.619*10^{-3}$ mol/L of eosin B in the aqueous solution used for the swelling process, the concentration of TEMPO$^+$ (0.0013 mol/g) units is sufficient to electrostatically complex the whole eosin B molecules. For the supernatant of the P(TEMPO-*r*-OEGMA) hydrogel the concentration in eosin B drops to $8{,}421*10^{-7}$ mol/L as determined from Beer-Lambert law. This means an excess of the eosin B molecules are sequestrated into the hydrogels (but not all as in the case of the P(TEMPO$^+$-*r*-OEGMA) hydrogel). Once again, this phenomenon could be explained by the formation of TEMPO hydrophobic domains inside the P(TEMPO-*r*-OEGMA) hydrogel as previously discussed to explain rheological data and cryo-TEM pictures. Some eosin B molecules could be encapsulated into those hydrophobic domains since eosin B also present hydrophobic aromatic groups beside its anionic groups. In order to release the eosin B molecules entrapped in the P(TEMPO$^+$-r-OEGMA) gels, we have tried to screen the electrostatic interactions between TEMPO$^+$ units and negatively charged eosin B. Our attempts

were however unsuccessful since addition of high amounts of salts resulted in a decreased solubility of OEGMA units because of salting-out effect on the one hand and on the other hand, as eosin B is double charged, this can lead to an additional reticulation inside the gel which explain why wasn't possible to release this molecule from the matrix of our hydrogel. The investigations in this direction will be presented in the next chapters of this thesis including a totally different design of the TEMPO-based hydrogels.

Thus, these preliminary experiments suggest that both P(TEMPO-*r*-OEGMA) and P(TEMPO$^+$-*r*-OEGMA) hydrogels could be useful for further encapsulation/release of molecules of interest.

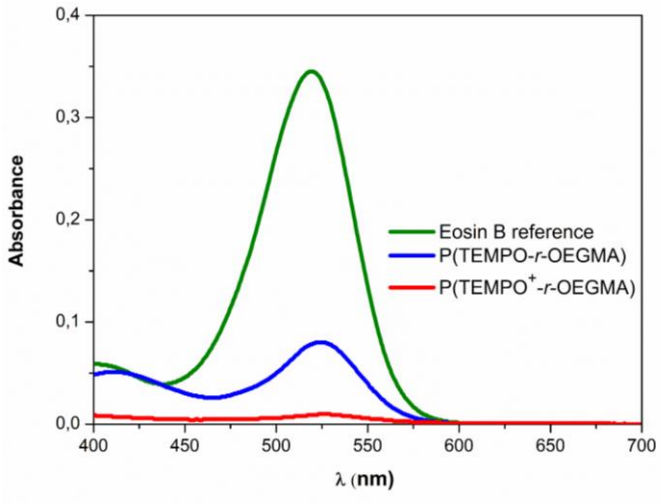

Figure 2.17 *UV-visible spectra of the supernatant of P(TEMPO-r-OEGMA) (blue line) and P(TEMPO$^+$-r-OEGMA) (red line) hydrogels after equilibrium swelling in eosin B solution (hydrogels prepared from the networks with X_{TEMPO} = 0.4 and X_{CL} = 0.03).*

2.7 Conclusions

In this chapter, the synthesis of redox-responsive hydrogels containing the 2,2,6,6-tetramethyl-1-piperidinyloxy methacrylate (TEMPO methacrylate) monomer has been disclosed. The amine-precursor of this monomer (TMPM) has been combined with

oligoethylene glycol methacrylate (OEGMA) to afford water solubility. The conventional radical polymerization technique used in this study proceeds in the quantitative incorporation of the comonomers into the polymeric network, allowing a perfect control over its composition.

The TMPM has been further quantitatively converted into TEMPO methacrylate by a simple oxidation reaction directly performed on the gel. Finally, the TEMPO nitroxide radical can be also quantitatively oxidized to the positively charged $TEMPO^+$ oxoammonium cation. Swelling tests have revealed that the optimum molar fraction of crosslinker, X_{CL}, is equal to 0.03 in order to obtain homogeneous gels displaying high swelling ratios. The amount of TEMPO units (expressed as X_{TEMPO} molar fraction) has been varied in the hydrogels. Cryo-TEM pictures and rheological tests suggest that TEMPO units form hydrophobic domains in the hydrogels. Rheological experiments have confirmed that our hydrogels are slightly chemically crosslinked hydrogels further re-inforced by physically crosslinked nanodomains resulting from the aggregation of hydrophobic TEMPO units.

Finally, the encapsulation abilities of the accordingly formed hydrogels have been explored by using eosin B as a model molecule. It has been demonstrated that the P($TEMPO^+$-*r*-OEGMA) hydrogel is very efficient to encapsulate eosin B molecules and electrostatic interactions have been anticipated. In the case of the P(TEMPO-*r*-OEGMA) hydrogel, some encapsulation of eosin B has been also monitored. In the latter case, hydrophobic interactions between eosin B and TEMPO domains are hypothesized. Those preliminary results have demonstrated the potential of the investigated hydrogels for further application. Next chapter will include a more detailed characterization of the rheological and temperature-responsive behavior of our hydrogels.

2.8 Experimental section

- **Materials**

All chemicals and monomers were purchased from Aldrich, Fluka, or Acros. Solvents were bought from Acros. Poly(ethylene glycol) methyl ether methacrylate (POEGMA, average molar mass of 300 g/mol, Aldrich) and di(ethylene glycol) dimethacrylate ($OEGMA_2$, Aldrich) were purified on a AlO_x-filtration column prior use in order to remove the inhibitor. The 2,2'-aziobutyronitrile (AIBN, 98% purity, Fluka) initiator was recrystallized twice from methanol prior use.

- **Instrumentation**

^{1}H NMR spectroscopy. Proton nuclear magnetic resonance (^{1}H NMR) spectra were acquired on a 300 MHz Bruker Avance II in deuterated chloroform from the supernatant of the polymerization medium and in acetonitrile for the hydrogel obtained after polymerization. ^{1}H NMR spectra were also recorded in the presence of an internal standard on the soluble fraction of oxidized gels swollen with an excess of D_2O in order to determine the fraction of chains that were not entrapped in the network.
^{1}H-NMR (300 MHz, CD_3CN) δ(ppm): 5.05 (s, $1H_3$), 4.08 (s, $2H_4$), 3.58 (m, $22H_{4',5,5'}$), 3.32 (s, $3H_6$), 2.16 (s, $4H_2$), 1.18 (s, $6H_1$), 1.11 (s, $6H_{1'}$).

Size exclusion chromatography (SEC). Apparent average molar masses (M_n and M_w) and dispersity ($Đ$) were measured on an Agilent SEC system equipped with an Agilent 1100/1200 pump (25 °C, eluent: chloroform/triethylamine/isopropanol (94/4/2), flow rate: 1 mL.min-1), an Agilent differential refractometer and two PSS SDV columns (1000 Å and 10000 Å). The calibration was performed using poly(methyl methacrylate) standards.

Fourier-transform infrared spectroscopy (FTIR). FTIR spectra were recorded with a Shimadzu FTIR-8400S spectrometer. The dried oxidized and reduced hydrogels were ground with KBr and pressed into pellets under reduced pressure.

UV-visible (UV-Vis) spectroscopy. After equilibration of the oxidized hydrogel swollen in eosin B solution, the supernatant was transferred into quartz cuvettes and measured in a Varian Cary 50 UV-Vis spectrophotometer with emission scans recorded from 250 to 800 nm.

Rheological measurements. Rheology experiments were performed on a Kinexus Ultra (Malvern Instruments) rheometer equipped with a heat exchanger and modified with a solvent trap. Measurements were carried out using a plate-plate steel geometry (8 and 20 mm diameter) with a gap adjusted between 450 and 1800 μm so that the geometry was completely filled. Oscillatory measurements were carried out in the linear regime (either at strain control of 1% or at stress control of 5 Pa). Strain sweep measurements have also been performed at a strain amplitude ranging from 0.3% to 1000% and at a frequency of 5 rad/s. Measurements were carried out at 20 °C, in a water saturated atmosphere in order to minimize evaporation of the solvent. Normal forces were checked to be relaxed to <0.05 N prior any measurement.

Swelling tests. The dry gels were swollen in distilled water at 25 °C in an isothermal water bath to study the equilibrium swelling kinetics. Mass measurements were taken at time points of 0, 0.5, 1, 2, 4, 8, 24, and 48h. The swelling factor was defined as the weight ratio between the difference in hydrogel weight in both dry and swollen state over the weight of the dry gel.

Electron Spin Resonance (ESR). The EPR spin count was determined as the mean value achieved from the EPR spectra of three samples of the TEMPO-containing gel. For comparison, the EPR spin count of a TEMPO-free gel was determined likewise. X-band EPR spectra were acquired on an EMXmicro CW-EPR spectrometer from Bruker, Germany (EMX micro EMM-6/1/9-VT control unit, ER 070 magnet,

EMX premium ER04 X-band microwave bridge equipped with EMX standard resonator, EMX080 power unit). The samples were investigated at room temperature and the data handling was done with the Bruker Xenon software package, version 1.1b86. The SpinCountQ software module was used for the determination of the spin count.

Electrochemical measurements. Charge/discharge tests were performed using an ARBIN Instrument Battery Tester (BT-2043). The cyclic voltammetry (CV) tests were carried out using a Parstat 3000. The CV measurements were performed at a scan rate of 0.1 mV/s. The electrodes were tested in half-cell configuration with lithium metal foil as counter and reference electrodes and porous polyethylene membrane as separator. The electrolyte used was 1 M of lithium hexafluorophosphate (LiPF6) in ethylene carbonate (EC) and diethyl carbonate (DEC) (1:1, v:v). All coin-cells were assembled under argon atmosphere (<0.1 ppm H_2O, <0.1 ppm O_2) in an Inert Lab glovebox.

Electrode preparation. The cathodes were prepared by blending the active gel material, conductive carbon black (Super C45, MTI), carboxymethyl cellulose (CMC) and Styrene-Butadiene Rubber (SBR) binder. The blend has the following composition, 60 wt. % of PTMA, 25 wt. % of carbon black and 5:10 wt. % of CMC:SBR binder. The ingredients were mixed uniformly at room temperature for 4 hours to yield the slurry. The slurry was cast on an aluminum foil using the doctor blade method (the thickness of the wet film was controlled to be 30 μm) and dried at 60 °C. Circular discs of 1 cm diameter were cut and used as cathodes for evaluating the electrochemical properties. Disks were subsequently punched and pressed at 6 tons/cm^2. Prior the cell assembly, the electrode was dried at 55 °C in vacuum for 12 hours. The coating mass was typically 0.5 to 1.5 mg/cm^2.

Cryogenic-transmission electron microscopy (Cryo-TEM). Samples for cryo-electron microscopy (cryo-EM) were prepared by applying a 4 μl droplet of sample suspension to lacey carbon copper grids (200 mesh, Science Services) and plunge frozen into liquid ethane using a Vitrobot Mark IV(FEI, Eindhoven, Netherlands)set at 4°C and 95 % humidity. Vitrified grids were mounted on a cryo transfer holder (Gatan 914,

Gatan, Munich, Germany) and transferred into a JEOL JEM-2100 (JEOL GmbH, Eching, Germany) transmission electron microscope for imaging. The microscope was operated at an acceleration voltage of 200 kV and a defocus of the objective lens of about 1.5–2 μm was used to increase the contrast. Micrographs were recorded with a bottom-mounted 4*4k CMOS camera (TemCam-F416, TVIPS, Gauting, Germany) at a magnification of 50 000x, corresponding to a pixel size of 2.32 Å at the specimen level. Total electron dose for each micrograph was kept below 20 $e^-/Å^2$.

- **Synthesis**

Typical procedure for the precursor poly(2,2,6,6-tetramethylpiperidin-4-yl methacrylate-random-oligoethyleneglycol methacrylate) (P(TMPM-*r*-OEGMA)) hydrogel synthesis. The synthesis of the polymeric network was carried out using conventional radical polymerization. Into a 50ml round-bottom flask, TMPM (different molar ratios of TMPM/(TMPM+OEGMA) (abbreviated as X_{TEMPO} in the following) were investigated 0.1, 0.2, 0.3 and 0.4) was dissolved in 2-propanol (IPA, 70 wt%), then OEGMA, $OEGMA_2$ (abbreviated as X_{CL}= $OEGMA_2$/(TMPM+OEGMA) was also varied 0.014, 0.02, 0.03, 0.04 and 0.05) and the initiator AIBN (0.5 eq.) were added and stirred until homogeneous blending. The solution was then degassed by three freeze pump-thaw cycles and filled with argon before it was stirred in an oil bath at 70 °C overnight. A transparent gel was formed.

Typical procedure for the poly(2,2,6,6-tetramethylpiperidinyloxy methacrylate-random-oligoethyleneglycol methacrylate) (P(TEMPO-*r*-OEGMA)) hydrogel synthesis. The secondary amine of TMPM units has been oxidized into a nitroxide radical to lead to TEMPO. For that, the remaining IPA of the polymerization gel solution was removed under reduced pressure. Then Na_2WO_4 (0.25 eq.), EDTA (0.15 eq.) and methanol were added and the gel was swollen for a

couple of hours before adding the oxidizing agent H_2O_2 (5eq.). The mixture was then stirred at 60°C overnight. An orange colored gel was obtained and washed four times with distilled water and methanol (1:1, v:v) and dried in vacuum at 40 °C overnight. An orange sticky gel was finally obtained.

Typical procedure for the oxidized (P(TEMPO$^+$-*r*-OEGMA)) hydrogel synthesis. The dried P(TEMPO-*r*-OEGMA) hydrogel was swollen in distilled H_2O (31.25 eq.). Then fluoroboric acid (HBF_4, 1 eq.) was slowly added dropwise over 1h at room temperature. After, sodium hypochlorite (NaClO, 0.5 eq.) was added over 1h at 0°C and stirred for an additional 1h at 0°C to lead to the oxidized hydrogel P(TEMPO$^+$-*r*-OEGMA).[70] Then the hydrogel was washed with ice-cold 5 wt% $NaHCO_3$, aqueous solution and ice-cold diethyl ether. The obtained yellow gel was finally dried overnight at 40°C in vacuum.

Bibliography

1 E. Caló and V. V. Khutoryanskiy, Eur. Polym. J., 2015, **65**, 252–267.

2 F. Ullah, M. B. H. Othman, F. Javed, Z. Ahmad and H. M. Akil, Mater. Sci. Eng. C, 2015, **57**, 414–433.

3 D. Klinger and K. Landfester, Polymer, 2012, **53**, 5209–5231.

4 W. Cheng and Y. Liu, Redox-responsive hydrogels, Elsevier Ltd, 2017.

5 I. Willner, Acc. Chem. Res., 2017, **50**, 657–658.

6 J. Yun, A. R. Oh, J. S. Im, H. Il Kim and Y. S. Lee, Macromol. Res., 2012, **20**, 1029–1036.

7 P. B. Kajjari, L. S. Manjeshwar and T. M. Aminabhavi, AAPS PharmSciTech, 2012, 13, 1147–1157.

8 S. Namkung and C. C. Chu, J. Biomater. Sci. Polym. Ed., 2007, **18**, 901–924.

9 Y. Li, T. Park, J. K. Quansah and S. C. Zimmerman, J. Am. Chem. Soc., 2011, **133**, 17118–17121.

10 Y. Z. You, Q. H. Zhou, D. S. Manickam, L. Wan, G. Z. Mao and D. Oupický, Macromolecules, 2007, **40**, 8617–8624.

11 E. U. Kulawardana, T. Kuruwita-Mudiyanselage and D. C. Neckers, J. Polym. Sci. Part A Polym. Chem., 2009, **47**, 3318-3325.

12 T. Satoh, K. Sumaru, T. Takagi and T. Kanamori, Soft Matter, 2011, **7**, 8030–8034.

13 B. S. Kaith, R. Jindal, H. Mittal and K. Kumar, Der Chem. Sin., 2010, **1**, 44–54.

14 D. Schmaljohann, Adv. Drug Deliv. Rev., 2006, **58**, 1655–1670.

15 D. Schmalijohann, J. Oswald, B. Jørgensen, M. Nitschke, D. Beyerlein and C. Werner, Biomacromolecules, 2003, **4**, 1733–1739.

16 J. Zhang and N. A. Peppas, Macromolecules, 2000, **33**, 102–107.

17 T. Okano, N. Yamada, M. Okuhara, H. Sakai and Y. Sakurai, Biomater. Silver Jubil. Compend., 1995, **16**, 297–303.

18 R. J. Mart, R. D. Osborne, M. M. Stevens and R. V. Ulijn, Soft Matter, 2006, **2**, 822–835.

19 R. Hoogenboom, H. M. L. Thijs, M. J. H. C. Jochems, B. M. Van Lankvelt, M. W. M. Fijten and U. S. Schubert, Chem. Commun., 2008, **1**, 5758–5760.

20 S. Glatzel, A. Laschewsky and J. F. Lutz, Macromolecules, 2011, **44**, 413–415.

21 J. F. Lutz, J. Polym. Sci. Part A Polym. Chem., 2008, **46**, 3459–3470.

22 S. Sugihara, K. Hashimoto, S. Okabe, M. Shibayama, S. Kanaoka and S. Aoshima, Macromolecules, 2004, **37**, 336–343.

23 S. Han, M. Hagiwara and T. Ishizone, Macromolecules, 2003, **36**, 8312–8319.

24 M. M. Ali and H. D. H. Stöver, Macromolecules, 2004, **37**, 5219–5227.

25 H. Kitano, T. Hirabayashi, M. Gemmei-Ide and M. Kyogoku, Macromol. Chem. Phys., 2004, **205**, 1651–1659.

26 D. Zhang and C. Ortiz, Macromolecules, 2004, **37**, 4271–4282.

27 M. Hrubý, S. K. Filippov and P. Štěpánek, Eur. Polym. J., 2015, **65**, 82–97.

28 X. Sui, X. Feng, M. A. Hempenius and G. J. Vancso, J. Mater. Chem. B, 2013, **1**, 1658–1672.

29 C. J. Pérez-Martínez, S. D. Morales Chávez, T. Del Castillo-Castro, T. E. Lara Ceniceros, M. M. Castillo-Ortega, D. E. Rodríguez-Félix and J. C. Gálvez Ruiz, React. Funct. Polym., 2016, 100, **12**–17.

30 R. E. Rivero, M. A. Molina, C. R. Rivarola and C. A. Barbero, Sensors Actuators, B Chem., 2014, **190**, 270–278.

31 J. P. Blinco, J. L. Hodgson, B. J. Morrow, J. R. Walker, G. D. Will, M. L. Coote and S. E. Bottle, J. Org. Chem., 2008, **73**, 6763–6771.

32 K. A. Hansen and J. P. Blinco, Polym. Chem., 2018, **9**, 1479–1516.

33 T. Yoshitomi, K. Kuramochi, L. Binh Vong and Y. Nagasaki, Sci. Technol. Adv. Mater., 2014, **15**, 1–7.

34 T. Janoschka, S. Morgenstern, H. Hiller, C. Friebe, K. Wolkersdörfer, B. Häupler, M. D. Hager and U. S. Schubert, Polym. Chem., 2015, **6**, 7801–7811.

35 A. Vlad, N. Singh, J. Rolland, S. Melinte, P. M. Ajayan and J. F. Gohy, Sci. Rep., 2014, **4**, 1–7.

36 O. Bertrand, A. Vlad, R. Hoogenboom and J. Gohy, Polym. Chem., 2016, **7**, 1088–1095.

37 J. M. Bobbitt, N. A. Eddy, C. X. Cady, J. Jin, J. A. Gascon, S. Gelpí-Dominguez, J. Zakrzewski and M. D. Morton, J. Org. Chem., 2017, **82**, 9279–9290.

38 G. Hauffman, J. Rolland, J.-P. Bourgeois, A. Vlad and J.-F. Gohy, Polym. Chem., 2013, **51**, 101–108.

39 Z. Zhai, L. Lei, J. Song, B. Song, X. Pei and Z. Cui, Soft Matter, 2016, **12**, 2715–2720.

40 L. G. D. Hawke, M. Ahmadi, H. Goldansaz, E. Van Ruymbeke, J. Rheol., 2016, **60**, 297-310.

41 D. R. Miller, C. W. Macosko, J. Polym. Sci. Pol. Phys., 1987, **25**, 2441-2469

42 D. R. Miller, C. W. Macosko, Macromolecules, 1976, **9**, 206-211

Chapter 3

Temperature and redox-responsive hydrogels based on nitroxide radicals and oligoethyleneglycol methacrylate

Table of contents

3.1 Introduction

Understanding the responsiveness of hydrogel structure and rheological properties to stimuli is essential for designing materials with desirable performance. Among the previously investigated stimuli, some studies have recently focused on redox-responsive hydrogels. As example the multi-stimuli responsive hydrogels based on ferrocene, a redox-active group, have been reported. Zhang and co-workers[1] fabricated ferrocenoyl phenylalanine (Fc-F) supramolecular hydrogels exhibiting a sharp phase transitions in response to redox potential. In another work, Wang et al.[2] described the fabrication of self-healing and multi-stimuli responsive hydrogels using the self-assembly of biodegradable ferrocene- modified chitosan in an acid aqueous solution at a low concentration of 10 mg/mL. It was shown that the resulting hydrogels possessed excellent redox, pH and ion responsiveness.

Moreover, the redox-stimulus has been rarely combined with temperature-responsive behaviour. Among the few works done in this topic, the work of Zheng et al.[3] can be cited here, where a thermo- and redox-responsive hydrogel based on the copolymerization of PNIPAM and poly(ionic liquid) network was synthetized. These hydrogels present a high thermo-responsive sensitivity and good redox-responsiveness which results from the transition of iron ions in the gel matrix between two oxidation states; making them very interesting in stimuli-responsive electronic devices or other self-adaptive electronics. Another example, a dual redox- and thermo-responsive hydrogel was synthesized based on PNIPAM and PFS-VIm polyionic liquid[4] where the FS-based poly(ionic liquid)s served as the macro-cross-linker and provided redox-responsive properties to the system. The LCST transition temperature of PNIPAM was influenced by the incorporation of the poly(ionic liquid) and the swelling ability and thermo-responsivity of the hydrogels could be tuned by the counterion type due to the presence of the poly(ionic liquid)s part.

This chapter is focused on the understanding of the relationships between structure-properties of redox and temperature responsive hydrogels through the study of their rheological properties. The

knowledge of such properties is fundamental because, on one hand, these properties can help us to decipher the hydrogel structure on the micrometer scale and, on the other hand, the gained knowledge allows the modulation and optimization of the hydrogel properties for application in different fields. More precisely, in the present paper, we evaluate the mechanical properties of redox and temperature responsive hydrogels by standard mechanical testing methods such as elastic or storage modulus (G') and viscous or loss modulus (G'') measurements, through dynamic mechanical tests at different deformation amplitudes. All rheological properties are evaluated through the use of rotational rheometers.

To this aim, the designed hydrogels described in chapter 2 exhibit the redox and temperature responsive properties: TEMPO groups as redox-active component and an OEGMA co-monomer containing 4/5 ethylene glycol units displaying a cloud-point of 65 °C. As stated above, the combination of redox and temperature-responsive behaviors in a same hydrogel has been rarely studied. Moreover, since the redox process utilized in this contribution results in the transformation of TEMPO which essentially behaves as an hydrophobic unit, into oxidized TEMPO ($TEMPO^+$) which is hydrophilic, an interplay between the redox and temperature behaviours is expected because the cloud point of polymers is known to be influenced by either the presence of neighbouring hydrophobic or hydrophilic units.[5]

In this chapter, we have focused on the effects of the covalent crosslinking degree and of the content of TEMPO units on the properties of the hydrogels at room temperature. We have demonstrated that the optimum molar fraction of crosslinker, X_{CL}, is equal to 0.03 in order to obtain homogeneous gels displaying high swelling ratios. By varying the amount of TEMPO units (expressed as X_{TEMPO} molar fraction) in the hydrogels, we have confirmed that our hydrogels are slightly chemically crosslinked further reinforced by physically crosslinked nanodomains resulting from the aggregation of hydrophobic TEMPO units.[6] In this chapter, our aim is to decipher the effects of temperature and redox stimuli on the rheological properties of reduced P(TEMPO-*r*-OEGMA) and oxidized P($TEMPO^+$-*r*-

OEGMA) hydrogels with varying TEMPO content at a fixed covalent crosslinking degree.

3.2 Synthesis

P(TEMPO-*r*-OEGMA) hydrogels with different X_{TEMPO} and X_{CL} equal to 0.03 **(Figure 3.1)** were synthesized using the same experimental protocol as described in chapter 2.

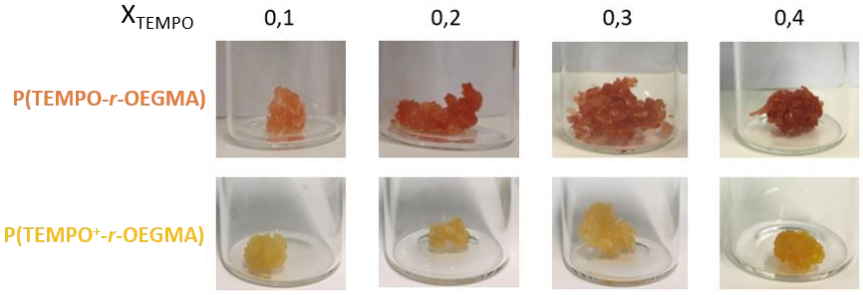

Figure 3.1 *Library of the reduced P(TEMPO-r-OEGMA) and oxidized P(TEMPO$^+$-r-OEGMA) hydrogels with X_{CL} = 0.03 and various X_{TEMPO}.* [12]

The cross-linker value (X_{CL}) was set to 0.03 since the accordingly obtained hydrogels present the highest swelling factor as detailed in section 2.5.1 of chapter 2. We showed that lower X_{CL} eventually leads to viscous fluids instead of gels and lower swelling factors are observed for higher X_{CL} since the increase of cross linker ratio leads to a decrease of the capacity of 3D polymer network to retain water due to the decrease in the mesh size of the network.

The P(TEMPO-*r*-OEGMA) hydrogels were converted into P(TEMPO$^+$-*r*-OEGMA) ones by the chemical oxidation of the nitroxide radicals into oxoammonium cations using NaClO. This reaction can be visually monitored by the change of color of the hydrogel from orange to yellow **(Figure 3.1)**. The UV-visible spectra of P(TEMPO-*r*-OEGMA) and P(TEMPO$^+$-*r*-OEGMA) are shown in **Figure 3.2**. FTIR spectroscopy also confirms the oxidation of P(TEMPO-*r*-OEGMA)

(with a characteristic N-O vibration at 1540 cm^{-1}) into P($TEMPO^{+}$-*r*-OEGMA) (with a characteristic N═ O vibration at 1570 cm^{-1}) as we showed in chapter 2. The yield of this reaction was determined to be close to 100% as we mentioned in chapter 2 by using electron spin resonance. Furthermore, cyclic voltammetry measurements confirmed the presence of redox responsive TEMPO groups in our materials and the reversibility of the redox reactions detailed in chapter 2.

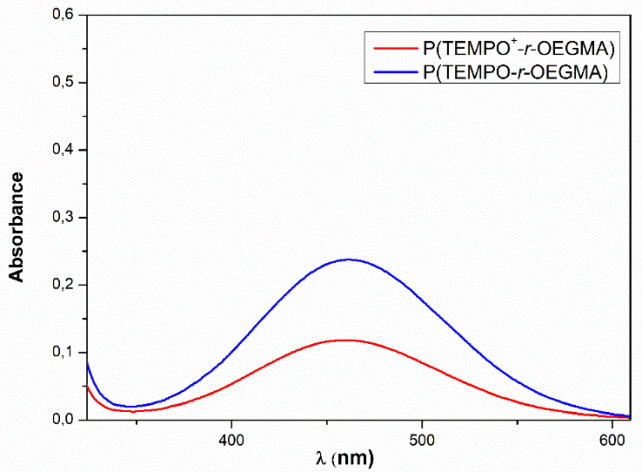

Figure 3.2 *UV-visible spectra of P(TEMPO-r-OEGMA) (blue line) and P($TEMPO^{+}$-r-OEGMA) (red line) hydrogels after equilibrium swelling in distilled water at room temperature (hydrogels prepared from the networks with X_{TEMPO} = 0.4 and X_{CL} = 0.03).*

In order to get some additional information about the structure of the gel, soluble fractions of the investigated hydrogels have been extracted and further analyzed by dynamic light scattering (DLS). Indeed, as demonstrated in chapter 2, our hydrogels are slightly chemically crosslinked and therefore contain a significant fraction of free or slightly crosslinked chains that can be extracted from the equilibrated hydrogels by bringing them into contact in an aqueous phase. The fraction of extracted was further quantified by ^{1}H NMR using an internal standard. Here, in addition to these previous experiments, we have carried out DLS experiments in order to get more information about the structure of the extracted species. In this respect,

objects with a mean hydrodynamic radius of 23 nm have been detected by DLS **(Figure 3.3)**. This can be explained by the fact that our hydrogels are not consisting of a single macroscopic network of crosslinked polymers but are rather cluster of smaller hydrogel particles linked together by entangled non-crosslinked polymer chains and/or hydrophobic TEMPO domains.

Figure 3.3 *Typical size distribution by light scattering for P(TEMPO-r-OEGMA) hydrogels with X_{CL} = 0.03 and for reference one without TEMPO units.*

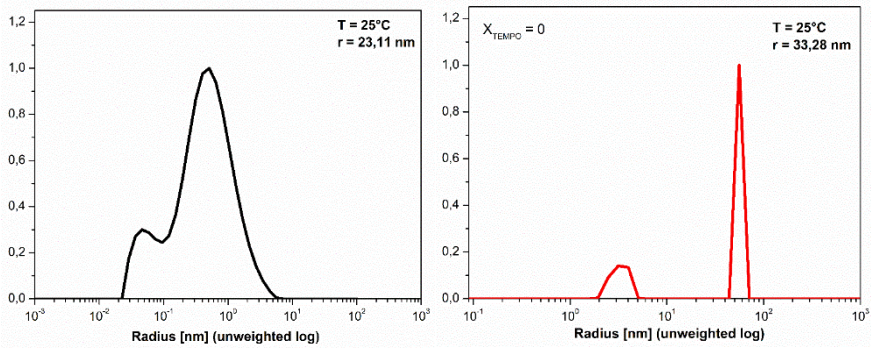

3.3 Mechanicals properties

3.3.1. Swelling test in function of time

Swelling tests were performed on the P(TEMPO-*r*-OEGMA) and P(TEMPO$^+$-*r*-OEGMA) hydrogels. The swelling factor was measured for all X_{TEMPO} values with X_{CL} equal to 0.03. The equilibrium state was determined by regularly weighting the hydrogel during the swelling process until it reached a constant weight. This was typically achieved after 24 h **(Figure 3.4)**. Swelling tests were performed on the P(TEMPO-*r*-OEGMA) and P(TEMPO$^+$-*r*-OEGMA) hydrogels. The swelling factor was measured for all X_{TEMPO} values with X_{CL} equal to 0.03. The equilibrium state was determined by regularly weighting the hydrogel during the swelling process until it reached a constant weight. This was typically achieved after 24 h **(Figure 3.4)**.

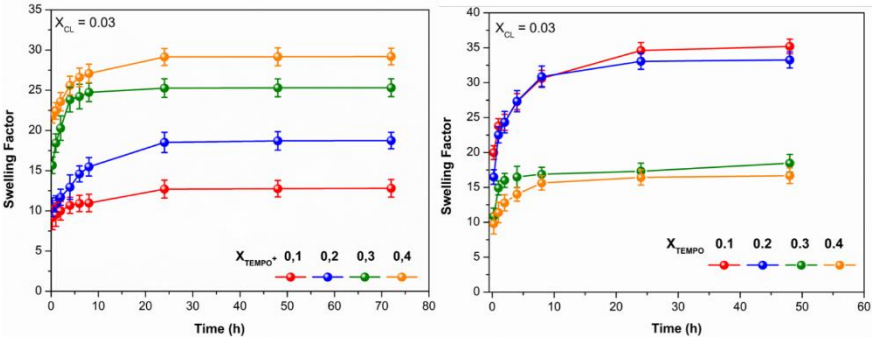

Figure 3.4 *Kinetic swelling study of the oxidized form P(TEMPO$^+$-r-OEGMA) and the reduced form P(TEMPO-r-OEGMA) hydrogels with varying X_{TEMPO}, error bars represent average swelling ratio ± standard deviation where n = 3.*

However, in order to be sure to be at the equilibrium, the hydrogels were further equilibrated for a total of 48 h or 72 h before measuring them again. P(TEMPO$^+$-*r*-OEGMA) hydrogels with varying X_{TEMPO} ratio and X_{CL} fixed to 0.03 display swelling factors around 12-18 for X_{TEMPO} of 0.1 and 0.2 **(Figure 3.5)** while for X_{TEMPO} of 0.3 and 0.4, the swelling factors increase by nearly a factor of 1.4. This increase of swelling factors with the content of X_{TEMPO} can be explained by the increase in hydrophilicity provided by the TEMPO$^+$ units. Indeed, P(TEMPO-*r*-OEGMA) hydrogels with varying X_{TEMPO} and X_{CL} fixed to 0.03 display an opposite effect **(Figure 3.4)**. In this case, the swelling factors decrease by nearly a factor of two when the amount of TEMPO units is increased (X_{TEMPO} of 0.3 and 0.4), which can be explained by the increase in hydrophobicity provided by the TEMPO units.

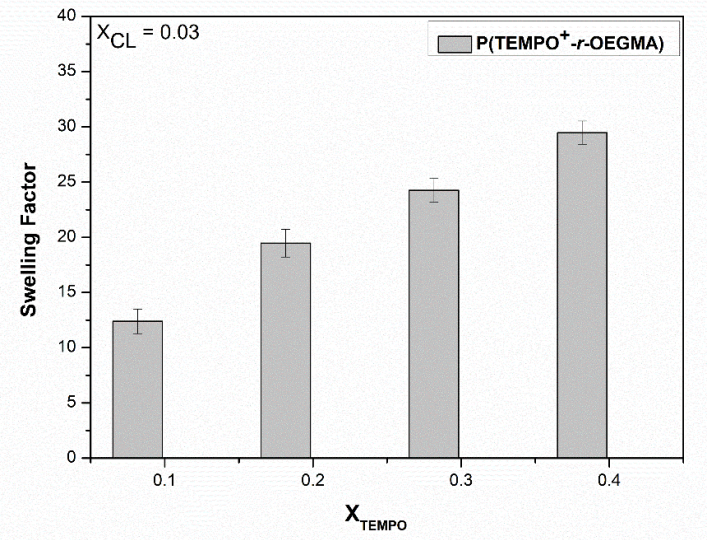

Figure 3.5 *The swelling factors at room temperature for oxidized P(TEMPO$^+$-r-OEGMA) hydrogels with different X_{TEMPO} and fixed X_{CL} = 0.03. Error bars represent average swelling ratio ± standard deviation where n=3.*

3.3.2. Swelling in function of temperature

The temperature-dependent swelling profiles of the P(TEMPO-*r*-OEGMA) and P(TEMPO$^+$-*r*-OEGMA) hydrogels with varying amounts of TEMPO units and X_{CL} equal to 0.03 are shown in **Figure 3.6**. In both cases, as temperature increases, the swelling factors decrease. The influence of temperature is complex to interpret since different effects are expected to come into play. For the P(TEMPO$^+$-*r*-OEGMA) hydrogels, the hydrophilic TEMPO$^+$ units are not expected to be influenced by temperature. In sharp contrast, OEGMA units are known to display a cloud-point in water due to the breaking of the hydrogen bonds between ether oxygens in OEGMA and water molecules as temperatures increases. The cloud-point of the OEGMA used here is reported to be located at 65 °C.[7] Thus, the hydrogel should collapse and become macroscopically turbid once the cloud-point is reached. This could ultimately lead to a macrophase separation between

a collapsed gel and an aqueous phase. However, the value of the cloud-point could be influenced by neighboring hydrophilic/hydrophobic groups.[5,8] Generally, hydrophobic groups lower the cloud-point while hydrophilic groups shift the cloud-point towards higher temperature.[9] In **Figure 3.6**, one can observe that, whatever the value of X_{TEMPO}^{+}, the swelling factors values are slightly decreasing as temperature increases and dramatically drop down between 70 and 80 °C. One can conclude that the cloud points of the P(TEMPO^{+}-*r*-OEGMA) hydrogels are located in this temperature range and slightly shifted to higher temperature compared to pure OEGMA due to the presence of hydrophilic TEMPO^{+} units as shown in **Figure 3.6**.

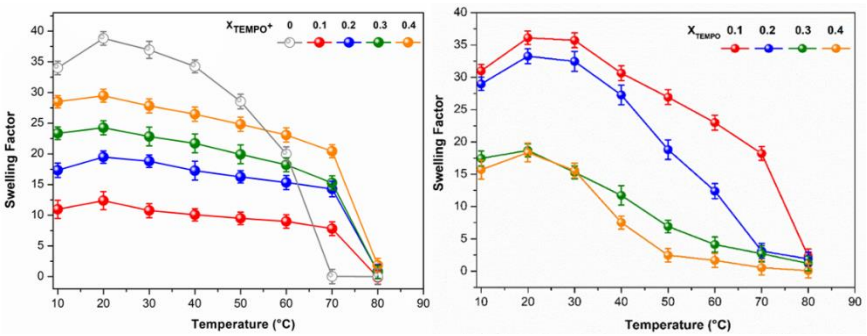

Figure 3.6 *Temperature-dependent swelling profiles of P(TEMPO^{+}-r-OEGMA) (left) and P(TEMPO-r-OEGMA) (right) hydrogels for different X_{TEMPO} and X_{CL}= 0.03. Error bars represent average swelling ratio ± standard deviation where n=3*

In the case of the P(TEMPO-*r*-OEGMA) hydrogels, the hydrophobic TEMPO units are expected to lower the cloud-point of OEGMA. In this respect, the swelling factor drops down to a value close to 0 at temperatures below 65 °C for the P(TEMPO-*r*-OEGMA) with X_{TEMPO} of 0.4 and 0.3, around 65 ° for X_{TEMPO} of 0.2 and close to 80 °C for the lowest value of X_{TEMPO} (0.1) **(Figure 3.6)**. To understand those values, it should be noted that an increase in temperature is known to increase the solubility of TEMPO units. Indeed, TEMPO-

methacrylate polymers are known to exhibit UCST behavior in water-containing solvents,[10] and thus to lead to the weakening or disintegration of hydrophobic TEMPO-rich domains. Thus, the two hypothesized effects are going in opposite directions: on one hand hydrophobic TEMPO units should decrease the cloud point of OEGMA (this effect is essentially observed for the hydrogels containing the highest amount of TEMPO, i.e. 0.4) and, on the other hand, TEMPO units start to be hydrophilic at higher temperature (this effect is essentially observed for the hydrogels containing the lowest amount of TEMPO, i.e. 0.1). For X_{TEMPO} values of 0.2 and 0.3, an intermediate behavior between the two extreme is observed. Those combined two effects could explain the evolution observed in **Figure 3.6** for the swelling factors of P(TEMPO-*r*-OEGMA) hydrogels as temperatures increases.

3.3.3 Rheological properties

The viscoelastic properties of the P(TEMPO-*r*-OEGMA) hydrogels were investigated by rotational rheometry. The viscoelastic response was first measured as a function of temperature for the reference hydrogel without TEMPO units and for the ones with X_{TEMPO} values equal to 0.1 and 0.4. As shown in **Figure 3.7**, the storage modulus (G') decreases when the temperature increases, while it increases when the value of X_{TEMPO} increases. The effect of X_{TEMPO} can be understood on the basis of the formation of hydrophobic TEMPO-rich domains acting as physical crosslinking nodes in the hydrogel. Those ones are added to the chemical crosslinking nodes afforded by $OEGMA_2$ units and are basically acting as mechanically reinforcing nodes, resulting in a higher G'. This effect is more pronounced as the content of TEMPO is increased in the hydrogels resulting in more or larger hydrophobic domains.

The effect of temperature has to be discussed with an approach similar to the one used for explaining the evolution of the swelling factor as a function of temperature. On the one hand, higher temperature increases the solubility of TEMPO that could ultimately lead to the disappearance of the TEMPO physical crosslinks within and between

the hydrogel particles. On the other hand, the solubility of the OEGMA decreases with increasing the temperature and OEGMA becomes insoluble once its cloud point is reached. As already discussed, the value of the OEGMA cloud point might vary with the composition of the hydrogel since it is likely influenced by the TEMPO units (in a rather complex way since the hydrophilic/hydrophobic character of TEMPO units also varies with temperature). Once the cloud point of OEGMA is reached, the hydrogel should collapse and become macroscopically turbid. This could ultimately lead to a macrophase separation between a collapsed gel and an aqueous phase. This situation has been observed for our gels at high temperature (above 60 °C) in line with the swelling factors measurements (in this case swelling factors of 0 have been measured). Due to the formation of heterogeneous systems composed of a flowing liquid and a solid phase, rheological measurements could not be performed above 60 °C. Below this temperature, as expected, the storage moduli of the investigated gels were found to decrease as temperature increases due to an increase in TEMPO solubility. **(Figure 3.7)**.

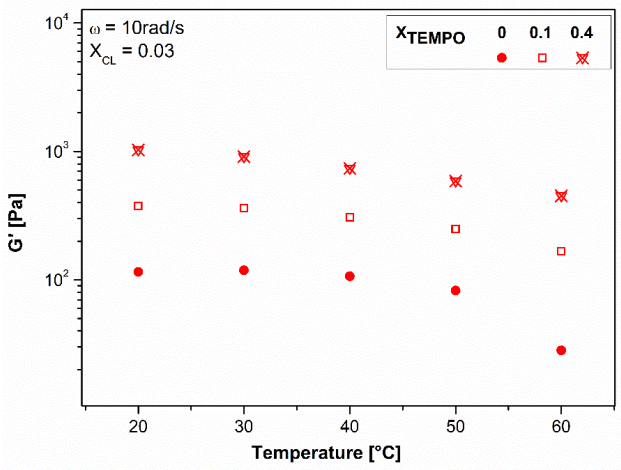

Figure 3.7 *Temperature-dependent of elastic modulus G' behavior of the hydrogel reference without TEMPO and for the P(TEMPO-r-OEGMA) hydrogels with the lowest and highest X_{TEMPO} values 0.1 and 0.4 respectively with X_{CL} 0.03.*

In order to investigate the reversible behavior of our hydrogels, strain sweep tests have been performed from low to high strain amplitude and then, from high to low strain. Results are shown in **Figure 3.8** for X_{TEMPO} = 0 (left) and for X_{TEMPO} = 0.1 and 0.4 (right). In the case of the hydrogel with no TEMPO unit **(Figure 3.8, left)**, a hysteresis is observed, which confirms the formation of hydrogels consisting of clusters of smaller hydrogel particles able to deform and held together via hydrogen bonds between OEGMA units and water molecules.

For the two samples containing TEMPO units, a hysteresis is also observed, which can be seen as a signature of reversible bonds. High strain leads to partial breaking of the hydrophobic interactions between TEMPO units, to allow the hydrogel particles to deform and adapt to the flow. When coming back to low strain amplitude, these interactions are formed again, and the initial value of the modulus is recovered. By increasing the amount of TEMPO units from 0.1 to 0.4, hydrophobic interactions are promoted, which leads to a higher modulus at low strain amplitude but also, to a shorter linear regime.

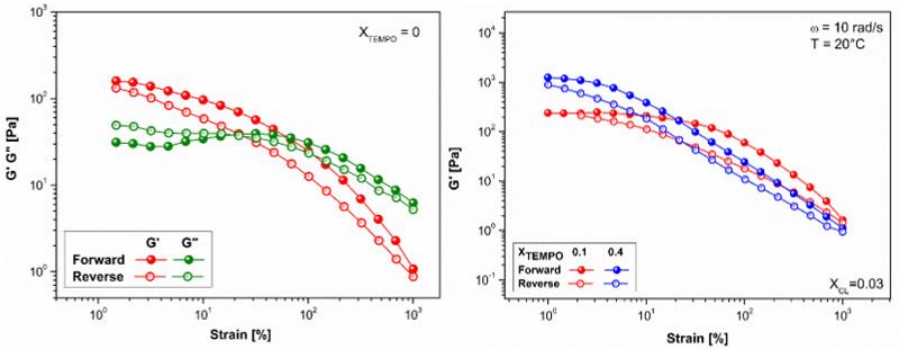

Figure 3.8 *(Left) Storage and loss modulus of the hydrogel without TEMPO units X_{CL}=0.03. (Right) Storage modulus of the hydrogels with the lowest amount of TEMPO units (0.1, red curve) and the highest amount (0.4, blue curve) with X_{CL}=0.03. From low to high (filled symbols) or high to low (empty symbols) amplitude of deformation.*

These results are also in line with the structure of our hydrogels that are poorly crosslinked and rather consist of clusters of hydrogel particles held together by TEMPO rich domains (hydrophobic interactions) and entangled free polymer chains.

Regarding the oxidized P(TEMPO$^+$-*r*-OEGMA) hydrogels, frequency sweeps were firstly performed to confirm gel formation **(Figure 3.9, left)**. While comparing the rheological properties of the P(TEMPO-*r*-OEGMA) and P(TEMPO$^+$-*r*-OEGMA) hydrogels **(Figure 3.9, left)**, the storage modulus of the charged gels decreases when the amount of TEMPO$^+$ units increases, in sharp contrast with the non-charged gels where G' increases when the amount of TEMPO units increases. This behavior can be explained by the lack of hydrophobic TEMPO units acting as mechanically-reinforcing physical crosslinks in the case of P(TEMPO$^+$-*r*-OEGMA) hydrogels.

Moreover, increasing the amount of TEMPO$^+$ units increases electrostatic repulsions in the system and therefore, the attractive interactions between hydrogel particles should vanish at the expense of repulsive ones. In turn, the macroscopic modulus of the hydrogels is expected to decrease as the amount of TEMPO$^+$ units increase in agreement with the situation observed in **Figure 3.9, left**. Frequency sweep measurements were also realized as a function of temperature for the charged P(TEMPO$^+$-*r*-OEGMA) hydrogels in comparison to the reference hydrogel with no TEMPO **(Figure 3.9, right)**. The evolution of G' as a function of temperature is similar to the one noted previously of the uncharged P(TEMPO-*r*-OEGMA) hydrogels. Since hydrophobic TEMPO domains are not existing in case of the P(TEMPO$^+$-*r*-OEGMA) hydrogels, one can hypothesize that the major effect playing here is the desolvation of OEGMA upon heating. As far as the structural features of the hydrogels are concerned, one can understand that desolvation of OEGMA units will reduce the interactions between the hydrogel particles and the number of hydrogen bonds connecting them, which will lead to lower values of storage modulus.

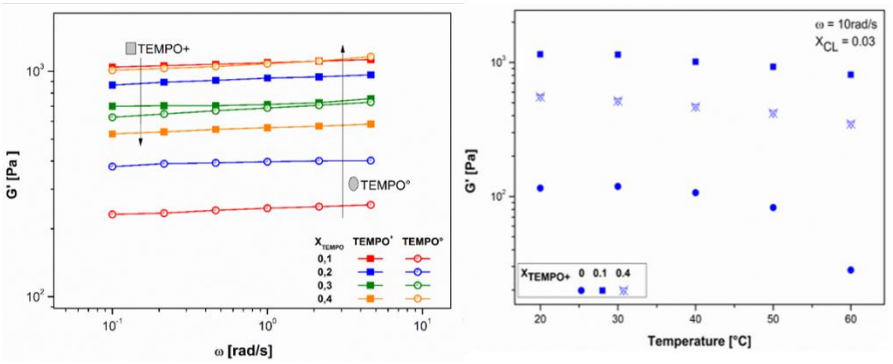

Figure 3.9 *(Left) Frequency sweep plots of storage moduli versus frequency for P(TEMPO-r-OEGMA) and P(TEMPO$^+$-r-OEGMA) hydrogels with X_{CL} = 0.03. (Right) Temperature-dependent of elastic modulus G' behavior of the hydrogel reference without TEMPO and for the P(TEMPO$^+$-r-OEGMA) hydrogels with the lowest and highest X_{TEMPO+} values of 0.1 and 0.4 respectively.*

Finally, strain sweeps tests have also been performed for the P(TEMPO$^+$-*r*-OEGMA) hydrogels from low to high strain amplitude and then, from high to low strain. Results are shown in **Figure 3.10** for X_{TEMPO+} = 0.1 and 0.4. For both samples, a hysteresis is observed, which can be seen as a signature of the deformability of the hydrogel particles and of the reversible bonds (only hydrogen bonds between OEGMA and the water molecule in this case). These results confirm again that our hydrogels are consisting of clusters of smaller hydrogel particles held together by non-covalent interactions.

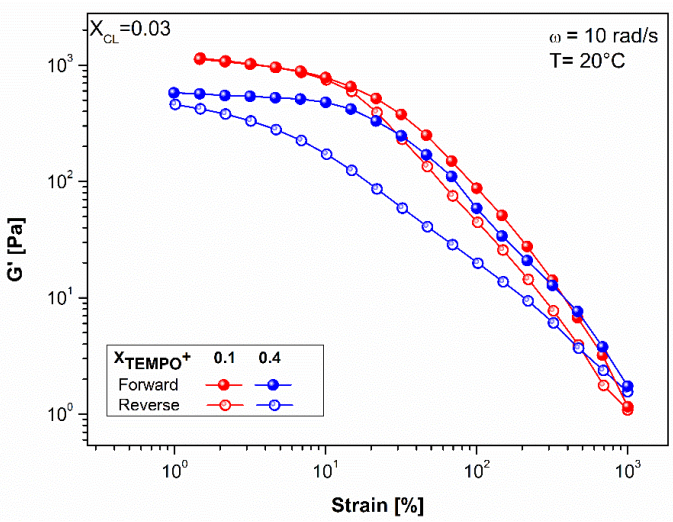

Figure 3.10 *Storage modulus of the hydrogels with the lowest amount of TEMPO units (0.1, red curve) and the highest amount (0.4, blue curve) with X_{CL}=0.03. From low to high (filled symbols) or high to low (empty symbols) amplitude of deformation.*

3.4 Conclusions

This chapter described the combination of redox and temperature-responsive behaviours in a same hydrogel, which has been rarely studied. As responsive groups, we selected OEGMA with a lower critical solubility temperature (LCST) resulting in temperature-responsive properties and TEMPO radicals as redox-responsive units.

The strategy of synthesis was based on the use of a low amount of difunctional monomer ($OEGMA_2$) to chemically crosslink the polymer network.[6] Therefore, the accordingly formed hydrogels obtained after swelling with water rather consisted of microgel particles with entangled polymer chains that are not chemically crosslinked, than a continuous polymer network swollen with water. On the basis of the rarely reported approaches on redox-responsive hydrogels,[11] this work has demonstrated that the TEMPO units in their radical form aggregate

into hydrophobic domains acting as physical crosslinking nodes in our hydrogels. Increasing the temperature resulted in two opposite effects. On one hand, the water solubility of TEMPO units increases as temperature increases resulting in the progressive swelling of the TEMPO domains. On the other hand, the solubility of the OEGMA groups decreases as temperature increases due to their dehydration. The oxidation of TEMPO into $TEMPO^+$ also resulted in a deep change in the hydrogel properties since $TEMPO^+$ units are essentially hydrophilic and do not aggregate into physical crosslinking nodes, thus resulting into hydrogels with weaker mechanical properties than TEMPO-containing hydrogels and with a degree of swelling increasing with the increasing content of $TEMPO^+$.

In conclusion, the effects of temperature and redox stimuli on the rheological properties of reduced P(TEMPO-*r*-OEGMA) and oxidized P($TEMPO^+$-*r*-OEGMA) hydrogels with varying TEMPO content at a fixed covalent crosslinking degree have been disclosed in this paper. In our future work, we will detail the concept of the encapsulation/release of a guest molecule from those hydrogels via an electrochemical oxidation of TEMPO group.

3.5 Experimental section

- **Materials and chemicals**

All chemicals and monomers were purchased from Aldrich, Fluka, or Acros. Solvents were bought from Acros. 2,2,6,6-tetramethyl-1-piperidyl methacrylate (TMPM), oligo(ethylene glycol) methyl ether methacrylate (OEGMA, average molar mass of 300 g/mol, Aldrich) and di(ethylene glycol) dimethacrylate ($OEGMA_2$, Aldrich) were purified on a AlO_x-filtration column prior use in order to remove the inhibitor. The 2,2'-azobisisobutyronitrile (AIBN, 98% purity, Fluka) initiator was recrystallized twice from methanol prior use.

- **Instrumentation**

Rheological measurements. Rheology experiments were performed on a Kinexus Ultra (Malvern Instrument) rheometer equipped with a heat exchanger and modified with a solvent trap. Measurements were carried out using a plate-plate steel geometry (8 and 20 mm diameter plate−plate geometries). Oscillatory measurements were carried out in the linear regime (by imposing either at strain amplitude of 1% or at stress amplitude of 5 Pa) with a gap adjusted between 450 and 1800 μm at given temperatures. A strain sweep test was performed with each sample, to determine the linear viscoelastic (LVE) range. Frequency sweep was then used to determine the storage modulus, G', and the loss modulus, G", as a function of angular frequency, ω. Normal forces were checked to be relaxed prior any measurement.

Swelling tests. The dry gels were swollen in distilled water at 25 °C in an isothermal water bath to study the equilibrium swelling kinetics. Mass measurements were taken at time points of 0, 0.5, 1, 2, 4, 8, 24, 48, 72 h. The swelling factor was defined as the weight ratio between the difference in hydrogel weight in both the dry and the swollen state over the weight of the dry gel. In order to perform a temperature swelling study, gels were swelled at temperature increments of 10°C from 10 to 80°C for 24h to reach equilibrium swelling, and mass swelling ratios at each temperature were calculated.

- **Synthesis**

Typical procedure for the synthesis of P(TEMPO -r-OEGMA) and P(TEMPO$^+$ -r-OEGMA) hydrogels. The investigated P(TEMPO-*r*-OEGMA) and P(TEMPO$^+$-*r*-OEGMA) hydrogels have been synthesized via a methodology described in our previous work.[6] Briefly, a P(TMPM-*r*-OEGMA) precursor hydrogel was prepared by conventional radical copolymerization of TMPM, OEGMA and $OEGMA_2$ (chemical crosslinking agent), followed by the oxidation of the secondary amine of TMPM units with H_2O_2 and Na_2WO_4 in methanol[10] to obtain the P(TEMPO-*r*-OEGMA) hydrogel. Different molar ratios of TMPM/(TMPM+OEGMA) (abbreviated as X_{TEMPO} in the following) were investigated (X_{TEMPO} = 0.1, 0.2, 0.3 and 0.4) to investigate the influence of increasing TEMPO content and the cross-linker molar ratio $OEGMA_2$/(TMPM+OEGMA) (abbreviated as X_{CL} in the following) was set to 0.03. Finally, the nitroxide radical units of TEMPO were oxidized into oxoammonium units (TEMPO$^+$) with NaClO in the presence HBF_4 to obtain the oxidized P(TEMPO$^+$-*r*-OEGMA) hydrogel.[12]

Bibliography

1 Z. Sun, Z. Li, Y. He, R. Shen, L. Deng, M. Yang, Y. Liang and Y. Zhang, *J. Am. Chem. Soc.*, 2013, **135**, 13379–13386.

2 Y. K. Li, C. G. Guo, L. Wang, Y. Xu, C. Y. Liu and C. Q. Wang, *RSC Adv.*, 2014, **4**, 55133–55138.

3 N. Sun, P. Sun, A. Wu, X. Qiao, F. Lu and L. Zheng, *Soft Matter*, 2018, **14**, 4327–4334.

4 X. Feng, K. Zhang, P. Chen, X. Sui, M. A. Hempenius, B. Liedberg and G. J. Vancso, *Macromol. Rapid Commun.*, 2016, **37**, 1939–1944.

5 A. García-Peñas, C. S. Biswas, W. Liang, Y. Wang, P. Yang and and F. J. Stadler, *Polymer (Guildf).*, 2019, **11**, 991.

6 M. Khodeir, B. Ernould, J. Brassinne, S. Ghiassinejad, H. Jia, S. Antoun, C. Friebe, U. S. Schubert, Z. Kochovski, Y. Lu, E. Van Ruymbeke and and J.-F. Gohy, *Soft Matter*, 2019, **15**, 6418–6426.

7 J. F. Lutz, *J. Polym. Sci. Part A Polym. Chem.*, 2008, **46**, 3459–3470.

8 T. Ise, K. Nagaoka, M. Osa and T. Yoshizaki, *Polym. J.*, 2011, **43**, 164–170.

9 P. J. Roth, F. D. Jochum, F. R. Forst, R. Zentel and P. Theato, *Macromolecules*, 2010, **43**, 4638–4645.

10 O. Bertrand, A. Vlad, R. Hoogenboom and J. Gohy, *Polym. Chem.*, 2016, **7**, 1088–1095.

11 N. Isobe, X. Chen, U. J. Kim, S. Kimura, M. Wada, T. Saito and A. Isogai, *J. Hazard. Mater.*, 2013, **260**, 195–201.

12 J. M. Bobbitt, *J. Org. Chem.*, 1998, **63**, 9367–9374.

Chapter 4

Application of redox-responsive hydrogels based on 2,2,6,6-tetramethyl-1-piperidinyloxy methacrylate and oligoethyleneglycol methacrylate

Table of contents

4.1 Introduction

TEMPO (2,2,6,6-tetramethyl-1-piperidinyloxy-methacrylate) a typical species that can undergo reversible oxidation–reduction reactions has been incorporated in hydrogels to achieve redox responsiveness[1] including our work presented in this thesis. The design of redox active networks usually involves the incorporation of redox responsive centers in the polymer main chain, in the side groups or as cross-linking moieties.[1] Especially valuable are hydrogels that are capable of responding reversibly, in a controllable and predictable way, to redox stimuli.[2] This redox stimuli may be applied chemically or electrochemically. This last possibility is particularly interesting since it does not require the addition of reactants to the hydrogel in order to observe the redox responsive behavior. However, the hydrogel should display a sufficient electric conductivity in order to be electrochemically addressed.

In chapters 2 and 3, we have described and characterized new redox-responsive hydrogels based on polymer networks containing 2,2,6,6-tetramethyl-1-piperidinyloxy (TEMPO) stable nitroxide radicals and oligoethylene glycol methyl ether methacrylate (OEGMA) as biocompatible co-monomer. TEMPO groups can undergo reversible oxidation-reduction reactions that lead to redox activity while OEGMA groups are hydrophilic and allow water swelling to obtain hydrogels. In the present chapter, the use of those hydrogels for two different applications is presented.

The first application presents the release of a guest molecule, namely aspirin, in response to an electrochemical redox trigger. The advantages of the electrochemical stimulus is that it can be localized in time, it does not require the addition of reagents and the trigger parameters, such as current intensity and reaction time, can easily by modulated to adequately comply with the system. Therefore, the amount of released guest molecule can be controlled and realized on demand.

The second application is based on the well-known use of TEMPO groups as catalysts for the oxidation of alcohols to obtain ketones,

aldehydes or carboxylic acids.[14–16] The oxidation of alcohols using TEMPO-based catalysts is often efficient, fast, selective, realized in mild conditions and can tolerate sensitive functional groups.[14–16] Here, we report a methodology using our hydrogels containing TEMPO groups as catalysts for the oxidation of benzyl alcohol into benzaldehyde in aqueous medium. This second application is inspired by the previous work of Hu et al.[3] Moreover, this application follows some of the principles of green chemistry since it uses water as solvent and it allows a very easy purification of the product of the reaction since the latter phase separates from the hydrogel. Therefore, the TEMPO-containing hydrogel can be easily recycled after the reaction to be used again.

4.2 Encapsulation-release application

In order to demonstrate the encapsulation abilities of P(TEMPO$^+$-*r*-OEGMA) hydrogels, we have designed a proof-of-concept experiment by taking opportunity of the presence of positively charged units in the oxidized P(TEMPO$^+$-*r*-OEGMA) hydrogels to encapsulate a negatively charged drug, namely acetylsalicylic acid commonly known as aspirin. In a first step, the equilibrium swelling of the P(TEMPO$^+$-*r*-OEGMA) hydrogel was realized with aspirin (0.1 g/L) dissolved in 0.1M aqueous $NaClO_4$ solution (at this pH close to 7 the aspirin is mainly negatively charged since its carboxylic group is in the carboxylate anion form). After the swelling step, a small piece (2 mm^2) of the hydrogel was cut and brought in direct contact with a printed carbon electrode to perform the electrochemical reduction of TEMPO$^+$ into TEMPO (**Figure 4.1)**. In this respect, cyclic voltammetry measurements (CV) for the P(TEMPO$^+$-*r*-OEGMA) hydrogel (X_{TEMPO} = 0.2 and X_{CL}= 0.03) loaded with aspirin show clearly the reversible reduction of the oxoammonium cations into nitroxide radicals (**Figure 4.2, a**).

Figure 4.1 *Electrochemical reduction of P(TEMPO$^+$-r-OEGMA) hydrogels, swollen in aqueous $NaClO_4$ and loaded with aspirin using the printed carbon electrode method (PCE).*

In order to demonstrate the release of aspirin molecules during the reduction step, the supernatant aqueous solution above the hydrogel was analyzed by mass spectrometry and the presence of aspirin molecules released from the hydrogel was detected (green mass spectrum in **Figure 4.2, b**)**.** In a second step, the electrochemical oxidation of the P(TEMPO-*r*-OEGMA) hydrogel into P(TEMPO$^+$-*r*-OEGMA) was performed and followed by CV (**Figure 4.2, a**). Once again, the supernatant aqueous solution above the hydrogel was analyzed by mass spectrometry but this time no aspirin molecules were detected (blue mass spectrum in **Figure 4.2, b**). This observation confirms that no aspirin molecules can be released from the P(TEMPO$^+$-*r*-OEGMA) hydrogel because electrostatic interactions between negatively charged aspirin molecules and positively charged TEMPO$^+$ groups are operating. A second explanation could be that all the encapsulated aspirin molecules have been released during the electrochemical reduction step and that the hydrogel contains no more

aspirin molecules. In order to clear out those questions, we have performed two additional experiments. In a first experiment, we have deposited a small amount of the 1M $NaClO_4$ solution on top of the aspirin loaded P($TEMPO^+$-*r*-OEGMA) hydrogel and we have let the system to equilibrate for 12h. Afterwards, the supernatant of the hydrogel has been analyzed by mass spectrometry and no aspirin molecules were detected confirming their strong electrostatic encapsulation in the hydrogel.

In a second experiment, UHPLC has been used to determine the amount of aspirin released in the supernatant of the P($TEMPO^+$-*r*-OEGMA) hydrogels after the electrochemical reduction. The determined concentration of aspirin molecules was 1372µM (247 ppm), for a total surface of 6.9 mm^2 (surface of the electrode) and a cutted gel surface of 2 mm^2 (**Figure 4.1**). The further calculation indicated that 100% of aspirin molecules were released in the whole supernatant, proving the efficiency of the electrochemically triggered release process.

All those results prove a new concept for the encapsulation/release of a negatively charged molecule from $TEMPO^+$-containing hydrogels via electrochemical oxidation/reduction.

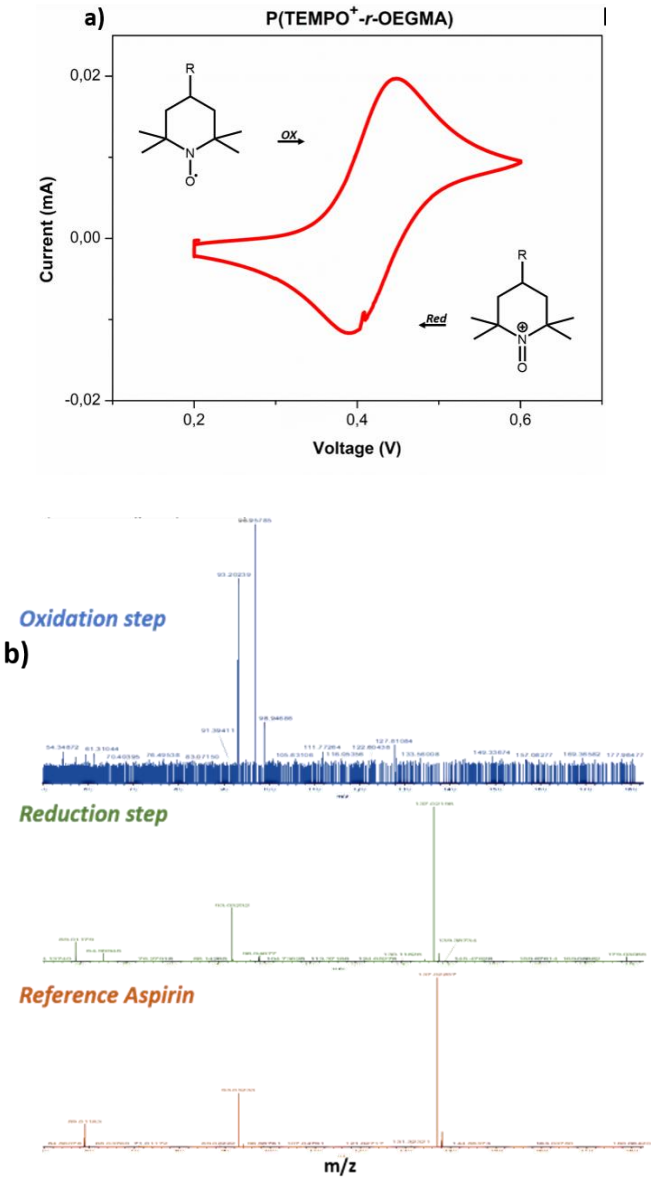

Figure 4.2 a) *Cyclic voltammetry of P(TEMPO$^+$-r-OEGMA) hydrogels. Analyses conducted in 0.1 M $NaClO_4$ in distilled water at a carbon electrode. Scan rate = 5 mV s^{-1}* ***b)*** *Mass spectroscopy analysis of the supernatant for the oxidation step (blue curve), reduction step (green curve) and the aspirin reference molecule (orange curve).*

4.3 Catalyst scaffold for alcohol oxidation

- P(TEMPO-*r*-OEGMA) hydrogels as catalytic scaffolds for the oxidation of alcohols

The catalytic activity of P(TEMPO-*r*-OEGMA) hydrogels (X_{TEMPO} =0.2 and X_{CL}=0.03) has been determined by monitoring the oxidation of benzylic alcohol under aerobic condition (**Figure 4.3**). Practically, the reaction was started by mixing in a 10 mL round-bottom flask the dry gel (153 mg) and all the reactants (benzylic alcohol, 0.52 mL; tert-butyl nitrite as a metal-free co-catalyst, 5 mol% and water, 1.5 mL) together and stirring for 2 hours at room temperature. In a second step, the temperature was raised to 50 °C to start the oxidation reaction for 4 hours. Then, the reaction was stopped by let it cool down to room temperature for 30 minutes and the supernatant of the gel was analyzed.

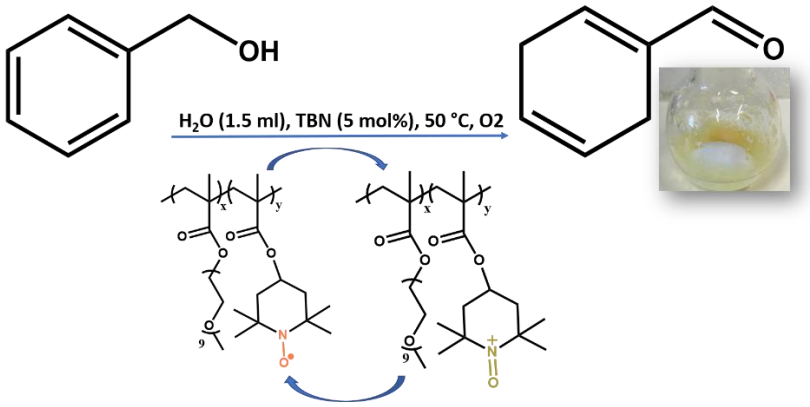

Figure 4.3 *Reaction conditions for benzyl alcohol oxidation.*

As shown by the GC-MS spectrum in **Figure 4.4**, the quantitative benzylic alcohol conversion was confirmed by utilizing tert-butyl-nitrite (TBN) as nitrite source with the peak characteristic of benzaldehyde appearing at 2.644 min with 83.45% relative area. Considering that the rest 16.55% relative area belonged to either some impurities or residual solvent, the actual benzaldehyde selectivity was close to 100%.

Such a high catalytic efficiency of the P(TEMPO-*r*-OEGMA) hydrogel could be mainly due to its composition allowing an important and uniform uptake of benzylic alcohol inside the hydrogel. In this respect, a homogenous system is observed when the P(TEMPO-*r*-OEGMA) hydrogel is added with the reactants and equilibrated. Benzylic alcohol was absorbed inside the matrix and as the reaction starts to proceed, a supernatant appears on top of the hydrogel essentially consisting of benzaldehyde (as determined by GC-MS, see above) that phase separates from the hydrogel. This last characteristic feature is very interesting since it allows the easy recovery of the product of the reaction and the easy recycling of the TEMPO catalyst.

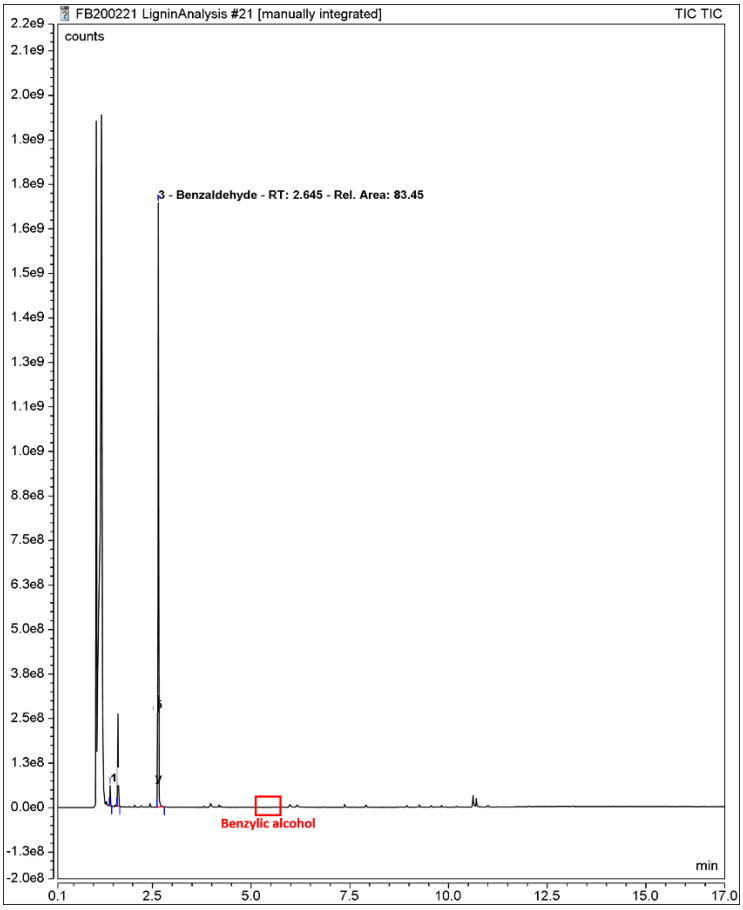

Figure 4.4 *GC-MS spectra of the solution obtained after oxidation.*

- Monitoring the kinetics of the reaction by in-situ infra-red spectroscopy

In order to get more information about the kinetics of the oxidation reaction of benzylic alcohol into benzaldehyde, an in-situ infra-red monitoring of the reaction was realized. Practically, the reaction was performed using the same experimental conditions as described above in the presence of an infra-red probe immersed in the reaction medium. The recording of the infra-red probe was started when temperature was raised to 50 °C to start the oxidation reaction. The infra-red data were

only usable to up to 90 minutes of reaction since technical problems were encountered later. Those problems were resulting either from an air bubble appearing on the probe window or from the gel itself impeding the movement of the solution to and from the probe window.

Nevertheless, the recorded data allow the deduction of two main trends corresponding to a linear disappearance of benzylic alcohol and a concomitant linear formation of benzaldehyde over time (**Figure 5.5**). This would indicate a zero order for the kinetics of the reaction as it is often the case for diffusion limited reactions due to the presence of a gel.[4]

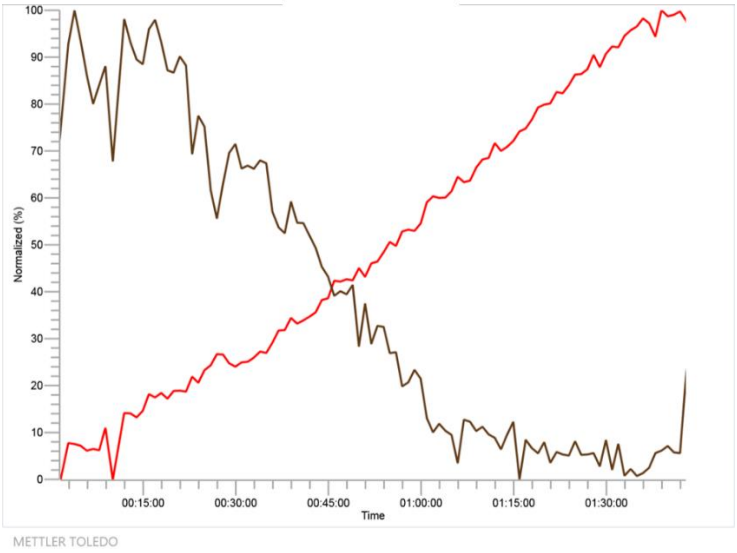

Figure 4.5 *Evolution of the normalized integration of the infra-red spectra of benzylic alcohol and benzaldehyde during the oxidation reaction of benzyl alcohol (black curve) into benzaldehyde (red curve) over time.*

The formation of benzaldehyde can be followed in the infra-red spectra by the peaks at 1700,1167 and 1204 cm^{-1} corresponding to vibrations associated to the aldehyde function. On the other hand, the peaks corresponding to the benzylic alcohol molecule in the area between 1605 and 1660 cm^{-1} are linearly vanishing with time (**Figure 4.6**).

All these results confirm the very efficient oxidation of benzylic alcohol to benzaldehyde using our redox hydrogels as catalyst.

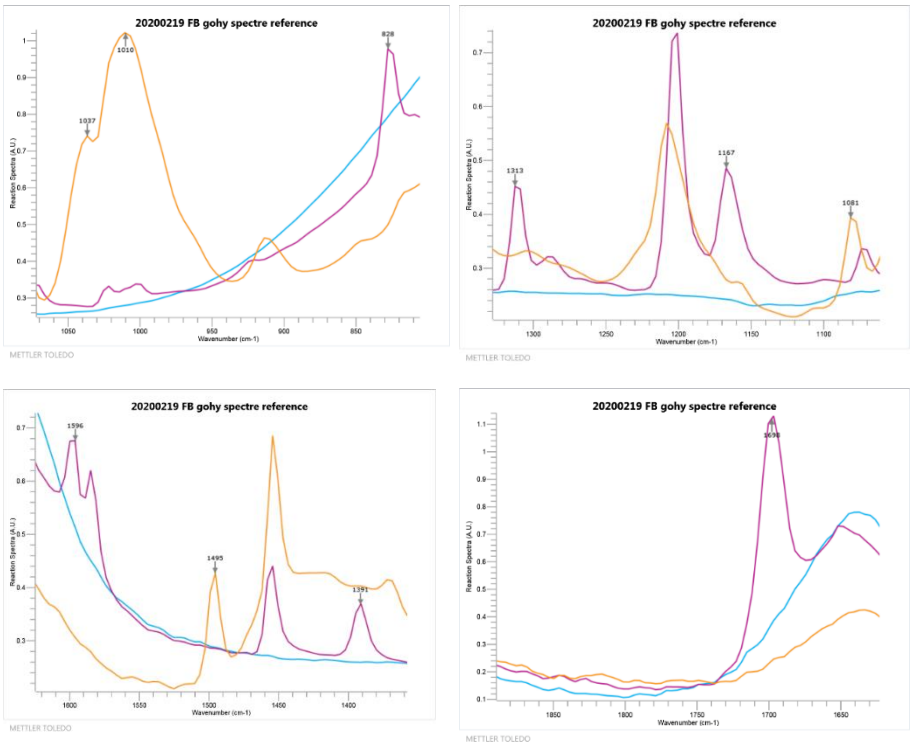

Figure 4.6 *Reference FTIR spectra (blue=water; yellow=alcohol/water, purple=aldehyde/water).*

Following characteristic peaks (cm^{-1}) are identified:

- Alcohol: 1010, 1081, 1037, 1495
- Aldehyde: 1698, 1596, 1391, 1313, 1167, 82

4.4 Conclusions

Redox-responsive hydrogels represent a highly interesting and versatile class of materials for loading and release applications in the biomedical field. In this chapter, we have taken advantage of the positive charge present on the oxidized form of TEMPO (oxoammonium cations in $TEMPO^+$) in our P(TEMPO-*r*-OEGMA) hydrogels to electrostatically complex a negatively charged model molecule (aspirin). We have demonstrated that aspirin is tightly bound to $TEMPO^+$ and cannot diffuse out the hydrogel. However, when $TEMPO^+$ groups are electrochemically reduced into TEMPO radicals, the electrostatic interaction between aspirin and $TEMPO^+$ disappears which allows the release of the aspirin molecule from the hydrogel. Furthermore, by using UHPLC, we have demonstrated that aspirin can be quantitatively released from the hydrogel. Finally, it should be pointed out that a very simple carbon printed electrodes has been used to electrochemically trigger our hydrogels (which have simply deposited on top of the electrode) proving that this set-up could be easily utilized for real life applications.

Finally, we have demonstrated the efficiency of our hydrogels as TEMPO-based catalysts for the oxidation of benzylic alcohols to the corresponding aldehydes under aerobic conditions. Moreover, the final products are easily separated from the hydrogel starting materials without using toxic organic solvents or complicated and costly process.

4.5 Experimental section

- **Materials**

All chemicals and monomers were purchased from Aldrich, Fluka, or Acros. Solvents were bought from Acros. Acetylsalicylic acid (ASA), 2,2,6,6-tetramethyl-1-piperidyl methacrylate (TMPM), oligo(ethylene glycol) methyl ether methacrylate (OEGMA, average molar mass of 300 g/mol, Aldrich) and di(ethylene glycol) dimethacrylate ($OEGMA_2$, Aldrich) were purified on a AlO_x-filtration column prior use in order to remove the inhibitor. The 2,2'-azobisisobutyronitrile (AIBN, 98% purity, Fluka) initiator was recrystallized twice from methanol prior use.

- **Instrumentation**

Electrochemical measurements. All electrochemical experiments were performed at room temperature using 0.1M $NaClO_4$ as supporting electrolyte. 5µL of sample were dropped on the working electrode (carbon screen printed electrode DRP-110-U75, Metrohm) and, after 60 s, cyclic voltammetry was performed in the potential range comprised between 0.2 and 0.6 V at a scan rate of 10 mV/s.

Ultra-high-pressure liquid chromatography (UHPLC) – electrospray ionization mass spectrometry (ESI) analysis. An UHPLC system consisting of a binary pump, an automatic injector, a column oven and an Agilent 1290 series UV detector was used. The separation was carried out on an Eclipse plus C18 RRHD column (100 × 2.1 mm, 1.8 µm) at a flow rate of 0.2 ml/min and using an aqueous solution containing 1.0% of acid formic acid and 5% acetonitrile (solvent A) and acetonitrile containing 0.1% formic acid (solvent B). The elution program was started at 90% solvent A for 1 min, then 90% solvent B for 6 min at a flow rate of 0.2 mL/min with UV detection at 280 nm. The injection volume was kept at 5 µL for the standard and all the other samples. The detection in mass spectrometry was carried out by an ESI jet stream Agilent 6150B mass spectrometer. The analysis was carried out at 200 ° C with a capillary voltage of 1500eV and a

voltage nozzle at 2000eV. The parameters were optimized for the detection of acetylsalicylic acid as follows: Nebulization pressure at 50 psi, drying gas at 4 L/min and power of fragmentary set at 75eV**.** The retention time of aspirin was observed at 5.52 ± 0.1 min for MS and 5.32 ± 0.1 min for UV. An aspirin standard (Sigma Aldrich) was dissolved in acetonitrile (ACN) containing 0.1% formic acid. A calibration curve ranging from 15µM (2.7 ppm) to 301µM (54.2 ppm) was injected. The aspirin was followed in LC-MS in SIM (-) mode for m/z of 179 and 225 and in UV at 280nm. 30µl of samples were diluted with 100µl of water (dilution factor 4.33)

Gas chromatography (GC) – mass spectrometry (MS) analysis. The chromatographic separation of benzaldehyde and benzylic alcohol was performed using a Thermo Scientific^{TM} TRACE 1310 GC coupled with a single quadrupole ISQ QD mass spectrometer. The GS was equipped with a RESTEK Rxi®-5Sil MS column (L = 30 m, d_c = 0.25 mm, and d_f = 0.25 μm). The GC temperature program started at a temperature of 60°C, ramped to 300°C (20°C/min, held 5min) with a constant flow of 2 ml/min, resulting in an overall analysis time of 17 min. Injection mode with split ratio of 1/10 was used. The MS was operated with source of mass at 305 °C and full scan mode (or TIC for total ions current) from 40 to 400 m/z.

Fourier-transform infra-red (FTIR) kinetic study. A probe 6.3 mm AgX DiComp (Au, Diamond, C22) was connected to a ReactIR 15 from Mettler Toledo. The probe was introduced in an Easymax reactor from Mettler Toledo.

- **Synthesis**

Typical procedure for the synthesis of poly(2,2,6,6-tetramethyl-1-piperidinyloxo ammonium methacrylate-random-oligo(ethylene glycol) methyl ether methacrylate) (P(TEMPO$^+$ -*r*-OEGMA)) hydrogels. The investigated P(TEMPO$^+$-*r*-OEGMA) hydrogels have been synthesized via a methodology described in our previous work.[5] Briefly, a P(TMPM-*r*-OEGMA) precursor hydrogel was prepared by conventional radical copolymerization of TMPM, OEGMA and $OEGMA_2$ (chemical crosslinking agent), followed by the oxidation of the secondary amine of TMPM units with H_2O_2 and Na_2WO_4 in methanol to obtain the P(TEMPO-*r*-OEGMA) hydrogel.[6] The molar ratio of TMPM/(TMPM+OEGMA) (abbreviated as X_{TEMPO} in the following) was set to 0.2 and the cross-linker molar ratio $OEGMA_2$/(TMPM+OEGMA) (abbreviated as X_{CL} in the following) was set to 0.03. Finally, the nitroxide radical units of TEMPO were oxidized into oxoammonium units (TEMPO$^+$) with NaClO in the presence HBF_4 to obtain the oxidized P(TEMPO$^+$-*r*-OEGMA) hydrogels.[7]

Bibliography

1 X. Sui, X. Feng, M. A. Hempenius and G. J. Vancso, *J. Mater. Chem. B*, 2013, **1**, 1658–1672.

2 B. Zoetebier, M. A. Hempenius and G. J. Vancso, *Chem. Commun.*, 2015, **51**, 636–639.

3 R. Liu, C. Dong, X. Liang, X. Wang and X. Hu, *J. Org. Chem.*, 2005, **70**, 729–731.

4 S. Dash, P. N. Murthy, L. Nath and P. Chowdhury, *Acta Pol. Pharm. - Drug Res.*, 2010, **67**, 217–223.

5 M. Khodeir, B. Ernould, J. Brassinne, S. Ghiassinejad, H. Jia, S. Antoun, C. Friebe, U. S. Schubert, Z. Kochovski, Y. Lu, E. Van Ruymbeke and and J.-F. Gohy, *Soft Matter*, 2019, **15**, 6418–6426.

6 O. Bertrand, A. Vlad, R. Hoogenboom and J. Gohy, *Polym. Chem.*, 2016, **7**, 1088–1095.

7 J. M. Bobbitt, *J. Org. Chem.*, 1998, **63**, 9367–9374.

Chapter 5

Synthesis and characterization of hydrogels containing redox-responsive 2,2,6,6-tetramethylpiperidinyloxy methacrylate and thermo-responsive *N*-isopropylacrylamide

Table of contents

5.1 Introduction

Polymers represent attractive candidates for smart materials because they may contain different domains or moieties, each of them with specific properties that may lead to multi-responsive systems. Moreover, polymers can form extended three dimensional structures which hold the solvent. Hydrogels are typical examples of such structures in which a crosslinked three-dimensional network of polymer holds water without dissolution. Depending on the monomers incorporated into the hydrogel and the conditions of the surrounding medium, hydrogels can exhibit a full range of properties. As a typical example, the work of Singh *et al.* showed that the swelling properties of poly(*N*-isopropylacrylamide) (PNIPAM) containing hydrogels could be tailored by incorporating various contents of poly(ethylene glycol) methacrylate (PEGMA) as well as by the conditions of polymerization.[1] In this respect, the lower critical solubility temperature (LCST) of PNIPAM was increased by increasing amount of PEGMA and was attaining a temperature of 37 °C after copolymerization with 10 wt% of PEGMA. Moreover, the copolymer composition also had a large effect on the cell growth and detachment.[1]

As already highlighted in the example before, hydrogels as biocompatible materials[2] are quite promising for applications in aqueous media.[3] And they become in particular useful when they are used as 'smart' materials.[3] As far as aqueous media are concerned, temperature and pH value changes are the most commonly studied stimuli since these parameters can be easily controlled. Thermoresponsive hydrogels have been recently increasingly investigated and are usually prepared from thermosensitive polymers with a lower critical solubility temperature (LCST).[4] More precisely, around the critical temperature, the polymer in aqueous solution exhibits a phase transition from a soluble to an insoluble state. Among the known LCST polymers, PNIPAM is one of the most promising because of its LCST (32°C) is close to human body temperature. There are numerous examples referring to PNIPAM hydrogels[5–8] and many applications are in aqueous medium in which they swell to a very high degree.[9–11] This requires a low density of slightly crosslinked PNIPAM

chains which makes the gels extremely poor in mechanical strength. This constitutes a great hurdle in their applications.

In chapter 2 and 3, we described the synthesis and characterization of redox hydrogels based on poly(2,2,6,6-tetramethylpiperidinyloxy methacrylate-*random*-oligoethyleneglycol methacrylate) (P(TEMPO-*r*-OEGMA)) copolymer networks. In these hydrogels, the OEGMA comonomer brings the hydrophilicity to the polymer network, the TEMPO methacrylate component being hydrophobic in its reduced form. Although, OEGMA is characterized by a LCST behavior, its cloud-point is located at a too high temperature (above 60 °C) to allow the hydrogel to be exploited for bio-applications.[12] This prompted us to replace it by NIPAM that exhibits a lower LCST value Therefore, the present chapter aims at synthesizing poly(2,2,6,6-tetramethylpiperidinyloxy methacrylate-*statistical*-*N*-isopropylacrylamide) (P(TEMPO-*s*-NIPAM)) copolymer networks, inspired by the strategy of Nistor et al.[13] who developed a semi-synthetic hydrogel based on poly(*N*-isopropyl acrylamide-*co*-diethylene glycol diacrylate) inserted onto a collagen porous membrane. The synthesis of those hydrogels was performed through radical copolymerization of *N*-isopropyl acrylamide (NIPAM) with diethylene glycol diacrylate (DEGDA) as crosslinking agent, using ammonium persulfate as initiator and *N,N,N',N'*-tetramethylethylene diamine as activator. A study of the effects of the redox and temperature stimuli on the mechanical and physicochemical properties of these hydrogels will be then performed.

5.2 Synthesis

The investigated P(TEMPO$^+$-*s*-NIPAM) hydrogels were synthesized via a three-step methodology as depicted in **Figure 5.1**. First, a P(TMPM-*s*-NIPAM) precursor hydrogel was prepared by conventional radical polymerization, followed by the oxidation of the secondary amine of the PTMPM units with H_2O_2 and Na_2WO_4 in methanol to obtain the P(TEMPO-*s*-NIPAM) hydrogel.

Different molar ratios of TMPM/(TMPM + NIPAM + DEGDA) (abbreviated as X_{TEMPO} in the following) were investigated (0.1, 0.2, 0.3 and 0.4) and the cross-linker molar ratio DEGDA/(TMPM + NIPAM + DEGDA) (abbreviated as X_{CL} in the following) was also varied (0.02, 0.03, 0.04, 0.05 and 0.13) to investigate the influence of increasing both TEMPO and DEGDA amounts on the characteristics of the hydrogels.

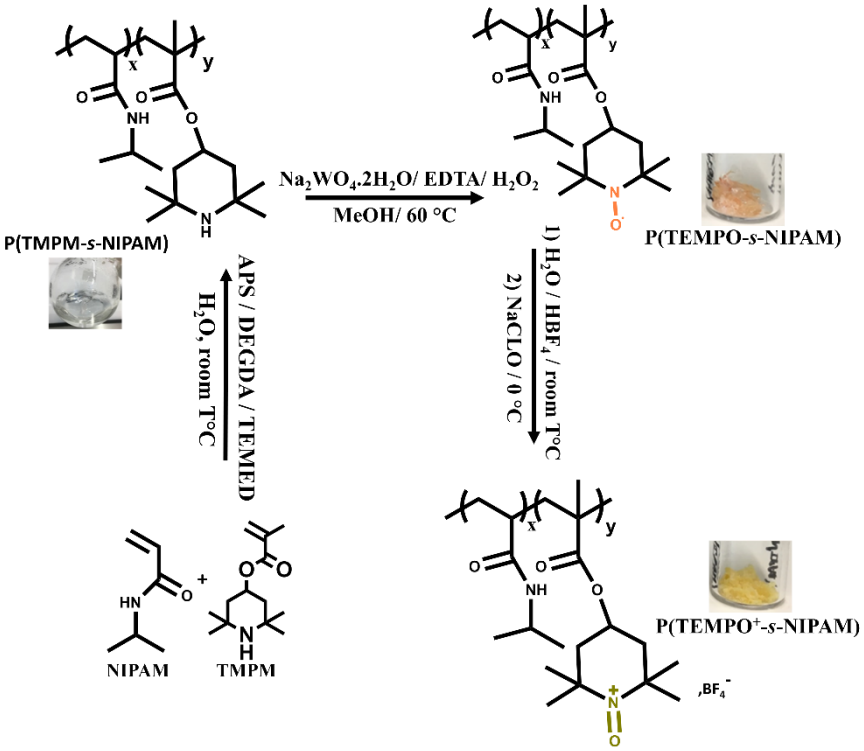

Figure 5.1 *Synthesis of P(TEMPO$^+$-s-NIPAM) hydrogels.*

The yield of the polymerization reaction was checked by ^{1}H NMR by dissolving the dry P(TMPM-*s*-NIPAM) network in $CDCl_3$ and recording a ^{1}H NMR spectrum of the soluble fraction. No signal corresponding to ethylenic protons was detected for all the investigated systems confirming a full conversion of the monomers (**Figure 5.2**). Signals corresponding to P(TMPM-*s*-NIPAM) polymer chains were however detected in the soluble fraction confirming that the obtained

P(TMPM-*s*-NIPAM) networks are slightly crosslinked and that some entrapped P(TMPM-*s*-NIPAM) free chains can be extracted from the hydrogel. The amount of extracted free chains was determined to be 10±1 wt% in agreement with our previously results on hydrogels based on OEGMA reported in chapter 2.

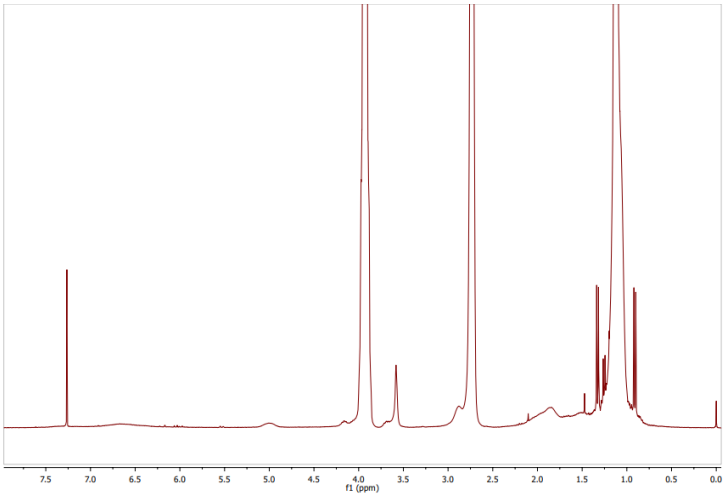

Figure 5.2 *Typically, ^{1}H-NMR spectrum of the supernatant of the polymerisation medium for the investigated P(TMPM-s-NIPAM) hydrogels after overnight polymerization in deuterated chloroform. (X_{TEMPO}=0.2; X_{CL}=0.03). Same results were obtained for all the synthetized networks.*

Finally, the nitroxide radical units of TEMPO were oxidized into oxoammonium units (TEMPO^{+}) with NaClO in the presence of HBF_4 to obtain the oxidized P(TEMPO^{+}-*s*-NIPAM) hydrogels. The macroscopic appearance of the synthesized hydrogels is listed in Table 1 in accordance to the X_{TEMPO} and X_{CL} parameters.

The fact that the synthesized P(TEMPO-*s*-NIPAM) networks do not always form hydrogels (**Table 5.1**) can be explained by different factors. Firstly, with too low concentrations of crosslinking agent (X_{CL} = 0.02, 0.03 and 0.04), it seems that the crosslinking density is too low to allow the formation of a macroscopic hydrogel. Secondly, the amount of TEMPO (or TMPM before oxidation) in the polymer

network is an important parameter driving the formation of a macroscopic hydrogel. Indeed, we have demonstrated in our previous reports that TEMPO (or TMPM before oxidation) units are essentially hydrophobic and aggregate into nano-domains.[25,26] Those hydrophobic interactions are leading to physical crosslinks summing up to the chemical crosslinks provided by the bifunctional DEGDA monomer.

X_{CL} \ X_{TEMPO}	0	0.1	0.2	0.3	0.4
0.02	Liquid	Liquid	Liquid	Liquid	Liquid
0.03	Liquid	Liquid	Liquid	Liquid	Liquid
0.04	Gel	Liquid	Gel	Liquid	Liquid
0.05	Gel	Gel	Gel	Liquid	Liquid
0.13	Gel	Gel	Gel	Gel	Gel

Table 5.1 *Macroscopic aspect of the P(TEMPO-s-NIPAM) hydrogels according to* X_{TEMPO} *and* X_{CL}.

5.3 Morphological analysis

- Dynamic light scattering

Since the synthesis of the P(TEMPO-*s*-NIPAM) networks is conducted in aqueous medium, one could consider that the presence of hydrophobic TEMPO nano-domains has little effect on the formation of a macroscopic hydrogel since those nano-domains will be present in all investigated samples. In that respect, the amount of DEGDA crosslinker seems to be the main factor dictating the formation of a macroscopic gel and a value of X_{CL} above 0.05 is needed to observe the systematic formation of hydrogels. This conclusion is corroborated by the expected reactivity ratios (r_1 and r_2) of the TMPM/NIPAM comonomers. Although we have not experimentally determined the

reactivity ratios in the present study, it is well known that methacrylate monomers are more reactive than acrylamide ones. As a typical example, Virtanen et al. have determined the reactivity ratios of NIPAM (monomer 1) and glycidyl methacrylate (monomer 2) and have found $r_1 = 0.39$ and $r_2 = 2.69$.[14] If we assume that a similar situation prevails in our case, we can assume that TMP is consumed first during the copolymerization reaction. Since we are reaching full conversion for the polymerizations carried out in the present study, TEMPO (or TMPM before oxidation) hydrophobic domains do form first during the course of polymerization from which NIPAM-rich blocks are growing in a next step. A significant part of the DEGDA crosslinker could be incorporated into the TEMPO (or TMPM before oxidation) rich domains, explaining why a significant amount of DEGDA is required to observed macroscopic gelation (see **Table 5.1**). If this hypothesis is valid, this would mean that kinds of nanogel or micellar structures should be formed during the copolymerization reaction. At the end of the copolymerization reaction those nanostructures will be eventually connected by chemical crosslinks in order to form the macroscopic hydrogel. In order to validate this hypothesis, we have performed dynamic light scattering (DLS) and cryo-transmission electron microscopy (cryo-TEM) analysis of samples that do not form a macroscopic gel. Indeed, those samples are liquids showing the typical blueish appearance of micellar solutions (**Table 5.1**). **Figure 5.3** shows a size distribution analysis obtained by DLS on the P(TEMPO-*s*-NIPAM) sample with and $X_{TEMPO} = 0.2$ and $X_{CL} = 0.03$. A single peak corresponding to a mean hydrodynamic radius of 25 nm is observed indicating the presence of micellar nano-objects or nanogel particles.

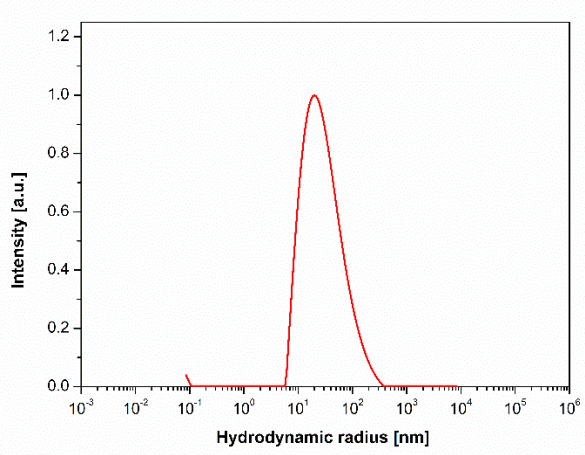

Figure 5.3 *Size distribution histogram obtained by DLS on a P(TEMPO-s-NIPAM) solution with* X_{TEMPO} *= 0.2 and* X_{CL} *= 0.03.*

- Cryo-TEM microscopy

Figure 5.4 shows a typical cryo-TEM picture for the same P(TEMPO-s-NIPAM) sample (diluted 100 times) with X_{TEMPO} = 0.2 and X_{CL} = 0.03 system. Spherical nano-object with diameters ranging from 30 to 50 nm were found. Those results agree with the DLS results and confirm our hypothesis concerning the formation of micellar nano-objects or nanogel particles containing TEMPO-rich hydrophobic domains when the amount of crosslinker is too low.

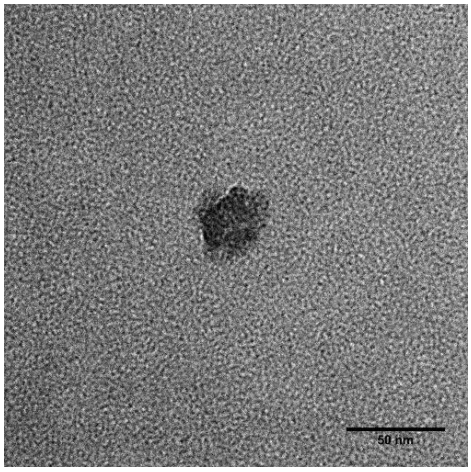

Figure 5.4 *Cryo-TEM image for a P(TEMPO-s-NIPAM) sample with* X_{TEMPO} *= 0.2 and* X_{CL} *=0.03.*

For higher amounts of crosslinker (i.e. 0.13), macroscopic gelation is observed (**Table 5.1** and **Figure 5.5**) meaning that the amount of crosslinker is sufficient to link together the micellar nano-objects or nanogel particles observed in **Figures 5.3** and **5.4**. Therefore, in the following of this paper, the focus will be on the hydrogel-forming samples with X_{CL} = 0.13 and different X_{TEMPO} = 0.1, 0.2, 0.3 and 0.4 (**Figure 5.5**).

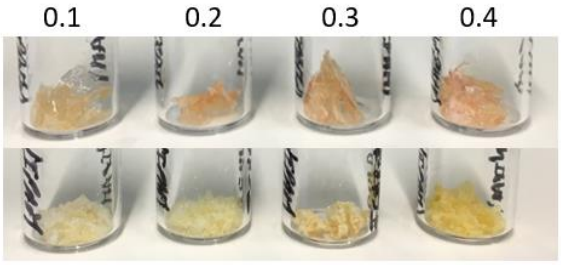

Figure 5.5 *Library of the reduced P(TEMPO-s-NIPAM) (top) and oxidized P(TEMPO*$^+$*-s-NIPAM)* (bottom) hydrogels with X_{CL} = 0.13 and different X_{TEMPO} (indicated on top).

5.4 Electrochemical performances

The oxidation of the P(TMPM-s-NIPAM) precursor into the P(TEMPO-*s*-NIPAM) hydrogel was macroscopically observed by the appearance of the orange color characteristic of nitroxide radicals (**Figure 5.5**). The oxidation yield of TMPM units into TEMPO ones was further determined by ESR. This method indicates an oxidation yield of ca. 99% and confirms that a high rate of oxidation has been reached for all the investigated hydrogels. As a typical example, **Figure 5.6** (red line) shows for the P(TEMPO-*s*-NIPAM) hydrogel with X_{TEMPO} = 0.4 and X_{CL} = 0.13 a spin density of around $1.15x10^{-3}$ mol g^{-1} with the typical signal shape for polymeric organic radicals, which confirms the presence of TEMPO radicals in this hydrogel.

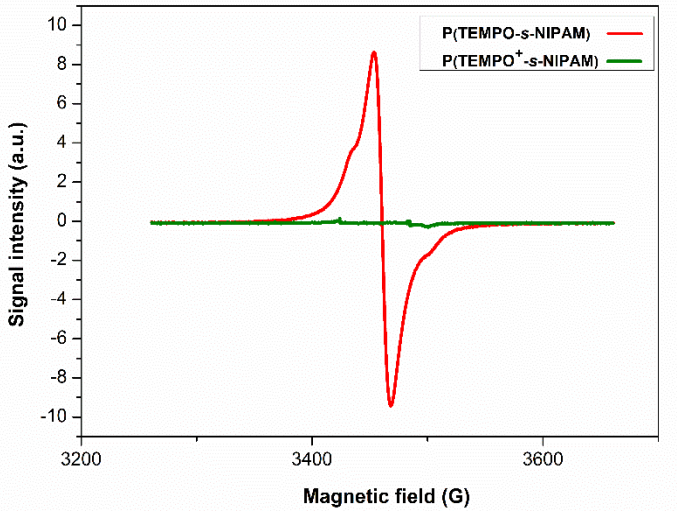

Figure 5.6 *Electron spin resonance spectra of the P(TEMPO-s-NIPAM) (red line) and P(TEMPO$^+$-s-NIPAM) (green line) hydrogels (X_{TEMPO} = 0.4 and X_{CL} = 0.13).*

Finally, the P(TEMPO-*s*-NIPAM) hydrogels were converted into P(TEMPO$^+$-*s*-NIPAM) ones by the chemical oxidation of the nitroxide radicals into oxoammonium cations using NaClO. This reaction can be visually monitored by the color change of the hydrogels from orange to yellow (**Figure 5.5**). ESR was also used to monitor this reaction. As a typical example, a spin ratio of ca. 10^{-6} mol g^{-1} was measured for the

P(TEMPO$^+$-*s*-NIPAM) hydrogel with X_{TEMPO} = 0.4 and X_{CL} = 0.13 and no characteristic signal belonging to radical species was clearly visualized (**Figure 5.6**, green line). From the spin density measurement, we deduce that only ca. 0.1% of the TEMPO units are not oxidized into TEMPO$^+$, which practically means that the conversion of the TEMPO units into TEMPO$^+$ ones is quantitative. Similar results have been obtained for all the investigated hydrogels.

5.5 Mechanical properties

5.5.1 Swelling test in function of time

Swelling tests were performed on the P(TEMPO-*s*-NIPAM) hydrogels with X_{CL} = 0.13 (**Figure 5.7**). The swelling factor, defined as [(Ws – Wd)/Wd] where Ws is the weight of the hydrogel in the swollen state at equilibrium and Wd is the weight of the hydrogel in the dry state, was calculated. The equilibrium state was determined by regularly weighting the hydrogel during the swelling process until it reached a constant weight (typically after 24 h).

However, the hydrogels were further equilibrated to reach a total time of 48 h before measurement. P(TEMPO-*s*-NIPAM) hydrogels with X_{TEMPO} of 0.1, 0.2 and 0.3 display swelling factors around 140 (**Figure 5.7, a**). For the hydrogel with X_{TEMPO} = 0.4, the swelling factor decreases by nearly a factor of two, which can be explained by the increase in hydrophobicity provided by the TEMPO units.

The swelling factors were significantly different for oxidized P(TEMPO$^+$-*s*-NIPAM) hydrogels with values around 85-90 for X_{TEMPO} = 0.1 and 0.2 (**Figure 5.7, b**) and around 110 for X_{TEMPO} 0.3 and 0.4. In this case, the value of the swelling factor increases with the content in TEMPO$^+$ groups which is expected since TEMPO$^+$ groups are hydrophilic in contrast to hydrophobic TEMPO groups. The swelling factor values are smaller for the P(TEMPO$^+$-*s*-NIPAM) hydrogels compared to the P(TEMPO-*s*-NIPAM) ones in agreement with our

previous studies on P(TEMPO-r-OEGMA) and P(TEMPO$^+$-r-OEGMA) hydrogels described in chapter 2 and 3.[25,26]

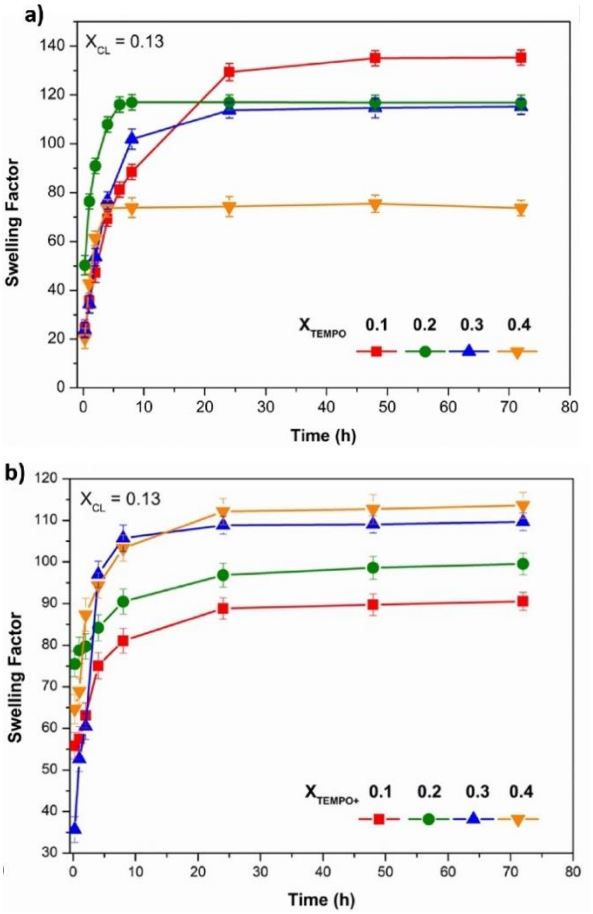

Figure 5.7 *Kinetic swelling study of a) P(TEMPO-s-NIPAM) and b) P(TEMPO$^+$-s-NIPAM) hydrogels with varying X_{TEMPO} (X_{CL} fixed to 0.13, error bars represent average swelling ratio ± standard deviation where n = 3).*

5.5.2 Swelling test in function of temperature

The temperature-dependent swelling profiles of the P(TEMPO-*s*-NIPAM) hydrogels with varying amounts of TEMPO units and X_{CL} equal to 0.13 are illustrated in **Figure 5.8**. As temperature increases, swelling decreases until 80 °C, when all gels totally collapsed. The swelling factors decrease significantly between 20 and 25 °C for all the investigated P(TEMPO-*s*-NIPAM) hydrogels in agreement with the desolvation of NIPAM units and in line with the milky macroscopic aspect of the hydrogels. This occurs at temperatures a bit lower than the reported LCST of PNIPAM (32 °C). This observation is expected since the presence of hydrophobic TEMPO units should shift the LCST to lower temperatures.[15] On the other hand, we have previously demonstrated that solubility of TEMPO units increases as temperature increases.[26] This effect would explain why a complete collapse of the P(TEMPO-*s*-NIPAM) hydrogels is not observed above the LCST of NIPAM units but rather a slow desolvation of the hydrogels as temperature increases (**Figure 5.8**).

As far as P($TEMPO^+$-*s*-NIPAM) hydrogels are concerned, the swelling factors are found to be constant whatever the temperature and the amount of X_{TEMPO+}. Therefore, it seems that the hydrophilic character of $TEMPO^+$ units is totally overwhelming the effect of the LCST of PNIPAM which has not been observed for the investigated samples. Indeed, all the P(TEMPO-*s*-NIPAM) hydrogels remains optically clear whatever the temperature meaning that the LCST of PNIPAM is not reached in our experimental window of parameters.

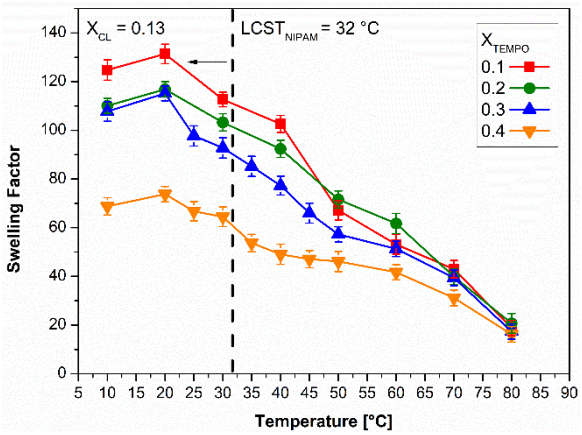

Figure 5.8 *Temperature-dependent swelling profiles of P(TEMPO-s-NIPAM) hydrogels for different X_{TEMPO} and X_{CL} = 0.13 (error bars represent average swelling ratio ± standard deviation where n = 3).*

5.5.3 Rheology experiment

The viscoelastic properties of the P(TEMPO-*s*-NIPAM) hydrogels were investigated by rotational rheometry. The viscoelastic response was measured as a function of the oscillation frequency for the different X_{TEMPO} values and for X_{CL} = 0.13. As shown in **Figure 5.9**, the storage modulus (G') is constant in the whole experimental frequency range, confirming the formation of a gel. By adding more TEMPO units in the hydrogel, G' increases. Since these units are insoluble in water, we hypothesize that TEMPO groups aggregate into hydrophobic domains that could be at the origin of the nanostructures observed by cryo-TEM (**Figure 5.4**). As suggested before, those hydrophobic domains could play the role of additional physical crosslinks to the chemical crosslinks provided by the DEGDA units, which nicely explains the increase of the elastic modulus of our hydrogels with increasing X_{TEMPO}. Regarding the oxidized P(TEMPO$^+$-*s*-NIPAM) hydrogels, frequency sweeps were also performed that confirm gel formation (**Figure 5.9**).

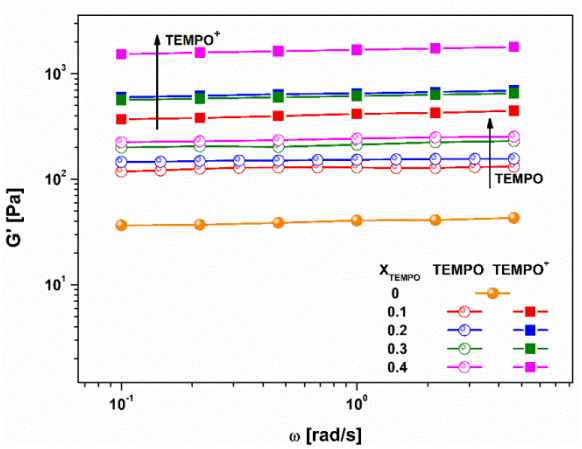

Figure 5.9 *Frequency sweep plots of storage versus frequency for P(TEMPO-s-NIPAM) and P(TEMPO$^+$-s-NIPAM) hydrogels with varying X_{TEMPO} and X_{CL} = 0.13.*

While comparing the rheological properties of the P(TEMPO-*s*-NIPAM) and P(TEMPO$^+$-*s*-NIPAM) hydrogels, we observe that the oxidized P(TEMPO$^+$-*s*-NIPAM) hydrogels display higher moduli than the P(TEMPO-*s*-NIPAM) ones although the physical crosslinks due to hydrophobic TEMPO domains disappear upon oxidation of the nitroxide radicals into soluble oxoammonium cations. As we discussed previously in this thesis, the elastic modulus of hydrogels varies depending on the presence or not of charged groups in their structure. We attribute the higher G' in P(TEMPO$^+$-*s*-NIPAM) hydrogels to a stiffening of the polymer network resulting from electrostatic repulsions among positively charged TEMPO$^+$ units and the effect of the electrostatic interactions of charged groups on the elastic free energy. This is consistent with the observation of the swelling behavior discussed above. The evolution of the storage modulus as a function of temperature is presented in **Figure 5.10** and is fully consistent with the temperature swelling data, i.e. G' decreases with temperature for P(TEMPO-*s*-NIPAM) hydrogels and is constant for P(TEMPO$^+$-*s*-NIPAM) hydrogels in the investigated temperature range.

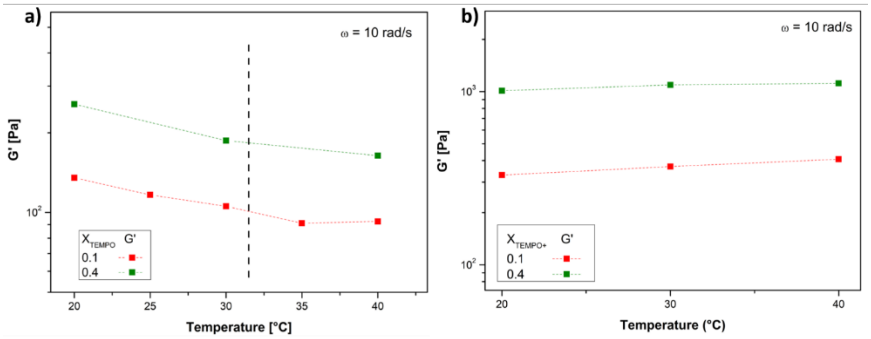

Figure 5.10 *Storage modulus of the a) P(TEMPO-s-NIPAM) hydrogels and b) P(TEMPO$^+$-s-NIPAM) hydrogels with the lowest X_{TEMPO} = 0.1; highest X_{TEMPO} = 0.4 and X_{CL} = 0.13.*

In order to investigate the reversible behavior of our hydrogels, strain sweeps have been performed from low to high strain amplitude and then from high to low strain. The results are shown in **Figure 5.11** for the P(TEMPO-*s*-NIPAM) hydrogels with X_{TEMPO} = 0.1 (lowest amount) and 0.4 (highest amount) and X_{CL} = 0.13.

For both samples, hysteresis is observed, which can be seen as a signature of reversible association operating in our hydrogels. While the network structure is partially broken at high strain in order to allow the sample to deform, the network is reformed when coming back to low strain amplitude. This behavior can be explained by the hypothesized structure of our hydrogels previously described in this chapter. Indeed, our hydrogels are believed to consist of micellar/nanogel particles containing a TEMPO-rich core that are usually linked together by chemical crosslinks. However, a significant amount of nano-objects could be trapped in the network structure through reversible association of the TEMPO groups, but without being covalently linked to this network. Therefore, upon deformation, those ones could dissociate from the covalent network compromising its integrity. Nevertheless, this behavior is reversible allowing the network to reform when deformation is stopped.

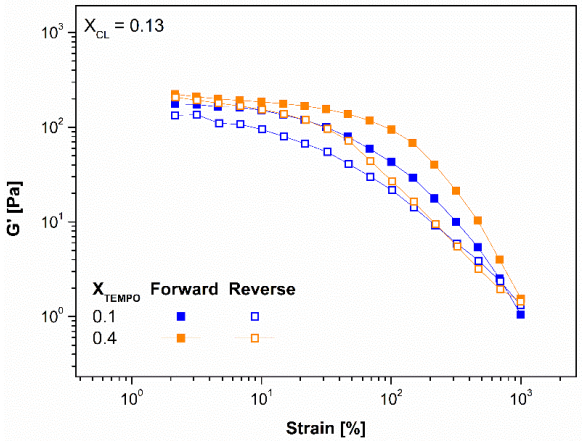

Figure 5.11 *Storage modulus of the P(TEMPO-s-NIPAM) hydrogels with X_{CL} = 0.13 and X_{TEMPO} = 0.1 (blue) or 0.4 (yellow), from low to high (filled symbols) or high to low (empty symbols) amplitude of deformation.*

The strain sweep experiment carried out on oxidized P(TEMPO$^+$-s-NIPAM) hydrogels basically show the same hysteresis behavior (**Figure 5.12**), confirming our hypothesis about the structure of the hydrogel. Those hydrogels are mechanically weak and can be reversibly disrupted which allow us to suggest that a fraction of nano-objects is simply entrapped in the network and can be disentangled when a mechanical deformation is applied.

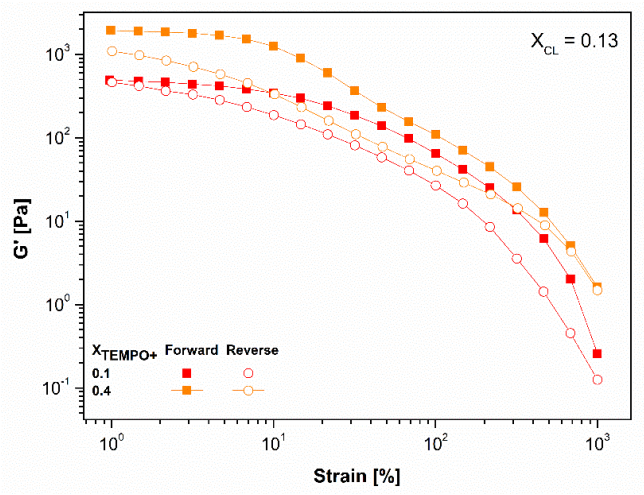

Figure 5.12 *Storage modulus of the P(TEMPO$^+$-s-NIPAM) hydrogels with X_{CL} = 0.13 and X_{TEMPO} = 0.1 (red) or 0.4 (orange), from low to high (filled symbols) or high to low (empty symbols) amplitude of deformation.*

In sharp contrast, the reference gel containing only NIPAM and DEGDA (and thus no TEMPO) keeps its integrity upon high deformation (**Figure 5.13**). However, in order to enter its nonlinear regime of deformation, covalent bonds have to break and the sample does not recover its initial state with lowering the strain amplitude. In this case, no micellar/nanogel substructure is present and only chemical crosslinking points are responsible for network formation.

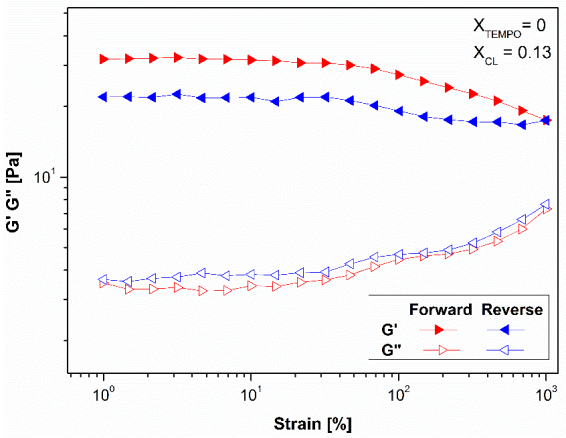

***Figure 5.13**. Storage modulus of the reference hydrogel without TEMPO units with X_{CL} = 0.13 from low to high (red) or high to low (blue) amplitude of deformation.*

5.6 Encapsulation properties

In order to demonstrate the encapsulation abilities of our hydrogels, we have designed a proof-of-concept experiment taking opportunity of the presence of positively charged units in the oxidized P(TEMPO$^+$-*s*-NIPAM) hydrogels to encapsulate a negatively charged model molecule, namely eosin B. Eosin B was selected since it can be easily visually followed by its pink-red color. In a first experiment water containing eosin B at a concentration of 0.012 g/L was used to realize the equilibrium swelling of either the P(TEMPO-*s*-NIPAM) or the P(TEMPO$^+$-*s*-NIPAM) hydrogels. As macroscopically observed in **Figure 5.14**, both P(TEMPO-*s*-NIPAM) and the P(TEMPO$^+$-*s*-NIPAM) (both prepared from the network with X_{TEMPO} = 0.4 and X_{CL} = 0.13) do form hydrogels with encapsulated eosin B. Nevertheless, the supernatant from the hydrogel prepared from the P(TEMPO$^+$-*s*-NIPAM) (**Figure 5.14**) seems to be colorless while the one from the P(TEMPO-*s*-NIPAM) sample (**Figure 5.14**) still presents the same characteristic pink color as the one of the starting eosin B solution at t_0. This preliminary observation suggests that ionic interactions are formed

between P(TEMPO$^+$-*s*-NIPAM) and eosin B that could explain the sequestration of eosin B molecules into the hydrogel. In the case of the P(TEMPO-*s*-NIPAM) hydrogel, eosin B seems to be homogeneously dispersed in the hydrogel and in the supernatant.

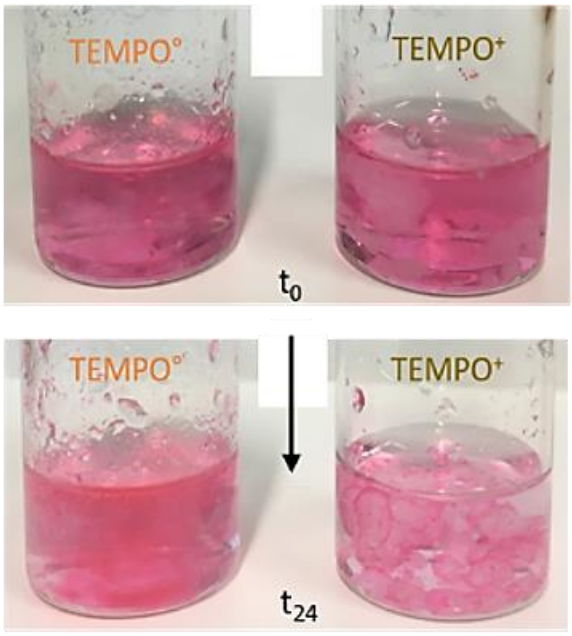

Figure 5.14 *Encapsulation of eosin B via two strategies: electrostatic interaction (for TEMPO$^+$ containing hydrogels and entrapping by swelling for TEMPO containing hydrogels (hydrogels with X_{TEMPO} = 0.4 and X_{CL} = 0.13).*

This observation was confirmed by UV-Vis measurements realized on the supernatant after equilibration. As observed in **Figure 5.15** the characteristic absorption peak of eosin B at 514 nm is still observed in the supernatant of the P(TEMPO-*s*-NIPAM) hydrogel (an encapsulation ability ~13% has been determined by using Beer-Lambert law) while it is not observed in the supernatant of the P(TEMPO$^+$-*s*-NIPAM) sample (encapsulation ability ~99%) confirming strong electrostatic interactions between the charged TEMPO$^+$ units and negatively charged eosin B molecules in the case of the P(TEMPO$^+$-*s*-NIPAM) hydrogel.

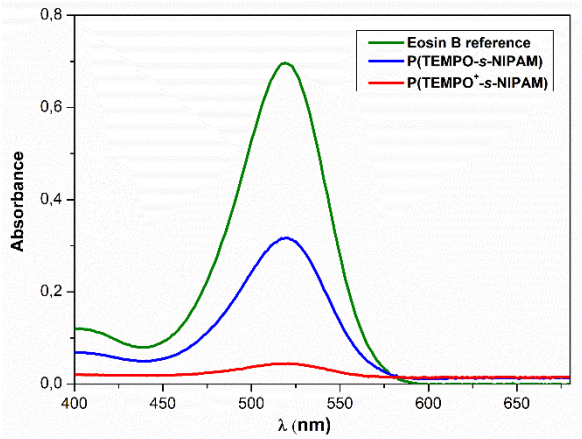

Figure 5.15 *UV-visible spectra of the supernatant of P(TEMPO-s-NIPAM) (blue line) and P(TEMPO$^+$-s-NIPAM) (red line) hydrogels after equilibrium swelling in eosin B solution (hydrogels prepared from the networks with X_{TEMPO} = 0.4 and X_{CL} = 0.13).*

5.7 Conclusions

In this chapter, we have described polymer-based hydrogels responding either to redox or temperature stimuli by introducing NIPAM and TEMPO comonomers into a polymer network. The LCST behavior of PNIPAM has been used to induce de-swelling of the hydrogels with increasing temperature while the oxidation of the nitroxide radicals of TEMPO into oxoammonium cations has allowed the transformation of hydrophobic TEMPO into hydrophilic TEMPO$^+$. The application of the redox and temperature stimuli has triggered important change in the mechanical behavior of the hydrogels as monitored by the determination of swelling factors and of rheological properties. Notably, it was observed that TEMPO units aggregate into hydrophobic nano-domains acting as supplementary physical crosslinking nodes in addition to the chemical crosslinking points provided by the difunctional crosslinking agent. Upon oxidation, those nano-domains are suppressed in favour of positively charged TEMPO$^+$ units conferring a polyelectrolyte character. In addition, we have shown that the thermo-responsive properties are influenced by the redox state of the TEMPO units. Indeed, hydrophobic TEMPO units tend to lower

the LCST of PNIPAM while hydrophilic $TEMPO^+$ groups seem to shift the LCST to higher temperatures or even suppress it.

Interestingly, we have also linked the microstructure of the polymer network to the macroscopic properties of the hydrogels. In this respect, the large difference in reactivity ratios between the comonomers leads to the formation of TEMPO-rich segments in the early stages of the polymerization that further aggregate into micellar nano-objects or nanogel particles. If too low amounts of bifunctional crosslinker are added, those nano-objects are not linked together in the later stage of the polymerization, leading to viscous solutions rather than macroscopic hydrogels. Those nanoparticles have indeed been observed by DLS and cryo-TEM. If the concentration of bifunctional crosslinker is high enough, the nano-objects are eventually linked together leading to a macroscopic hydrogel. The accordingly obtained hydrogels are however rather mechanically weak and can be reversibly disrupted through strain sweep experiments. This suggests that a fraction of nano-objects is simply entrapped in the network and can be disentangled when a mechanical deformation is applied.

To end, the encapsulation abilities of those hydrogels have been tested by encapsulating a negatively charged guest molecule through electrostatic interactions with the positively charged $TEMPO^+$ units. These novel stimuli-responsive hydrogels can be very relevant for many applications in material science and biotechnology.

5.8 Experimental section

- **Materials**

All chemicals and monomers were purchased from Aldrich, TCI, or Acros. Solvents were bought from Acros and VWR. *N*-Isopropylacrylamide (NIPAM, Acros) and diethylene glycol diacrylate (DEGDA, Aldrich) were purified on an AlOx-filtration column prior use in order to remove the inhibitor.

- **Instrumentation**

^{1}H NMR spectroscopy. Proton nuclear magnetic resonance (^{1}H NMR) spectra were acquired on a 300 MHz Bruker Avance II in acetonitrile for the hydrogel obtained after polymerization.

UV-visible (UV-vis) spectroscopy. After equilibration of the oxidized hydrogel swollen in eosin B solution at a concentration of 0.012 g/L, the supernatant was transferred into quartz cuvettes and tested using a Varian Cary 50 UV-vis spectrophotometer with emission scans recorded from 250 to 800 nm.

Rheological measurements. Rheological experiments were performed on a Kinexus Ultra (Malvern Instruments) rheometer equipped with a heat exchanger and modified with a solvent trap. Measurements were carried out using a plate–plate steel geometry (8 and 20 mm diameters) with a gap adjusted between 450 and 1800 mm so that the geometry was completely filled. Oscillatory measurements were carried out in the linear regime (either at strain control of 1% or at stress control of 5Pa). Strain sweep measurements have also been performed at a strain amplitude ranging from 0.3% to 1000% and at a frequency of 5 rad.s^{-1}. Measurements were carried out at 20 °C in a water saturated atmosphere in order to minimize evaporation of the solvent. Normal forces were checked to be relaxed to ~ 0.05 N prior to any measurement.

Swelling tests. The dry gels were swollen in distilled water at 25 °C in an isothermal water bath to study the equilibrium swelling kinetics. Mass measurements were taken at time intervals of 0, 0.5, 1, 2, 4, 8, 24, and 48 h. The swelling factor was defined as the weight ratio between the difference in hydrogel weight in both the dry and the swollen state over the weight of the dry gel. A temperature swelling study was conducted, gels were swelled from 10 to 80 °C with increments of 5 °C. An equilibration time of 24 h was used before each measurement and mass swelling ratios at each temperature were calculated.

Electron spin resonance (ESR). The EPR spin count was determined as the mean value achieved from the EPR spectra of three different samples of the same TEMPO-containing gel. For comparison, the EPR spin count of a TEMPO-free gel was determined likewise. X-band EPR spectra were acquired on an EMXmicro CW EPR spectrometer from Bruker, Germany (EMX micro EMM-6/ 1/9-VT control unit, ER 070 magnet, EMX premium ER04 Xband microwave bridge equipped with an EMX standard resonator, EMX080 power unit). The samples were investigated at room temperature and the data handling was done with the Bruker Xenon software package, version 1.1b86. The SpinCountQ software module was used for the determination of the spin count.

Cryogenic-transmission electron microscopy (Cryo-TEM). For the cryo-electron transmission microscopy (cryo-TEM) measurements, a 4 ml droplet of diluted sample suspension was dropped onto lacey carbon copper grids (200 mesh, Science Services) and plunge frozen into liquid ethane using a Vitrobot Mark IV (FEI, Eindhoven, Netherlands), which was set at 4 °C with 95% humidity. Vitrified grids were then mounted on a cryo transfer holder (Gatan 914, Gatan, Munich, Germany) and transferred into a JEOL JEM2100 (JEOL GmbH, Eching, Germany) transmission electron microscope for imaging with a bottom-mounted 4x4k CMOS camera (TemCam-F416, TVIPS, Gauting, Germany). The microscope was operated at an acceleration voltage of 200 kV and a defocus of the objective lens of about 1.5–2 mm was used to increase the contrast. The total electron dose for each micrograph was kept below 20 $e^{-}Å^{-2}$.

- **Synthesis**

Typical procedure for the precursor poly(2,2,6,6 tetramethylpiperidinyl methacrylate-statistical-NiPAM) (P(TMPM-s-NIPAM)) network synthesis. The synthesis of the polymer network was carried out using conventional radical polymerization. Into a 50 mL round-bottom flask, TMPM was dissolved in water then NIPAM and diethyleneglycoldiacrylate (DEGDA) crosslinker were added and stirred until a homogeneous blend was achieved. The solution was then degassed by three freeze–pump–thaw cycles. The initiator ammonium persulfate (APS; 0.5 eq.) and activator tetramethylethylenediamine (TEMED; 0.5 eq.) were then introduced under argon flux. The solution was immersed in water bath at 25 °C and stirred overnight. A transparent gel was formed.

Typical procedure for the P(TEMPO-s-NIPAM) network synthesis. The secondary amine of the TMPM units has been oxidized into a nitroxide radical to lead to TEMPO. For that, water has been evaporated under pressure from the P(TMPM-s-NIPAM) hydrogel obtained after polymerization. Then Na_2WO_4 (0.25 eq.), EDTA (0.15 eq.) were added and the mixture was swollen in methanol for a couple of hours before adding the oxidizing agent H_2O_2 (5eq.). The mixture was then stirred at 60 °C overnight.[28] An orange colored gel was obtained, washed four times with distilled water and methanol (1:1, v:v) and dried in a vacuo at 40 °C overnight. An orange sticky material was finally obtained.

Typical procedure for the oxidized P(TEMPO$^+$-s-NIPAM) hydrogel synthesis. The P(TEMPO-s-NIPAM) network was swollen in distilled H_2O (31.25 eq.). Then fluoroboric acid (HBF_4, 1 eq.) was slowly added dropwise over 1 h at room temperature.[26] Sodium hypochlorite (0.5 eq.) was then added over 1 h at 0 °C and stirred for an additional 1 h at 0 °C to lead to the oxidized P(TEMPO$^+$-s-NIPAM) hydrogel. Then the hydrogel was washed with ice-cold 5 wt% $NaHCO_3$, distilled water and ice-cold diethyl ether. The obtained yellow gel was finally dried overnight at 40 °C *in vacuo*.

Bibliography

1 D. Singh, D. Kuckling, V. Koul, V. Choudhary, H. J. Adler and A. K. Dinda, *Eur. Polym. J.*, 2008, **44**, 2962–2970.

2 J. Kopecek, *Nature*, 2002, **417**, 388–391.

3 G. Li, I. Dobryden, E. J. Salazar-Sandoval, M. Johansson and P. M. Claesson, *Soft Matter*, 2019, **15**, 7704–7714.

4 E. Isikci Koca, G. Bozdag, G. Cayli, D. Kazan and P. Cakir Hatir, *J. Appl. Polym. Sci.*, 2019, **48861**, 1–10.

5 M. A. Haq, Y. Su and D. Wang, *Mater. Sci. Eng. C*, 2017, **70**, 842–855.

6 P. Li, X. Hou, L. Qu, X. Dai and C. Zhang, *Polymers (Basel).*, 2018, **10**, 2–12.

7 B. Strachota, A. Strachota, M. Šlouf, J. Brus and V. Cimrová, *Soft Matter*, 2019, **15**, 752–769.

8 M. Cao, Y. Wang, X. Hu, H. Gong, R. Li, H. Cox, J. Zhang, T. A. Waigh, H. Xu and J. R. Lu, *Biomacromolecules*, 2019, **20**, 3601–3610.

9 M. V. Martinez, M. Molina and C. A. Barbero, *J. Phys. Chem. B*, 2018, **122**, 9038–9048.

10 S. Shekhar, M. Mukherjee and A. K. Sen, *Adv. Mater. Res.*, 2012, **1**, 269–284.

11 X. Feng, K. Zhang, P. Chen, X. Sui, M. A. Hempenius, B. Liedberg and G. J. Vancso, *Macromol. Rapid Commun.*, 2016, **37**, 1939–1944.

12 M. Khodeir, S. Antoun, E. Van Ruymbeke and J. Gohy, *Macromol. Chem. Phys.*, 2020, **1900550**, 1–7.

13 M. Nistor, A. P. Chiriac, C. Vasile, L. Verestiuc and L. Elena, *Colloids Surfaces B Biointerfaces*, 2011, **87**, 382–390.

14 J. Virtanen and H. Tenhu, *J. Polym. Sci. Part A Polym. Chem.*, 2001, **39**, 3716–3725.

15 G. Gürdağ and B. Kurtuluş, *Ind. Eng. Chem. Res.*, 2010, **49**, 12675–12684.

Conclusions and Perspectives

The motivation for this work arose in the context of challenging technological developments, namely smart materials. In this respect, the goal of this thesis was to access novel polymeric hydrogel materials with precise control over their dynamic mechanical properties and highlighting the possible application of these materials. To this aim, a design strategy was developed based on the introduction into the hydrogel of the 2,2,6,6-tetramethyl-1-piperidinyloxy (TEMPO) stable nitroxide radical that can be reversibly oxidized into an oxoammonium cation ($TEMPO^+$). Hydrophilicity in the system is provided by the presence of (oligoethylene glycol) methacrylate (OEGMA) for the first type of hydrogel (chapters 2, 3 and 4) and N-isopropylacrylamide (NIPAM) for the second type of hydrogel (chapter 5).

A state of the art has been presented in **chapter 1**, that summarized the progresses achieved to date in the field of the so-called "smart" hydrogels, encompassing the concepts and basics of hydrogels synthesis and properties. This part showed that researchers accomplished significant progress in developing hydrogels with higher sophistication and complexity in contrast to the early days of hydrogels. Increasing demand on the properties and functionalities of such materials led us to provide novel methods for the production of 'smart' hydrogels.

In this thesis, **chapter 2** reported the development of P(TEMPO/$TEMPO^+$-*r*-OEGMA) stimuli responsive hydrogels that can encapsulate a guest molecule via electrostatic interactions. The electrochemical and mechanical characterizations showed that those gels exhibit interesting physicochemical properties making them very promising candidates for practical use in a wide range of applications.

Moreover, the combination of redox (TEMPO radical) and temperature-responsive (OEGMA comonomer) behaviours in a same hydrogel has been rarely studied. On the basis of the rarely reported approaches on redox-responsive hydrogels, **chapter 3** described the effect of temperature and redox stimuli on the rheological properties of reduced P(TEMPO-*r*-OEGMA) and oxidized P($TEMPO^+$-*r*-OEGMA) hydrogels with varying TEMPO content at a fixed covalent crosslinking degree. Since we use a rather low amount of di(ethylene glycol) dimethacrylate ($OEGMA_2$) to chemically crosslink the polymer network, the accordingly formed hydrogels obtained after swelling with water consist of microgel particles with entangled polymer chains that are not chemically crosslinked. By varying the amount of TEMPO in the polymer network, we have demonstrated that the radical form of TEMPO aggregates into hydrophobic domains acting as physical crosslinking nodes in our hydrogels and further increasing the cohesion between microgel particles. Increasing the temperature results in two opposite effects on the solubility of TEMPO and OEGMA units. The oxidation of TEMPO into $TEMPO^+$ also results in a deep change in the hydrogel properties since $TEMPO^+$ units are essentially hydrophilic and do not aggregate into physical crosslinking nodes.

Chapter 4 that layouts the application of those redox-responsive hydrogels based on 2,2,6,6-tetramethyl-1-piperidinyloxy methacrylate and oligoethyleneglycol methacrylate that have been synthesized and characterized in chapters 2 and 3. In the first application, we have demonstrated the electrochemically-triggered release of an encapsulated drug, namely aspirin. For this application, we immobilized first via ionic interactions negatively charged aspirin molecules in the oxidized hydrogels containing positively charged oxoammonium cations. Then the aspirin loaded hydrogels was deposited on a carbon screen-printed electrode and the reduction of oxoammonium cations into nitroxide radicals was electrochemically triggered. This led to the disruption of electrostatic interactions responsible for the immobilization of aspirin molecules in the hydrogel. Finally, we analysed the supernatant of the hydrogels by mass spectrometry to identify the presence of released aspirin molecules and

quantify their amount by high-pressure liquid chromatography. In a second application, we have used the hydrogels containing nitroxide radicals as catalysts for the oxidation of benzylic alcohol into benzaldehyde. The kinetics of the reaction was followed by in-situ infra-red spectroscopy and the yield of the reaction is determined by gas chromatography coupled to mass spectrometry. In the used experimental conditions, a quantitative transformation of benzylic alcohol into benzaldehyde was observed. Moreover, the formed benzaldehyde phase separates on top of the benzylic alcohol loaded hydrogel making the separation of the product of the reaction extremely easy as well as the recovery of the redox hydrogel catalyst.

A second type of smart hydrogels containing 2,2,6,6-tetramethylpiperidinoxy methacrylate (TEMPO) and *N*-isopropylacrylamide (NIPAM) that undergo reversible redox behavior was prepared and investigated in **chapter 5**. Several polymer networks were first prepared by free radical copolymerization of varying amounts of TEMPO, NIPAM and a crosslinker (diethyleneglycol diacrylate, DEGDA) and subsequently swelled with water to lead to hydrogels. In order to investigate the effects of the redox activity of TEMPO units and of the lower critical solution temperature (LCST) of NIPAM on the hydrogel properties, a study of the swelling ratio of the polymer networks in water at different temperatures was performed for the two forms of TEMPO, the reduced (TEMPO) and oxidized ($TEMPO^+$) one. Moreover, the rheological properties were also measured for both hydrogel forms. Finally, the encapsulation abilities of the oxidized hydrogels were demonstrated via electrostatic interactions between positively charged $TEMPO^+$ units and negatively charged guest molecules, supporting future application of our system in the biomedical and environmental fields.

In summary, the hydrogels based on the OEGMA comonomer display advantages over the NIPAM-containing hydrogels by being more biocompatible, showing stronger mechanical behavior in aqueous medium and because their TEMPO groups can be electrochemically oxidized leading to a better control of their redox responsive activity and opening a wide landscape of application.

In terms of structure and morphology, OEGMA-containing hydrogels consist of a weakly chemically crosslinked OEGMA network containing an important fraction of entangled non-crosslinked polymer chains in which TEMPO methacrylate monomers are essentially randomly dispersed. Since TEMPO-methacrylate units are poorly soluble in water, they tend to aggregate into small hydrophobic clusters adding some weak physical crosslinks to the chemically crosslinked OEGMA network. In contrast, the NIPAM-containing hydrogels are believed to consist of highly segregated TEMPO-rich domains embedded in a NIPAM-rich network due to a high difference in reactivity ratios between the two comonomers. Moreover, the crosslinking difunctional units have a strong tendency to be incorporated into the TEMPO-rich domains and therefore relatively high amounts of crosslinker have to be incorporated in order to observe macroscopic gelation. Since TEMPO-methacrylate and NIPAM units are highly incompatible and phase separate at the nanoscale, the morphology of those hydrogels can be seen as a network of micellar nanoparticles consisting of crosslinked TEMPO-rich cores surrounded by NIPAM-rich corona. When the amount of difunctional crosslinker is sufficient, crosslinking molecules are also incorporated into the micellar NIPAM corona resulting in a network of crosslinked micelles. The observation of micellar nanoparticles from slightly crosslinked NIPAM-based hydrogels in chapter 4 gives credit to this hypothesis. In both cases, the thermo-responsive properties are clearly influenced by the redox state of the TEMPO units. However, a systematic determination of the LCST should have been carried out in order to clearly understand those effects. As expected, the redox state also influences the mechanical properties of hydrogels including the swelling capacity and the rheological behavior.

Our results can be compared with previous studies on the effect of temperature and redox state on acrylamide and methacrylate-based hydrogels used for guest molecule delivery application. We can cite for example the work of S. Dutta et al.[1] They developed a novel pH, thermo and redox responsive semi-interpenetrating network (SIPN) by free radical polymerization of *N*-isopropylacrylamide (NIPA), methacrylated carboxymethylcellulose and a redox sensitive cross-linker. The temperature dependent swelling behavior revealed that those SIPNs exhibited a LCST around 32 ◦C, which is very close to the LCST of PNIPA hydrogels and that the amount of methacrylated carboxymethylcellulose had no significant influence on the LCST of the hydrogels.

For future work, we propose on one hand testing the following points which were not investigated in this thesis: trying to polymerize the TEMPO monomer directly in the form of a nitronium cation, copolymerizing NIPAM with TEMPO acrylate rather than methacrylate in order to obtain a statistical distribution of the comonomers and systematically determining the LCST for our hydrogels by UV-VIS turbidimetry[2] or by differential scanning calorimetry (DSC).[3]

In another hand, testing these families of stimuli-responsive hydrogels for in vitro drug delivery experiments. In this case, the cytotoxicity of the gels in their oxidised P(TEMPO$^+$-*r*-OEGMA) and reduced P(TEMPO-*r*-OEGMA) forms will be measured. Monitoring the effect of the electrical stimulation on the cell viability will be also evaluated. Finally, the drug loaded hydrogels will be used in real conditions for their purpose, i.e. the electrical induced drug release to cancerous or ill cells.

Moreover, materials composed of TEMPO moieties can be valuable to other application than drug delivery. As stated in chapter 1, TEMPO can act as a scavenger of reactive oxygen species (ROS) and as an imaging agent. Thus, the exploration of other therapeutic applications could be considered for our hydrogels. As example, the adaptiveness of P(TEMPO-*r*-OEGMA) hydrogels for ROS scavengers and the

evaluation of the effect of our material on damaged cells could be used to feed a future with effective novel therapeutic systems.

1 S. Dutta, P. Samanta and D. Dhara, *Int. J. Biol. Macromol.*, 2016, **87**, 92–100.
2 H. Zhao, H. An, B. Xi, Y. Yang, J. Qin, Y. Wang, Y. He and X. Wang, *Polymers*, 2019, **11**, 490.
3 J. H. Park, J. W. Jang, J. H. Sim, I. J. Kim, D. J. Lee, Y. H. Lee, S. H. Park and H. Do Kim, *Int. J. Polym. Sci.*, 2019, **2019**, 1–7.

Refereed publications

1) **M. Khodeir**, B. Ernould, J. Brassinne, S. Ghiassinejad, H. Jia, S. Antoun, C. Friebe, U. S. Schubert, Z. Kochovski, Y. Lu, E. Van Ruymbeke and and J.-F. Gohy, *Soft Matter*, **2019**, 6418–6426.

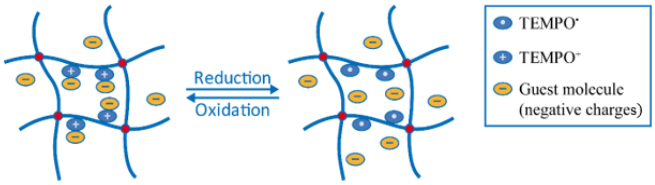

2) **M. Khodeir**, S. Antoun, E. Van Ruymbeke and J.-F. Gohy, *Macromol.Chem. Phys.*, **2020**, 1900550, 1–7.

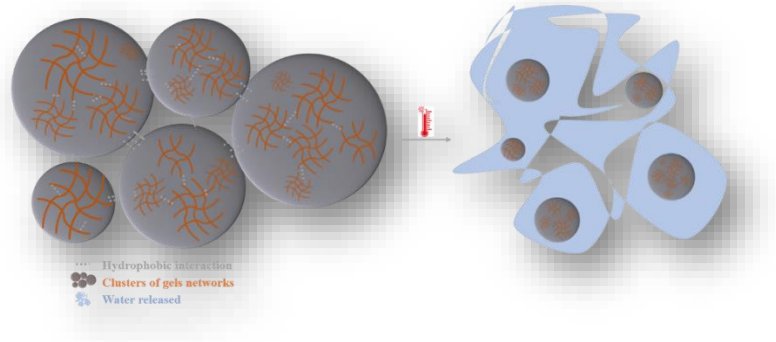

3) **M. Khodeir**, H. Jia, S. Antoun, C. Friebe, U. S. Schubert, Y. Lu, E. Van Ruymbeke and J.-F. Gohy,
J. Polym. Sci.,***2020***,*1-11.